INGEGNERIA

SCUOLA DOTTORALE / DOTTORATO DI RICERCA IN

XXVI

CICLO DEL CORSO DI DOTTORATO

Lifetime investigations on Novel Thermal Barrier Coating systems for Gas Turbine applications

Titolo della tesi

Ahmed Umar Munawar

Nome e Cognome del dottorando firma

Prof. Ing. Giovanni Cerri

Docente Guida/Tutor firma

Prof. Ing. Edoardo Bemporad

Coordinatore: firma

Abstract

In this study, relatively new materials for ceramic top coat, bond coat and substrate applications are studied and their effect on the lifetime of TBC systems is investigated with the aim of increasing the temperature capabilities of gas turbines and/ or improving the lifetime of current TBC systems. The standard TBC system tested for comparison is IN100/ NiCoCrAlY/ 7YSZ. During the study, each component of the standard system is replaced by an relatively advance material and the effect on lifetime is investigated. The material tested for ceramic top coat material is Gadolinium Zirconate (GdZ) which is well known for its lower thermal conductivity and higher thermal stability. Recently, studies demonstrated very good resistance of GdZ against CMAS and volcanic ash attack. In a gas turbine application, with the internal cooling present, GdZ will definitely reduce the temperature at the underlying metal surface due to its lower thermal conductivity. The aim of this study is however to investigate the effect of GdZ on the lifetime of TBC systems. For substrate effect, IN100 superalloy is compared with a more advance, CMSX-4 superalloy. CMSX-4 is a 2nd generation, single crystal superalloy manufactured by Cannon Muskegon Corporation and is well known for its improved high temperature properties. To investigate the bond coat effect, the performance of standard NiCoCrAlY has been compared with a Hf- doped version of NiCoCrAlY deposited on CMSX-4 substrate. Furthermore, the effect of higher Y-content has also been investigated by doping the NiCoCrAlY bond coats with extra Y and depositing on IN100 substrate. All the depositions have been carried out by Electron- beam physical vapor deposition (EBPVD) techniques. The lifetime investigations have been carried out by furnace cyclic testing (FCT) where the TBC samples are kept at 1100°C for 50mins and are cooled down to room temperature by forced air cooling for 10mins. The whole experimental research for this study, from the deposition of samples to the microstructural analysis, has been carried out at German Aerospace Center (DLR) in Cologne, Germany.

This study showed that GdZ on NiCoCrAlY bond coat improves the lifetime of TBC systems considerably. This improvement of lifetime has been observed for both IN100 and CMSX-4 substrates. However, CMSX-4 and NiCoCrAlY based TBC systems show a lower lifetime than the IN100 based counterparts, irrespective of the ceramic top coat material. During thermal cycling, GdZ has been found to undergo a chemical reaction with the TGO on NiCoCrAlY bond coats and a new phase forms at the TBC- TGO interface. In the beginning, this new phase is formed in random patches at different locations, however, with increasing the number of thermal cycles; this new phase becomes continuous at the TBC- TGO interface. GdZ undergoes an ordering transformation from cubic fluorite to pyrochlore phase during thermal cycling. This pyrochlore phase has a very high thermal stability and is the main motivation behind using GdZ as ceramic top coat material. It has been observed that this fluorite to pyrochlore transformation is not detrimental for the lifetime of TBC systems as GdZ based TBCs show a very high lifetime despite this transformation.

In case of NiCoCrAlY version with higher yttrium content, referred to as NiCoCrAlY-2 in this study, it was observed that Yttria forms at the TBC-TGO interface in the form of elongated islands even before the deposition of ceramic top coat. This yttria layer interacts with the TGO during thermal cycling and forms different Y- aluminates. When GdZ-NiCoCrAlY-2 TBC system is thermally cycled, the chemical reaction between GdZ and the TGO results in a reaction zone consisting of alternating Gd- and Y rich phases. GdZ-NiCoCrAlY-2 TBC systems show a significantly longer lifetimes, however, 7YSZ-NiCoCrAlY-2 TBC systems showed relatively shorter lifetime than the standard 7YSZ-NiCoCrAlY TBC systems.

The effect of Hf has also been investigated on CMSX-4 substrate. It has been observed that doping NiCoCrAlY bond coats with 0.6 wt. % Hf improves the lifetime by around 10 times. This improved lifetime doesn't change much when the ceramic top coat is replaced from 7YSZ to GdZ. In the CMSX-4 based TBC systems, diffusion of refractory elements has been found from the substrate towards the TGO. In the NiCoCrAlY-Hf systems, additional diffusion of Hf is also observed and Hf can be seen at the TBC-TGO interface, in the TGO and in the bond coat. In this study, an attempt has been made to understand the mechanisms which effect the lifetime of TBC systems by investigating diffusion of elements in TBC systems, phase changes, chemical reactions and sintering effects.

ACKNOWLEDGEMENTS

I would like to express my deepest gratitude to my supervisor Prof. Giovanni Cerri for all his technical guidance, his moral support, encouragement and patience. His kindness and cooperative nature helped me throughout my PhD and I'd like to carry these attributes in my life as well. I feel lucky to be a part of this research group at the University of Roma Tre and I am thankful to all my colleagues here for their support and cooperation.

I owe special thanks to Dr. Uwe Schulz from German Aerospace Center (DLR) where I carried out all my experimental research. With all his experience and knowledge in the field of Thermal Barrier Coatings, I could not have found a better supervisor than him. He supported me very well throughout my PhD and was always cooperative and understanding. In the end, he read and corrected my PhD thesis even when I was not a part of DLR. I am also thankful to my colleagues at DLR for all the good time I had over there.

I would like to thank my family as well especially my wife Nabawiya Mattke for her support. My children, Zainab and Daud, are source of inspiration for me and I always get motivation and energy when I look at them. My parents always encouraged and motivated me for higher education and I would like to give special gratitude to them for all their unconditional love and support. Without the support of my family, I could never have accomplished so much in my life.

CONTENTS

List of Figures

List of Tables

Nomenclature (List of Abbreviations)

TBC = Thermal Barrier Coatings

EB-PVD= Electron Beam Physical Vapor Deposition

PS = Plasma Spraying

RE = Reactive Elements

DS = Directionally solidified

SC = Single crystal

GdZ = Gadolinium Zirconate

7YSZ = 7 wt % yttria stabilized zirconia

TGO = Thermally Grown Oxide

CMAS = Calcium Magnesium Alumino Silicates

DySZ = Dysprosia stabilized Zirconia

CeSZ = Ceria stabilized Zirconia

FCT = Furnace Cyclic Testing

XRF = X-ray Fluorescence

XRD = X- ray Diffraction

SEM = Scanning Electron Microscopy

EDX = Energy Dispersive X-ray Spectroscopy

DEDICATION

I would like to dedicate this thesis to the source of all the good things in my life !

1- Introduction and Motivation

A gas turbine is an internal combustion engine that is used to deliver mechanical power and/ or thrust. It consists of three main parts which are 1- compressor, 2- combustion chamber and 3- turbine or expander. A compressor increases the pressure and temperature of inlet air to 200-600°C and directs it towards a combustion chamber [1]. The fuel is introduced in a highly atomized spray form in the combustion chamber and the compressed air/ fuel mixture is ignited thereby creating a gaseous product which is very high in stored energy and exists at a very high temperature. These gases are directed to the turbine section which converts the stored energy in the gas to rotational mechanical energy of the turbine rotor. In aircraft engines, these gases can be fed through another set of nozzles in the exhaust of the turbine to convert even more energy to thrust, and the use of an afterburner can increase thrust even further in military applications. A gas turbine for jet engine application is shown in Fig. 1.1.

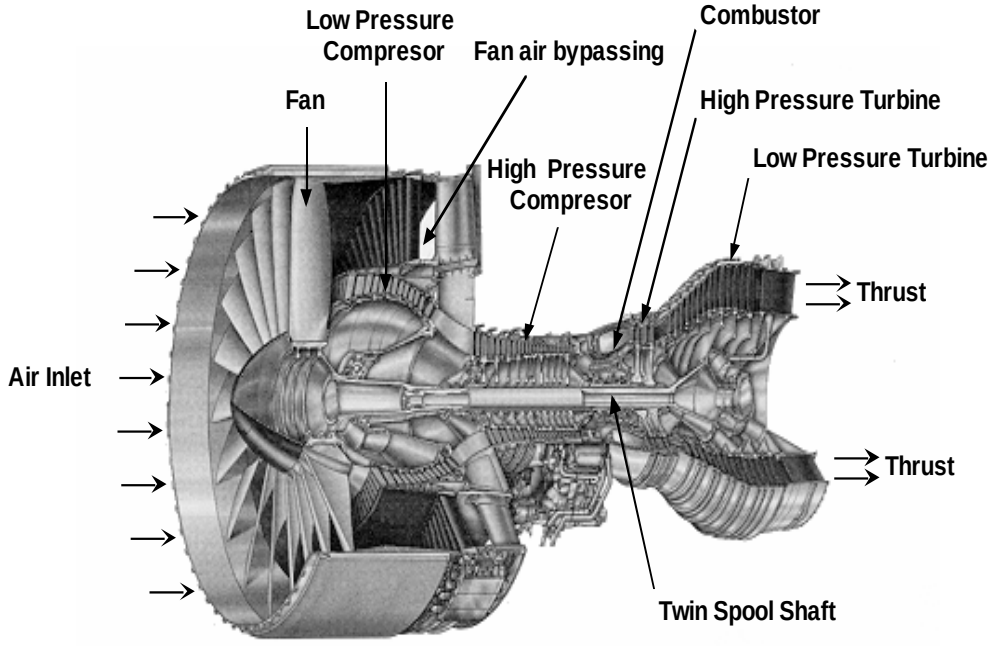

Fig. 1.1: Schematic diagram of Rolls Royce Trent 800 engine, which powers the Boeing 777 aircraft [2].

The efficiency of all types of a gas turbine engines (aircraft, terrestrial and marine) is strongly dependent on the turbine inlet temperature (TIT). From a performance standpoint, stoichiometric combustion with turbine inlet temperature of around 2,000°C would be a thermodynamic ideal as no work would be "wasted" to compress air needed to dilute combustion products [3, 4]. As a result, the current industry trend pushes the turbine inlet temperature closer to the fuel

stoichiometric temperature, especially for military aircraft engines. However, allowable component metal temperatures, even for the most advanced alloys and manufacturing processes, cannot exceed 1000°C. To operate gas turbines at gas temperatures well above this limit, a highly efficient cooling system is required. Improvement in cooling technology is very important to achieve higher turbine inlet temperatures. For advanced aero engines turbine inlet temperatures (TIT) close to 1700°C and compressor pressure ratios around 40:1 are becoming a reality [4]. For industrial engines the major requirement is long-term durability without frequent inspections and overhauls. The TIT limit for a modern industrial gas turbine is established presently in the range of 1250- 1400°C and the components are expected to endure at least 30000 hours between overhauls, with potential to be repairable such that the engine life can be extended to 100,000 hours [4, 5].

The most common cooling techniques are based on the application of the air bled from the compressor discharge or intermediate stages. Introduction of this turbine cooling air results in degradation of turbine performance because less work is extracted from the compressed cooling air. At the same time there is lesser amount of air available for the combustor which makes liner cooling and emission control more difficult. The major challenge in designing such a cooling system is to achieve targeted metal temperature by a minimum amount of cooling air and to produce the smallest negative impact on engine durability, performance, weight, emission, cost, and fabrication complexity. Another type of cooling technique is to allow the coolant to penetrate the airfoil surface through a porous wall. This is a very efficient air cooling technique available but it has significant limitations due to required small size of the pores and the potential problem of their blockage. However to minimize these problems, the cooling air can be discharged through relatively large holes mixing subsequently with a relatively small velocity mainstream flow [4].

The use of coatings in the protection of underlying metal from high temperature degradation has been seen as important for the last 100 years [6, 7]. There has been a significant development in coatings technology and composition since then. The first coating for protection against high temperature was an early form of aluminium diffusion coating and was patented by Van Aller in 1911 [6]. The first use of coating in gas turbines was in 1942 by Anselm Franz who aluminized low alloy steel to substitute more expensive high alloy steels. Use of both ceramic and metallic coatings to increase the turbine inlet temperature even further was first use in military aircrafts. These advancements were then passed down to civil aero engine applications and led to a significant increase in engine efficiency through reduction of internal cooling requirements [7-9]. This combination of ceramic and metallic coatings to withstand high temperature in gas turbines is called Thermal Barrier Coating (TBC) system. TBC coatings allow gas turbines to operate at a higher temperature, as shown in Fig. 1.2.

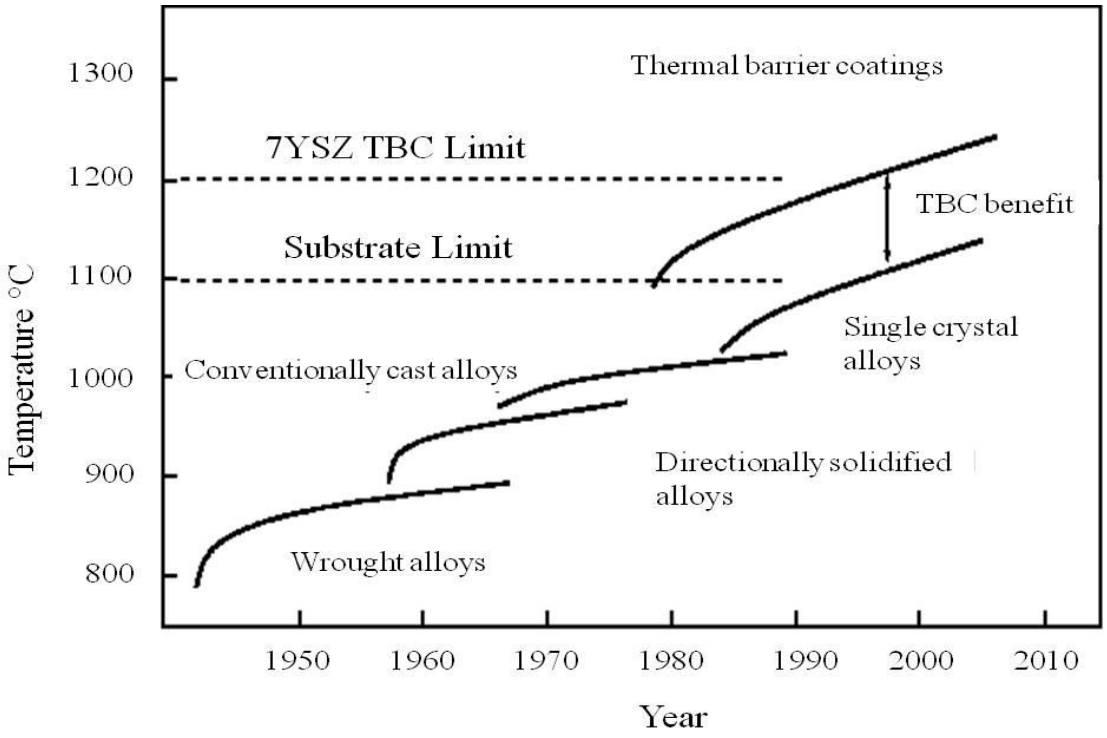

Fig. 1.2: Effect of TBC system on the temperature capabilities of gas turbines [10].

These days film cooling is frequently used in combination with previously mentioned cooling techniques to provide cooling for gas turbine components. The coolant flowing through the internal sections of the turbine blades remove the heat flowing from the metal. In the internal convection heat transfer phenomena; flow velocity and composition of the coolant gas and, architecture and geometry of the blades play the most important part. Between the ceramic and metallic layers of the TBC system, conduction heat transfer takes place which depends mainly on the thermal conductivity and thickness of ceramic top coat. A lower thermal conductivity and a higher thickness of ceramic top coat layer will definitely reduce the temperature at the underlying metal surface. Apart from thermal conductivity, higher thermal stability of the ceramic top coat is also very important to operate the gas turbines at higher TIT.

The aim of this study is to investigate the mechanisms affecting the lifetime of relatively new TBC systems. In this study gadolinium zirconate (GdZ) is studied as the ceramic top coat layer which is well known for its higher thermal stability and lower thermal conductivity. GdZ is deposited on different bond coats and substrate materials and lifetime investigations are carried out at elevated temperature.

2- Literature Survey

2.1 TBC System

Together with internal cooling, TBC systems allow gas turbines to operate at a higher temperature and/ or improve the lifetime of components. In TBC systems, a metallic and a ceramic coating is deposited on the base or substrate material which is usually a Ni or Co based substrate to withstand high temperature, stress, and high temperature oxidation & corrosion conditions in gas turbines. A TBC system is shown schematically in Fig. 2.1.

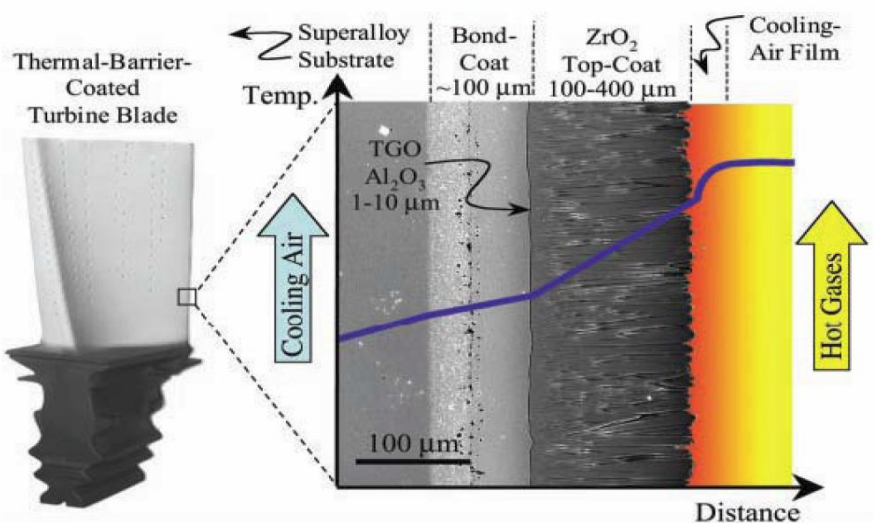

Fig. 2.1: A schematic diagram of TBC system [5].

During the deposition of ceramic top coat, an oxide layer starts to grow at the interface of ceramic top coat and bond coat. During the operation of TBC system this oxide layer continues to grow and as a result stresses accumulate in the TBC system, which play an important role in the failure of TBC system. Different components of a TBC system are explained in detail in the upcoming sections.

2.2 Substrate

High temperature nature of the applications requires the use of superalloys to make various components of gas turbines. Usually, the high temperature is defined from the aspect of material rather than that of the application itself. For this reason, it is important to mention the fraction of melting temperature T_m, also called the homologous temperature, of the alloys used. Superalloys are those which have the capability to operate in excess of $0.5T_m$. Ni- based superalloys are well-known for their outstanding combination of high temperature strength, toughness and resistance to degradation in corrosive or oxidizing environments [11]. Therefore turbine blades, which are a critical component in both aeronautical and stationary gas turbines, are made from Ni- base

superalloys. As the performance of gas turbines is closely related to the capability of materials to withstand high temperatures, there has been a tremendous development in superalloys. Ni- base superalloys have a γ phase matrix with a face- centered cubic (FCC) structure, containing a dispersion of intermetallic precipitate particles of γ′- Ni_3Al [11].

In the beginning, superalloys were cast with equiaxed structure with a higher γ′ volume fraction in order to improve the creep strength at higher temperatures. The grain boundaries of these equiaxed superalloys were strengthened by adding the elements C, B, Zr or Hf [12]. it was observed that the grain boundaries represent the weak points in the system. In 1960s, the creep strength and ductility were significantly improved by the elimination of grain boundaries perpendicular to the principal stress axis, by means of directionally solidified (DS) blades [12, 13]. In DS blades, the columnar grains are aligned to the blades axis, as shown in Fig. 2-2. It is because the major failure mechanisms for turbine blades involved nucleation and growth of cavities along transverse grain boundaries. DS blades improved the temperature capability of turbine blades by around 20°C, compared to the conventional cast alloys. Later development in the turbine blades resulted in a total elimination of grain boundaries as grain boundaries represented the weak points and stresses tend to concentrate there. Single crystal superalloys also eliminated the requirement of grain-boundary strengthening elements (C, B, Zr, Hf). The evolution of turbine blades cast in different microstructures is shown in Fig. 2.2.

Single crystal superalloys represent the best microstructure; industry has to offer currently, where strength is considered. However, there has been tremendous development in single crystal superalloys with respect to high temperature properties and at the same time the composition has become more complicated [13-15]. The first original modification of SC superalloy chemistry has been the introduction of rhenium (Re). This refractory element imparts significant creep advantages over the 1^{st} generation superalloys due to solid solution strengthening effects [15]. In addition Re, due to its low diffusion rate, slows down all thermally activated mechanisms controlling the high temperature deformation and damage mechanisms. Rene N5, CMSX-4 and PWA1484, which have been developed by General Electric, the Cannon Muskegon Corporation and Pratt & Whitney respectively, are typical example of 2^{nd} generation superalloys containing about 3wt. % Re. These three superalloys are widely used these days in a variety of aircraft engines as well as in land-based gas turbine engines for power generation. Further increase of Re content to about 6wt. % leads in the development of third generation superalloys such as Rene N6 and CMSX-10 by General Electric and Cannon Muskegon Corporation respectively. However, the addition of Re is not a panacea as it also imparts some drawbacks such as high cost, limited availability, increase of the density and higher proneness to deleterious topologically close-packed (TTP) phase precipitation [14]. To overcome these problems from the 3^{rd} generation superalloys, addition of Ruthenium (Ru) has been found to be useful which has also become a basis for the latest 4^{th} generation superalloys [14, 15].

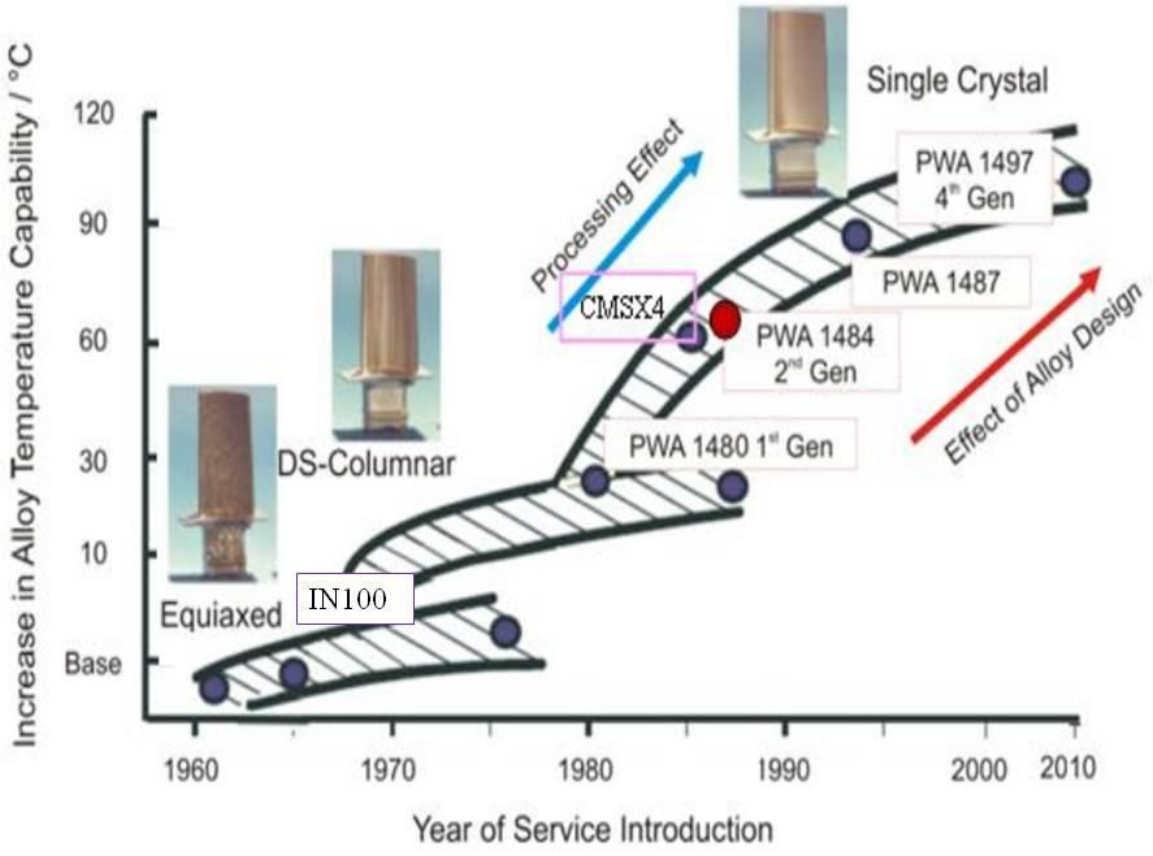

Fig. 2.2: The evolution of superalloy microstructure and the improvement in temperature capability [16].

Strengthening mechanisms used for Ni- base superalloys are precipitation and solid- solution hardening. In precipitation hardening, the solute atoms precipitate in creating a fine and uniformly dispersed second phase. In Ni- base superalloys precipitation hardening is the most important mechanism where γ′ Ni_3Al precipitates provide the most important mechanism for strengthening by acting as coherent barrier to dislocation movement. The creep resistance is dependent on slowing the dislocations speed within the crystal structure. There are many elements (such as Ti, Ta, Al, Mo etc.) which promote the creation of γ′ phase. The size of γ′ phase particles can be precisely controlled by careful precipitation hardening heat treatments. Many modern superalloys consist of square γ′ particles finely dispersed in γ matrix. The γ′-Ni_3Al phase is not strictly stoichiometric as the Ni sites may also contain Co, Cr, Re, W and Mo, while Al sites may contain Ti and Nb. Strengthening by γ′ precipitates is attributed to the slight structural difference between the γ and γ′ phases i.e. long range order and lattice misfit. Dislocations can only move through γ′ precipitates in pairs, called superdislocations. The energy required for the superdislocation to pass through γ′ precipitates is called anti-phase boundary

(APB) which is a result of different slip planes between the two phases [2]. Modern superalloys may contain up to 70 % volume fraction of γ′ phase for the purpose of strengthening. These γ′ precipitates are distributed homogeneously in the γ matrix and have sizes less than 1μm [14].

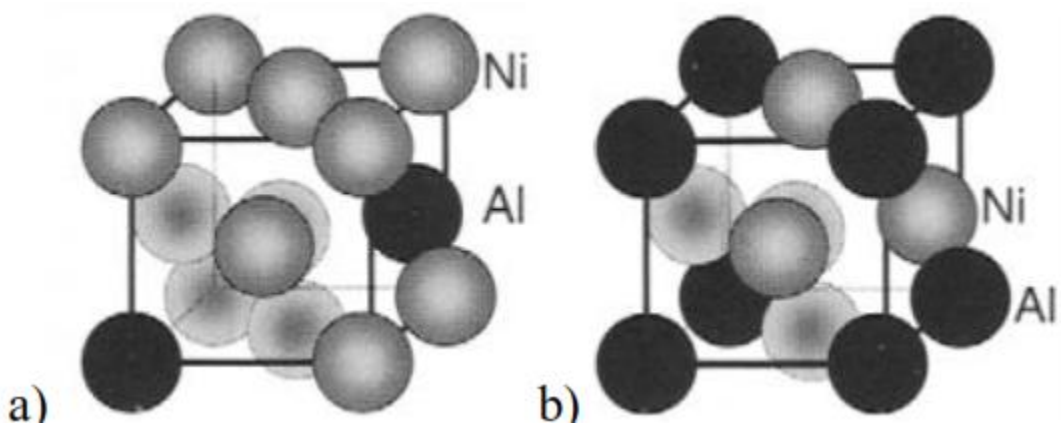

Fig. 2.3: FCC phases in Ni-base superalloys, a) γ- Ni matrix and b) γ′- Ni_3Al [15].

2.3 Bond Coat:

Bond coat gets the name from its function of providing bonding between the ceramic top coat layer and the metallic substrate in a TBC system. It is also supposed to provide necessary protection against hot oxidation and corrosion by forming a protective oxide film which is mostly alumina. Chromia has been another protective oxide which is used for protection at temperatures between 600-900°C in many applications such as catalytic converters [8, 17, 18]. However, it tends to evaporate above 1000°C and hence it is not used for such applications. As explained in previous section, the refractory content of substrate material has been increased continuously over the recent years to improve its strength. This has resulted in a decrease in the Al and Cr content which is harmful for the oxidation and corrosion resistance of superalloy substrates for long term applications. Consequently, it is very important to deposit a bond coat layer which protects the underlying substrate material against high temperature oxidation and corrosion by forming a suitable oxide layer. The structure and composition of this oxide layer which is called thermally grown oxide (TGO) depends on the bond coat material and plays a very important role in determining the lifetime of TBC systems.

The earliest coatings used for protection against hot oxidation and corrosion have been diffusion aluminide coatings based on intermetallic compound NiAl [19-22]. These coatings have enough reservoir of Al to form Al_2O_3 at high temperature. However, major limitations of these coatings are their lack of ductility at temperatures below 600°C and a considerable reduction in the lifetime above 950°C [8]. With the passage of time, many alloying additions have been made in NiAl coatings to improve their properties and lifetime. Espe8cially, with the addition of Pt in

NiAl coatings, the lifetime has been improved significantly. PtAl bond coats are usually manufactured by electroplating a thin layer of Pt on the superalloy and then aluminizing by chemical vapor deposition (CVD) technique or by pack cementation process. The other type of bond coats are overlay coatings, which will be discussed in detail in the upcoming section. The thickness of a bond coat is usually in the range of 75- 150μm.

2.3.1 Overlay Coatings as Bond Coats

Overlay coatings are based on MCrAlY (where M = Ni, Co or a combination of these) and are deposited by low-pressure plasma spraying (LPPS) or by physical vapor deposition (PVD) techniques. Overlay coatings are about 2-4 times more expensive than the diffusion processes; however, much better control on the coating composition can be achieved since the composition is dictated by the coating source. This provides flexibility in depositing different bond coat compositions, however, knowledge of vapor pressure, deposition efficiency and spatial distribution of all the chemical elements is required [23].

MCrAlY coatings are composed of Al- rich and finely divided β-NiAl precipitates in γ-Ni(Co, Cr, Al)- solid solution. This β phase acts as Al- reservoir during the TGO growth at high temperature. As in case of superalloy, the different elements present in the bond coat also serve different roles. Nickel being the element in majority, reduces the phenomenon of inter-diffusion with substrate material. Aluminum provides a reservoir to constantly replenish the oxide during the working of a TBC system. Chromium promotes the formation of α-alumina which is stable at higher temperature and has a very low diffusivity of oxygen resulting in a slow TGO growth. The oxidation of MCrAlY coating is directly proportional to the formation rate of continuous alumina scales present on its external surface. The rate of formation of the scale is related to aluminum activity. Cr also plays an important role in increasing the aluminum activity. Further, the addition of Cr effectively lowers the aluminum content required to form and maintain the oxide film. Overlay coatings can be Ni or Co based, depending upon their applications. Generally, at higher temperatures where oxidation is dominant failure mode (900°C), Ni based over-lay coatings are preferred while for applications at 650-800°C, where corrosion is dominant failure mode, Co- based overlay coatings outperform Ni- based ones because of their higher Cr content [24]. Composition of different overlay coatings according to their application is shown in Fig. 2.4.

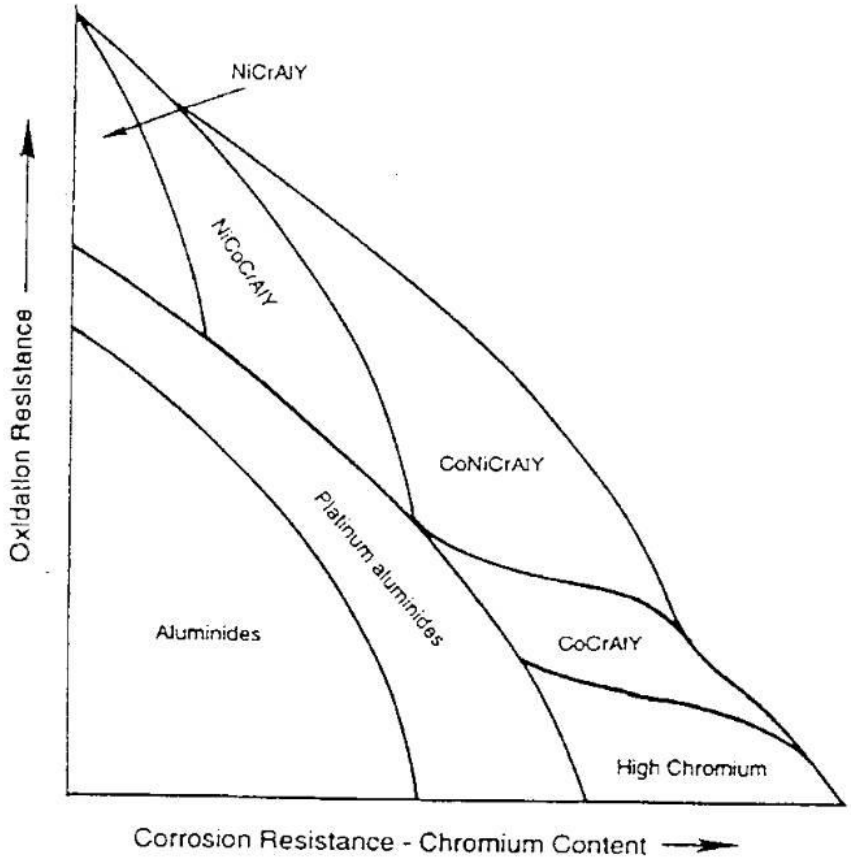

Fig. 2.4: Relative oxidation and corrosion resistance of high temperature coating systems [23].

2.3.2 Effect of Reactive elements on Oxide Scale Adhesion

Reactive elements (REs, e.g., Y, Zr, Hf etc.) are frequently added in overlay coatings to improve adhesion of coatings, however, their role is still not completely understood [27-31]. The addition of Yttrium to the coating promotes scale adhesion. Y has limited solubility in MCrAlY, therefore the excess quantities precipitate within grain boundaries as yttria. This yttria forms pegs, which protrude into the coating alloy and its surface scale. The coating alloy and the alumina film are thus mechanically pinned together and hence scale adhesion is improved [5, 25, 26]. Hf has been found to form oxide stringers in the bond coat and thus improves the coating adhesion by causing an "anchoring" effect. It has been demonstrated that Hf reduces growth rate of alumina scale by a factor of 10 and this reduction has been explained by suppression of Al- grain boundary transport by the segregation of RE ions to the grain boundaries [32]. As a result, such thinner scales can significantly improve scale adhesion as the strain energy release rate upon cooling is direction proportional to the scale thickness. RE in bond coats also increase the oxide scale plasticity and hence result in improve the oxide scale adhesion. However, a contrary result has been reported

where a faster TGO growth has been reported because of Hf- doping of NiCoCrAlY [33]. It has been mentioned that the diffusion through NiCoCrAlY bond coat deposited by Electron Beam Physical Vapor Deposition (EB-PVD) method is faster because of relatively fine-grained structure of NiCoCrAlY [33].

It has been demonstrated that reactive elements segregate at the grain boundaries of TGO and limit the outwards diffusion of Al [34]. As a result there is a change in the rate-limiting step of oxidation and in oxide microstructure and oxide grain size is reduced. It has been proposed in some studies that reactive elements segregate at the metal-oxide interface and grain boundaries as shown in Fig. 2.5 and inhibit interfacial void growth, thus improving the oxide scale adhesion [30, 34, 35].

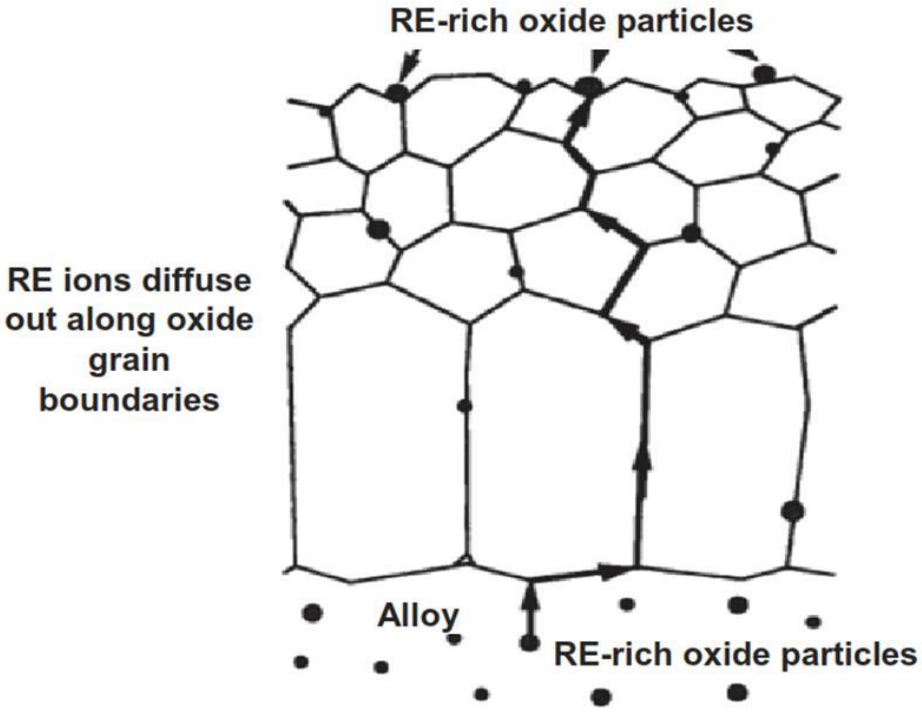

Fig. 2.5: Diffusion of reactive elements through bond coat [29].

In one of the studies, adhesion between different ceramic/ metal interfaces has been measured and it was observed that Zr, Ti, Y, Si and Sc improve the adhesion between Ni/ Al_2O_3 interface [24]. It has also been mentioned that Hf doping to the bond coat can considerably improve the adhesion between bond coat and TGO [36, 37]. Some mechanisms to improve oxidation resistance by reactive elements addition have been stated in the literature which are; enhanced oxide-scale plasticity, a graded seal mechanism, modification of the oxide's growth process, chemical bonding, a vacancy sink model and "pegging" by other oxides [24].

Apart from oxidative corrosion, sulfur also reduces the adhesion at alloy/ oxide interface. It enhances pore formation by lowering its nucleation energy and weakens the interface by accelerating crack propagation between pores [38]. Addition of RE also lowers the extent of sulfur segregation at the metal/ oxide interfaces and hence improves the oxide adherence. It has been stated that Y reacts with the indigenous S to form stable sulfide, thus preventing S from degrading the scale adhesion [5, 39]. In another study, Y-segregation at the alloy-oxide interfaces has been mentioned which lowers the driving force for sulfur segregation at these interfaces and thus eliminates its detrimental role. Apart from Y; Ta, Zr and Hf have also been reported to form pegs which improve the adherence between metal/ oxide interface.

2.4 Thermally Grown Oxide

At high temperature, an oxide film starts to grow at the interface of the bond coat and the ceramic top coat and is called thermally grown oxide (TGO). TGO serves the purpose of protecting the underlying bond coat from further damage, however, it is also a source of strain incompatibility between the different layers of a TBC system. Due to its continuous growth, stresses accumulate at the TGO- bond coat and TGO- ceramic top coat interfaces which play an important role in the failure of TBC system. The composition and structure of TGO depends mainly on the bond coat. An ideal bond coat is engineered so that the TGO forms as α- alumina and that its growth is slow, uniform and defect free [5]. Such a TGO has a very low ionic diffusivity and is quite stable at high temperature. In general, the growth of TGO takes place by inward diffusion of oxygen [40, 41] however in some cases outward diffusion of Al also becomes important [42, 43]. At high temperature, the formation of θ- and/ or γ Al_2O_3 and its conversion to the stable α-Al_2O_3 in the TGO has been mentioned to have a profound effect on the structural integrity of the TGO during thermal cycling [44, 45]. Some properties of different isoforms of alumina are mentioned in Table 2.1.

Table 2.1: Some properties of the main alumina isoforms [153]

	α- alumina	γ- alumina	θ- alumina
Structure	Rhombohedral	Monoclinic	Modified FCC
Density (Kg/m^3)	3980-3990	3560-3600	3200-3700
Melting Point (°C)	2051		
Transition Temperature (°C)		Transition to α-alumina ~925	Transition to δ-alumina 700-800

Thus annealing of bond coats prior to the ceramic top coat deposition is done to obtain an "optimum" TGO that only consists of α-Al_2O_3 so that the reliability and durability of TBCs are improved [46]. However, it has been reported in [47] that the only element to oxidize upon vacuum annealing of a NiCoCrAlY bond coat at 1080°C for 4hrs is yttrium. Formation of yttria after 4hrs of annealing prior to ceramic top coat deposition is shown in Fig. 2. 6.

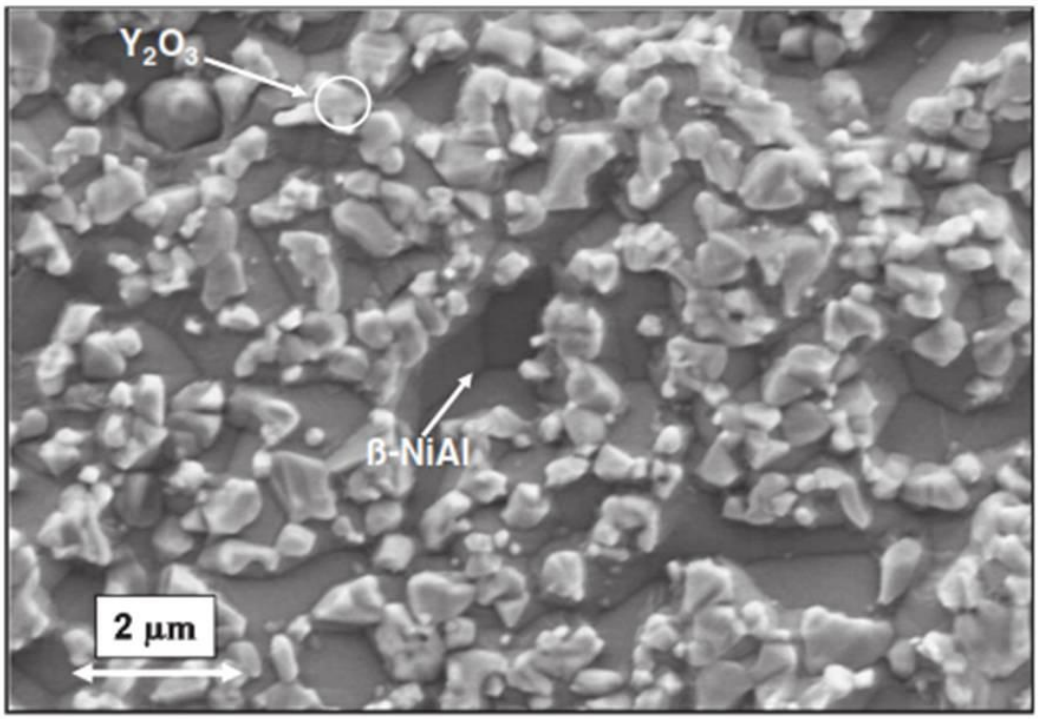

Fig. 2.6: SEM micrograph of a NiCoCrAlY top view after annealing for 4hrs at 1080°C. Different phases identified by EDX are mentioned [47].

It has been reported that formation of yttria doesn't take place for the annealing temperatures below 1050°C [47]. Therefore, the formation of alumina or yttria as a result of annealing depends upon the temperature at which annealing is done. Further, TBC systems where vacuum annealing prior to ceramic top coat deposition is done above 1050°C showed a higher lifetime than the systems where vacuum annealing is done below 1050°C, which clearly shows the benefit of depositing ceramic top coat after yttria is formed at the interface [48] . As deposition of ceramic top coat is done on a pre-heated substrate, the yttria islands formed during the vacuum annealing step lose direct contact with the bond coat due to the formation of $NiAl_2O_4$ spinel layer below the yttria islands [46]. The relatively higher oxygen partial pressure and the steady temperature ramp covering the range from the room temperature to 1000°C within 10mins favor the formation of transient oxides such as spinels at this stage otherwise NiCoCrAlY system is known as a strong alumina former [49]. Till the deposition of ceramic top coat, TGO is approximately 0.5µm thick corundum layer including a periodic sequence of plug-shaped Y- rich

precipitates at the TGO- TBC interface at a spacing of approximately 1- 1.5μm. As the TGO transforms from metastable θ- and/ or γ Al_2O_3 to the stable α-Al_2O_3, the excess zirconia precipitates out. This mixture of dark alumina with white zirconia particles is called a mixed zone. However, the convoluted TGO sections below the yttria islands contain very few zirconia particles, as the pure yttria islands act as a diffusion barrier restricting zirconia supply to the TGO. Such a discontinuous mixed zone structure is termed as "off-plane" mixed zone in the literature. Below the mixed zone, TGO grows in the form of columns and this region is also called columnar alumina zone (CAZ). The growth kinetics of the CAZ demonstrate protective diffusion- controlled parabolic or sub-parabolic growth rates which are typical for alumina-forming alloys. The thickness of the mixed zone, however, remains nearly constant over long periods [50].

2.5 Ceramic Top Coat:

Ceramic top coat is deposited on top of the bond coat to withstand high temperature and to cause a maximum possible temperature drop across its thickness by having very low thermal conductivity [51-54]. For the last two decades, different polymorphs of zirconia have been extensively studied for the ceramic top coat application. Zirconia, in its pure state, has extremely low thermal conductivity and relatively high strength and fracture toughness. In fact, the thermal conductivity of zirconia is lower than most of the other engineering ceramics by over an order of magnitude. In practical terms, this means that even a thin zirconia film (less than one millimeter thickness) can potentially reduce the temperature of the underlying alloy several hundred degrees Celsius when thermal gradient is there. Furthermore, the linear thermal expansion coefficient and elastic modulus of zirconia (especially the tetragonal phase) match very well to several popular nickel-based superalloys, compared to possible alternative ceramics. These properties play a very important role in surviving thermal cycling during TBC applications.

Zirconia exhibits polymorphism as a function of temperature and hence it has to be regulated in order to control its properties [55, 56]. Out of the monoclinic, tetragonal and cubic phases formed by zirconia over different temperature ranges, partial stabilization of tetragonal phase has been found to inhibit stress-induced micro crack propagations. Attempts have been made to control or eliminate the polymorphism by adding different oxides to zirconia. It has been observed that adding 6-8.5wt. % (~3-4.5mol.%) Y_2O_3 forms a partially stabilized tetragonal phase while adding higher amounts of Y_2O_3 form fully stabilized cubic phase. Similarly, adding CeO_2, CaO or MgO also result in a fully stabilized zirconia. TiO_2 as stabilizing oxide has been found to be less effective, however, when added to Y_2O_3 or CeO_2 stabilized ZrO_2 has been shown to produce zirconia polycrystals with favorable properties [5, 57]. Yttria-zirconia phase diagram has been shown in Fig. 2.6 with metastable T′ phase being highlighted.

During the initial TBC development during the 1970s, it has been demonstrated that addition of 6- 8.5wt. %(~ 3- 4.5 mol. %) Y_2O_3 gives the longest TBC lifetime in burner rig tests, even

though zirconia was not fully stabilized. This conclusion has been drawn with different test temperatures and different bond coat compositions. Time to first crack in thermal cycle tests as a function of Y_2O_3 content has been shown in Fig. 2.7. The lifetime of TBCs decreased dramatically at concentrations exceeding these optimum values. It has to be pointed out that, after extensive research for the last two decades to identify better top coat compositions, 6-8 wt. %(~3-4.5 mol. %) Y_2O_3 content in ZrO_2 continues to be optimum.

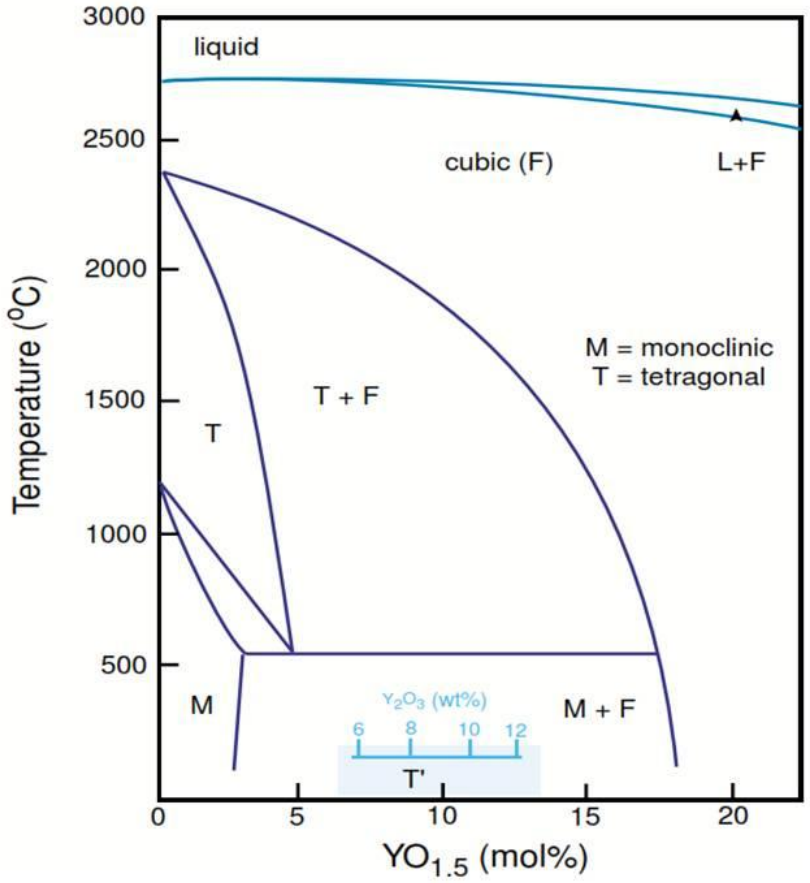

Fig. 2.7: Relevant part of yttria- zirconia phase diagram [23].

2.5.1 Yttria Stabilized Zirconia

Ceramic top coat material must possess a combination of properties to be effective. These properties include a low thermal conductivity, high coefficient of thermal expansion, better resistance to spallation, good erosion resistance, phase stability and pore morphological stability.

7 wt. % Y_2O_3 stabilized zirconia (YSZ) has very low thermal conductivity at elevated temperatures (~2.3W.m^{-1}.K^{-1} at 1273K for a fully dense material). 7YSZ has a high thermal-expansion coefficient (~11 x 10^{-6} K^{-1}), which helps to reduce stress in TBC systems arising from the thermal-expansion mismatch between the ceramic top-coat and the underlying metal (~14 x 10^{-6} K^{-1}) [5, 52]. To further alleviate these stresses, microstructural features like inter- and intra-columnar porosity and feather arms are deliberately engineered into the top-coat to make it highly compliant (elastic modulus ~ 50GPa) and "strain tolerant". 7YSZ has a relatively low density (~6.4Mg.m^{-3}), which is important to reduce the "parasitic-weight" in rotating engine components. 7YSZ also has a hardness of ~14GPa, which makes it resistant to erosion and foreign-body impact. It is resistant to ambient and hot corrosion and furthermore has a high melting point, making it suitable for high temperature applications.

2.6 Coating Processes:

Two most important methods used for TBC top-coat deposition are 1- plasma pray (PS) deposition and 2- electron beam physical-vapor deposition (EBPVD). These techniques will be discussed in detail in the upcoming sections.

2.6.1 Plasma Spray Deposition:

Plasma spray deposition is a type of thermal spraying which is extensively used because of its ability to deposit various compositions readily. In plasma spraying, the material to be deposited is introduced into the high temperature plasma gas stream in the form of powder. Spraying can be done under atmospheric or low pressure conditions. The molten powder particles are then carried into the plasma and propelled onto the substrate, which is heated to a controlled temperature in order to control stress. Thermal spraying processes are not practical for complex components with coatings required in narrow passages since it is a "line-of-sight" process. The advantages of thermal spraying are that it is relatively inexpensive, part size is not a concern, and deposition rates are high. The coating surface produced is, however, usually rough (an R_a of few hundred) and subsequent finishing operations are usually required for airfoil aerodynamics. Plasma spraying can be used to deposit ceramic thermal barrier coatings, MCrAlY oxidation-resistant overlays and abradable seal systems in both the compressor and the turbine.

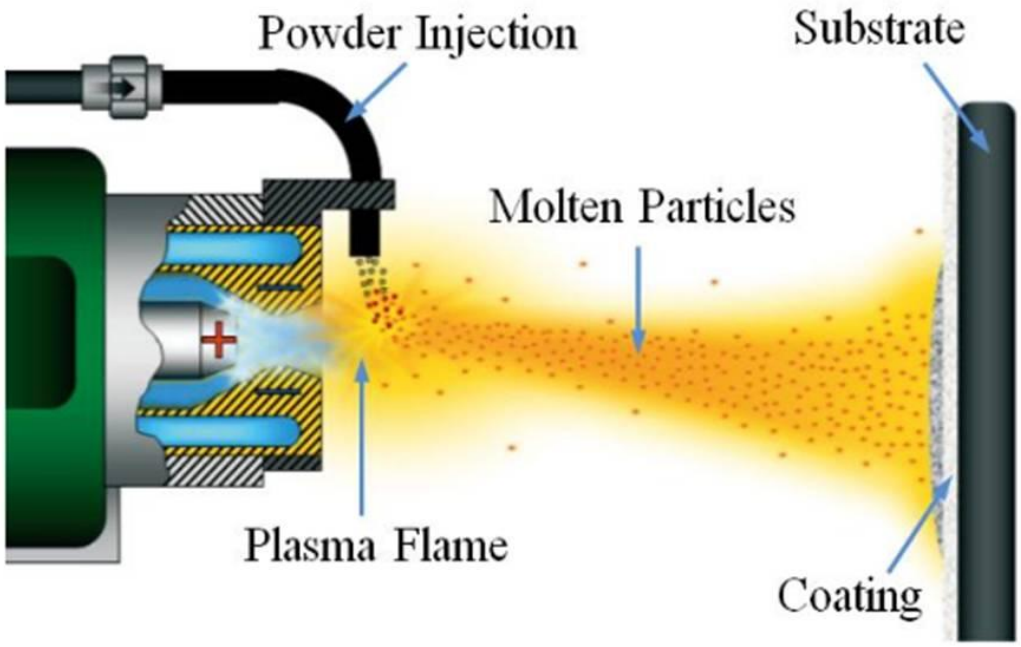

Fig. 2.8: Schematic diagram of Plasma spraying process [58].

2.6.2 Electron Beam Physical-Vapor Deposition:

Electron beam physical-vapor deposition (EBPVD) is a commonly used physical vapor deposition (PVD) technique in which an electron beam is used to melt and subsequently vaporize the solid ingot. High energy electron beam is produced by thermionic emission and is subsequently accelerated and concentrated by electromagnetic fields. During vaporization, a vapor cloud is formed which contains the atoms to be deposited. The substrate to be coated is mounted on to a sample holder and immersed in the area of vapor space where the vapors condense onto the substrate [59, 60]. The substrate is pre-heated to a controlled temperature to optimize coating residual stresses. EB-PVD process is shown in Fig. 2.9.

EB-PVD process results in a columnar microstructure of ceramic top coat where each column represents one grain. The final morphology and orientation of the columns depends on angle at which vapors condense on to the substrate. This is called vapor incidence angle (VIA) and represents the angle between the substrate normal and the average direction of vapor incidence. To control the vapor incidence angle, EB-PVD deposition can be carried out in perpendicular or oblique stationary mode, or conventional or oblique rotating mode. It has been observed that a fibrous column texture with mainly <111> and <110> preferred growth directions are achieved for coatings deposited by stationary perpendicular and oblique modes [59, 61]. However,

coatings deposited at different substrate temperature and rotation speed in conventional rotating mode exhibit a <100> column growth direction [62].

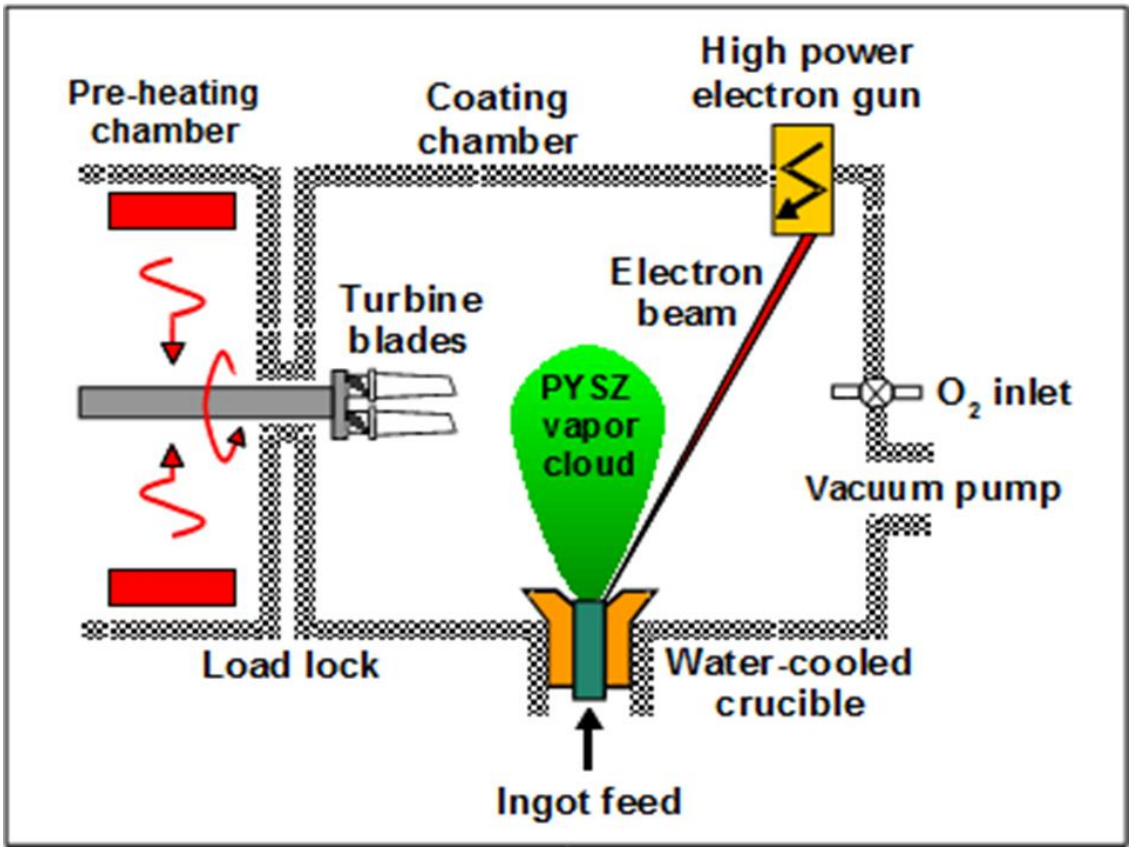

Fig. 2.9: Schematic diagram of EB-PVD process [59]

The complexity of the EB-PVD process vastly increases as the compositional complexity of the coating increases for example, in case of MCrAlY- type coating. It is because the vaporization pressures of each of the elements of interest must be considered in producing controlled alloy chemistry [63]. In addition, issues like melting and evaporation behavior of source material, deposition rate and efficiency and EB power and oxygen additions are also important in EB-PVD deposition [23]. As during the vapor phase processing, most of the compounds decompose into their individual constituents, it is important to consider the evaporation behavior of sub-oxides during the search for potential EB-PVD coating candidates. Fig. 2.10 shows the vapor pressure against different temperatures for some of the oxides currently in consideration for ceramic top coat materials.

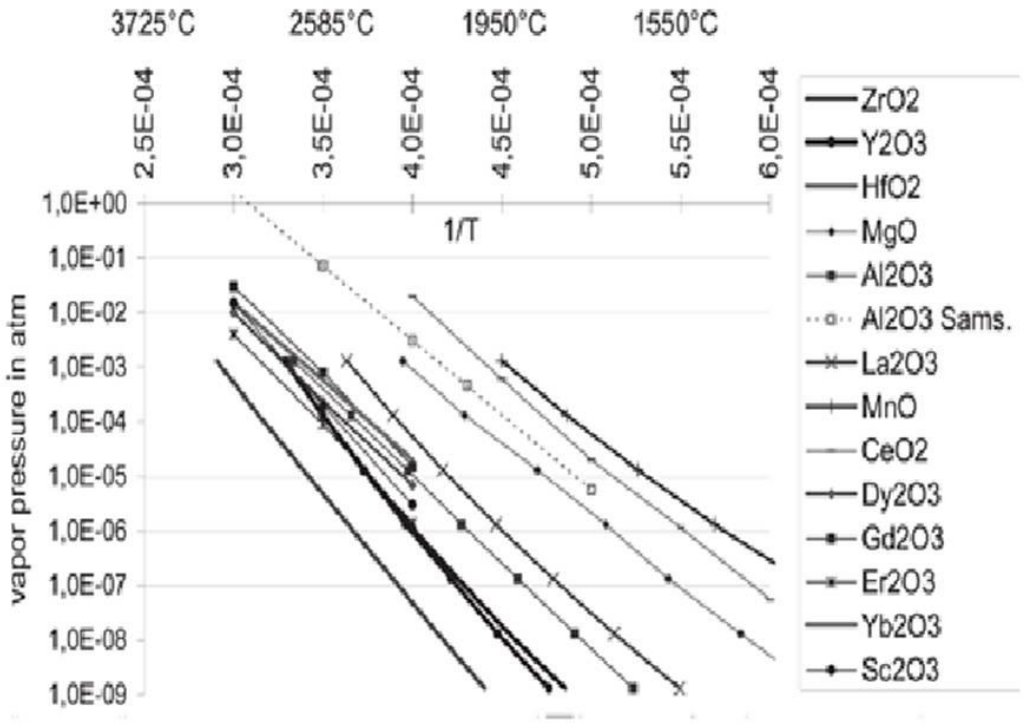

Fig. 2.10: Vapor pressure of different oxides for EB-PVD process [54].

PVD processes are of a "line-of-sight" type and produce a coated surface which replicates the substrate surface, i.e. a smooth substrate surface initially will result in a smooth coated surface. In this way, subsequent coating finishing operations may be eliminated or minimized. Thickness uniformity and deposition rate are usually good but will vary with coating composition [63].

2.6.3 Effect of Coating Process on TBC properties:

The performance of a TBC coatings system depends on morphology of the ceramic top coat as well. This is evident from the properties of ceramic top coats when they are deposited with PS or EB-PVD techniques. Coatings deposited by PS have a thermal conductivity in the range of 0.8 – 1.0 W/mK at 25°C which is significantly lower than the 1.5 – 1.9 W/mK reported for EB-PVD coatings at 25°C [5, 64-66]. This means that the PS coatings provide superior thermal protection. However, the lifetime of PS TBC layers has been found to be lower than that of EB-PVD coatings which is mainly due to the higher strain tolerance of EB-PVD coatings [5, 23, 67]. Consequently, EB-PVD TBC layers are preferred for aerospace gas turbine applications.

The morphology of ceramic top coats is obtained when deposited with PS or EB-PVD techniques which results in different thermal and mechanical properties. In case of PS coatings, the microstructure mainly consists of "splats" which contain pores that are mostly aligned parallel to

the substrate surface. These pores are further accompanied by micro-cracks and fine grain boundaries as shown in Fig. 2.11.

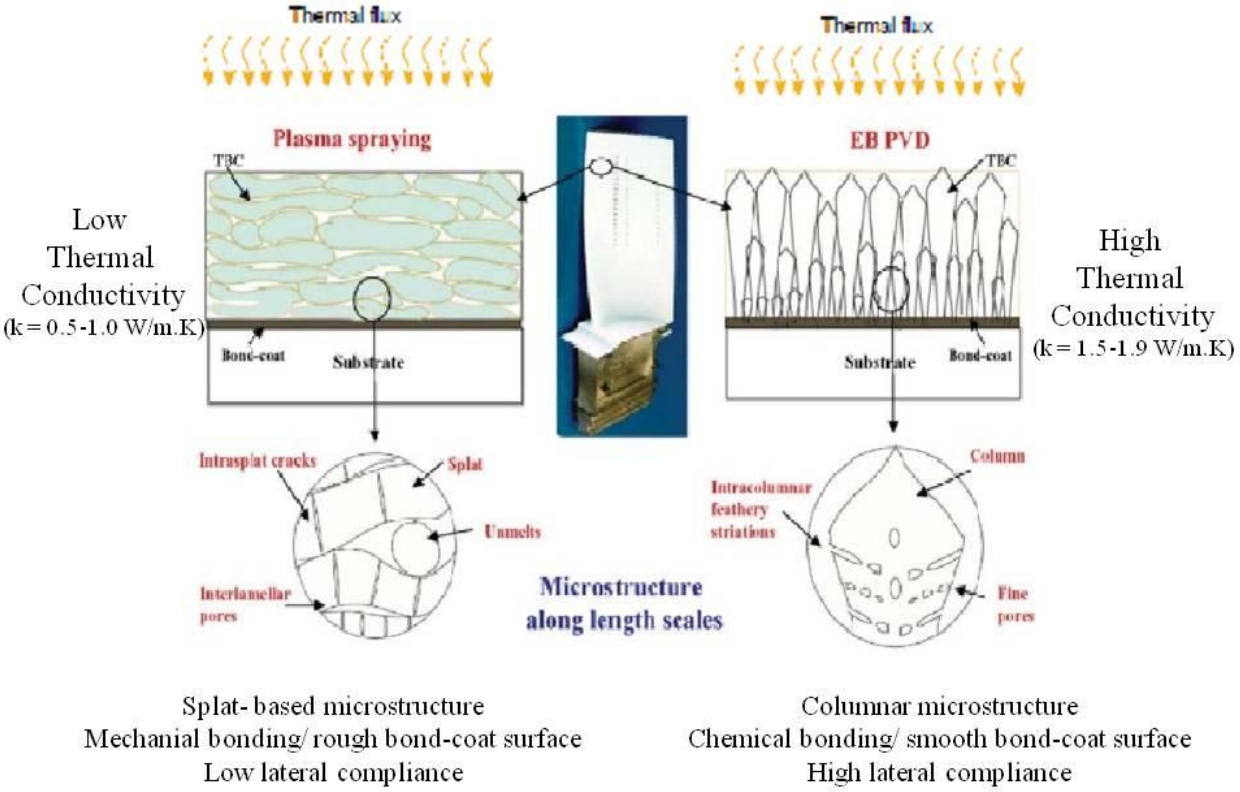

Fig. 2.11: Microstructures resulting from different deposition processes [23].

In case of EB-PVD top coats, the microstructure consists of columnar grains which are separated to each other by inter-columnar porosity. There is also porosity present within the EB-PVD columns as shown in Fig. 2.11. The porosity present in EB-PVD coatings helps in improving the strain tolerance or compliance of EB-PVD coatings which leads to an improved lifetime. However, as inter-columnar pores are parallel to the thermal flux, such porosity doesn't reduce the thermal conductivity as much as the pores perpendicular to the thermal flux do in case of PS coatings [5, 23, 54, 64, 66-69]. It has been mentioned that the thermal conductivity of ceramic top coat decreases as the pore volume fraction increases in case of PS coatings. It is because the pores provide a high impedance to heat flow through the thickness of coatings [5, 23, 66, 68, 69].

Further, PS coatings are believed to have a lower erosion resistance than EB-PVD coatings [70, 71]. On the other hand, PS coatings are less expensive than the EB-PVD coatings. Choice of PS or EB-PVD coatings is made after considering all the above mentioned characteristics.

2.7 Microstructure of EB-PVD Coatings

The early grains formed in EB-PVD process under both, conventional rotation and stationary, modes are of equiaxed type with no preferred crystal orientation [72-74]. This is assumed to be due to the low temperature of the substrate at the beginning of the EB-PVD process, thermal stresses at this state and interaction with the TGO. For conventionally rotated samples, the rotating movement dictates the crystallographic texture and morphology of the columns [75]. The microstructure consists of numerous single-crystal columns of fine diameter which start to grow on the equiaxed grains formed earlier. The growth of columns takes place continuously in a preferred growth direction enlarging their diameter and consequently reducing the number of columns due to a competitive growing process. Screening out of columns with unfavorable orientation allows a gradual broadening of favorable oriented ones. Due to the rotation of substrate, a "sunrise-sunset" line of sight shadowing effect takes place from the neighboring column which influences the favored growth of columns and impedes the vapor flux to reach the bottom of the valleys between the column tips. As a result nano-sized secondary columns and voids in between feather arms are formed throughout the column periphery. These voids between feather-arms can be designated as opened intra-columnar pores created at the columns periphery due to lower vapor flux

The effect of substrate temperature on the microstructure of EB-PVD coatings has been explained by a physical model from Movchan and Demchisin [76]. According to this model, three microstructural zones are emerged by the increase in the substrate temperature which are designated as Zone 1, Zone 2 and Zone 3. These zones are separated by two transition temperatures which are mentioned as T1 and T2 (Fig. 2.10). These temperatures have been experimentally determined to be $T_1 \sim 0.3\ T_m$ and $T_2 \sim 0.5\ T_m$ for metals while $T_1 \sim 0.26\ T_m$ and $T_2 \sim 0.45\ T_m$ for oxides [74]. In the Zone 1 region, there is low surface diffusivity of the deposited adatoms and the resulting grains are cone shaped with rounded tips containing a highly porous cross-section. In the Zone 2 region, surface diffusion activity defines the appearance of parallel columnar grains with faceted tips with low porosity volumes. The thickness of these columnar grains increases by increasing the temperature. In the Zone 3 region, additional activation of volume diffusion results in re-crystallized equiaxed grains with a flat top surface.

Zone 2 region from the Movchan and Demchisin's model has been further explained by the deterministic model for polycrystalline growth by Van Der Drift [77]. In this model, it is described that the growth of EB-PVD coatings under stationary conditions is controlled by surface diffusion influencing the nucleation and growth of columnar crystals. Such conditions are

controlled by several factors like the combined effect of vapor deposition direction, surface diffusion and crystallographic condensation coefficients.

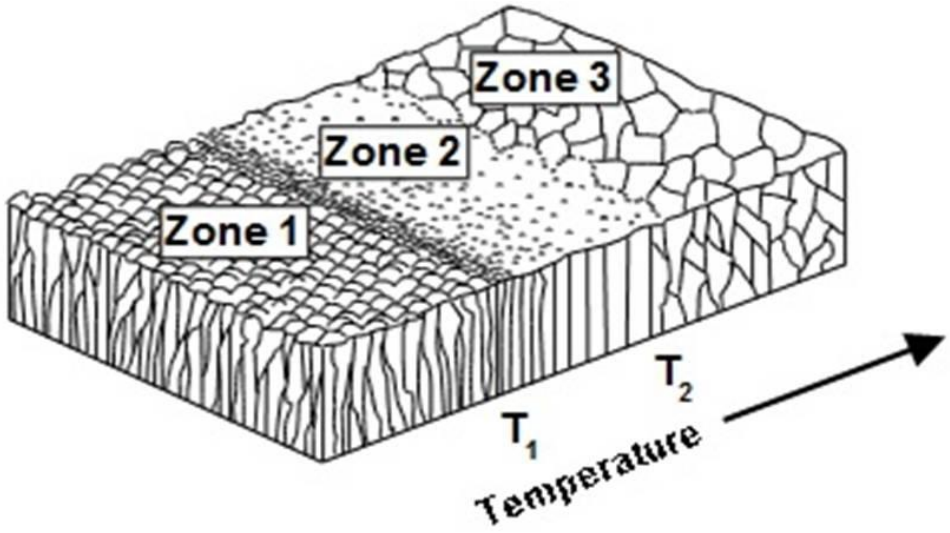

Fig. 2.12: Movchan model for the effect of substrate temperature on the microstructure of EB-PVD columns [76].

2.8 New Materials for ceramic top coat:

7YSZ on prolonged exposure at high temperature decomposes into high yttria and low yttria phases. The low yttria phase on cooling transforms into monoclinic phase with a large volume increase associated with this phase change. This phase change eventually proves to be catastrophic and results in TBC spallation. Hence the upper temperature limit for the use of 7YSZ as ceramic top coat has been set to 1200°C [56, 78, 79]. In addition, sintering also reduces the high temperature capability of 7YSZ as it leads to a loss of strain tolerance and results in early failure [80]. Therefore, alternate materials with higher temperature capabilities sought with main focus on a lower thermal conductivity and higher thermal stability.

2.8.1 Zirconia based Compositions

Apart from 7wt% yttria stabilized zirconia, many other forms of zirconia have been tested because of their better properties. One approach has been to increase the amount of yttria in zirconia which results in fully stabilized cubic zirconia. In this way, the problem of phase

transformation can be eliminated. In addition, thermal conductivity 20-30% lower than that of 7YSZ has been observed. However, fully stabilized zirconia based TBCs showed lower lifetime results in both burner rig and cyclic furnace test and more importantly, their erosion resistance has been very poor [81-84].

Another approach has been made by stabilizing zirconia with Ceria. Ceria- stabilized zirconia (CeSZ) provides good corrosion resistance and superior phase stability at high temperature. In addition, the thermal conductivity has been found to be lower than that of 7YSZ and better lifetime and thermocyclic resistance have been reported [84-88]. However, the vapor pressures of ceria and zirconia differ considerably and problems with process control have been experienced in EB-PVD deposition. Nevertheless, improvements have been achieved by dual-source evaporation, enhanced pool control, beam pattern and crucible design.

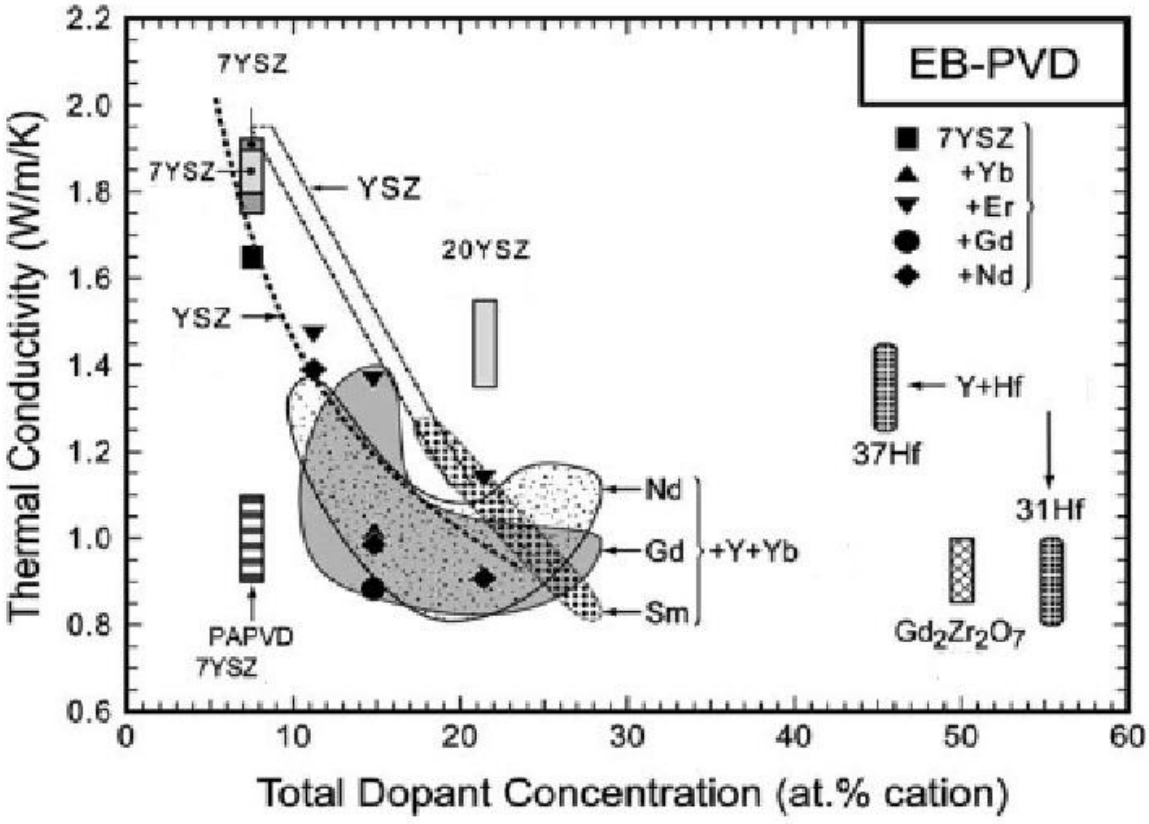

Fig. 2.13: Thermal conductivity values for different zirconia-based materials [89].

Other rare-earth oxide stabilizers like dysprosia and ytterbia behave similar to yttria. It has been observed that an optimized version with 12 mol% DySZ reduces thermal conductivity up to 40% compared to 7YSZ [90, 91]. For Scandia and Scandia-yttria stabilized zirconia, higher phase stability, excellent resistance to hot corrosion, longer oxidation resistance and easy

manufacturing has been demonstrated [54, 92, 93]. For zirconia with 19 mol% SmO, a 30% reduction in thermal conductivity and with gadolinia- zirconia compositions (that do not form the pyrochlore structure but instead a cubic) a 50% reduction in thermal conductivity has been achieved [54]. Many more zirconia based compositions have been covered by patents; however, real data on EB-PVD processed coatings or properties has not been given.

2.8.2 Pyrochlores

For applications above 1200°C, ceramic materials with pyrochlore structure $A_2B_2O_7$ have been found to be very attractive compared to 7YSZ. Several zirconate pyrochlores have lower thermal conductivity [89, 94, 95] which means they can reduce the temperature at the bulk metal considerably, provided internal cooling is there. Also, their thermal stability is excellent which can be due to the fixed positions of cations in the crystal. Gadolinia- Zirconia phase diagram is shown in Fig. 2.14 where it can be seen that pyrochlore compound gadolinium zirconate (GdZ) has temperature stability up to 1500°C.Improved sinter resistance has been found for EB-PVD pyrochlore TBCs, especially for $Gd_2Zr_2O_7$ [96] and $Sm_2Zr_2O_7$ [54, 97-103]. Recently, GdZ has shown excellent resistance against CMAS and volcanic ash attack [104-106]. Among the widely investigated pyrochlores are the rare-earth zirconates ($Ln_2Zr_2O_7$), where Ln is any or combination of La, Gd, Sm, Nd, Eu and Yb [54, 97, 99-103].

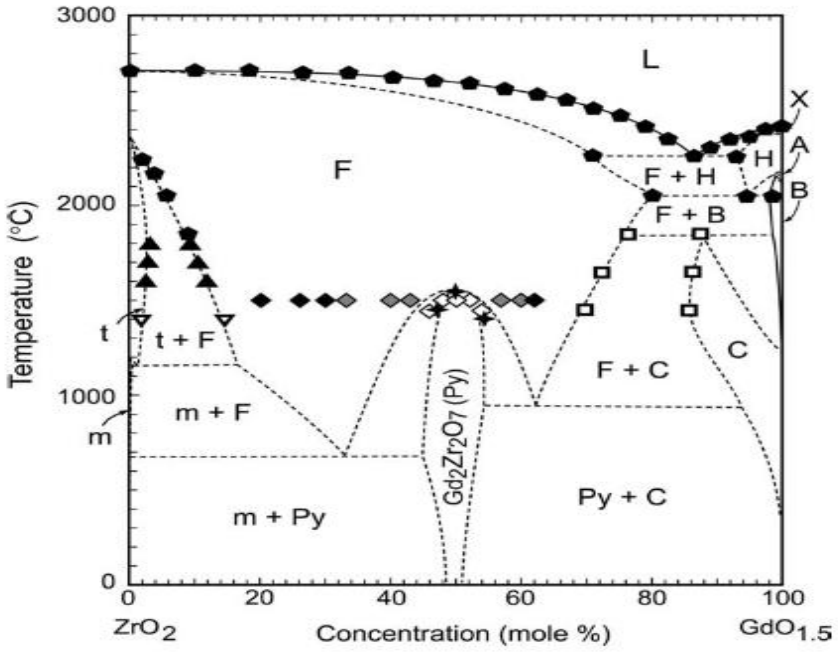

Fig. 2.14: Suggested $GdO_{1.5}ZrO_2$ binary phase diagram constructed from a summary of the literature data [107].

Among the pyrochlores, $La_2Zr_2O_7$ (LnZ) seems to have the most promising bulk properties suitable for ceramic top coat applications. It has a high thermal stability up to 2000°C, a low thermal conductivity of 1.56W/m K and a low sintering tendency [102]. However, it has a relatively low thermal expansion coefficient (CTE) of about 9 x 10^{-6} K^{-1} compared to 7YSZ which has a CTE of 10-11 x 10^{-6} K^{-1}. This can lead to higher thermal stresses due to the thermal expansion mismatch. In this regard, $Gd_2Zr_2O_7$ with a relatively higher CTE value of 10.5 x 10^{-6} K^{-1} seems to be advantageous [102].

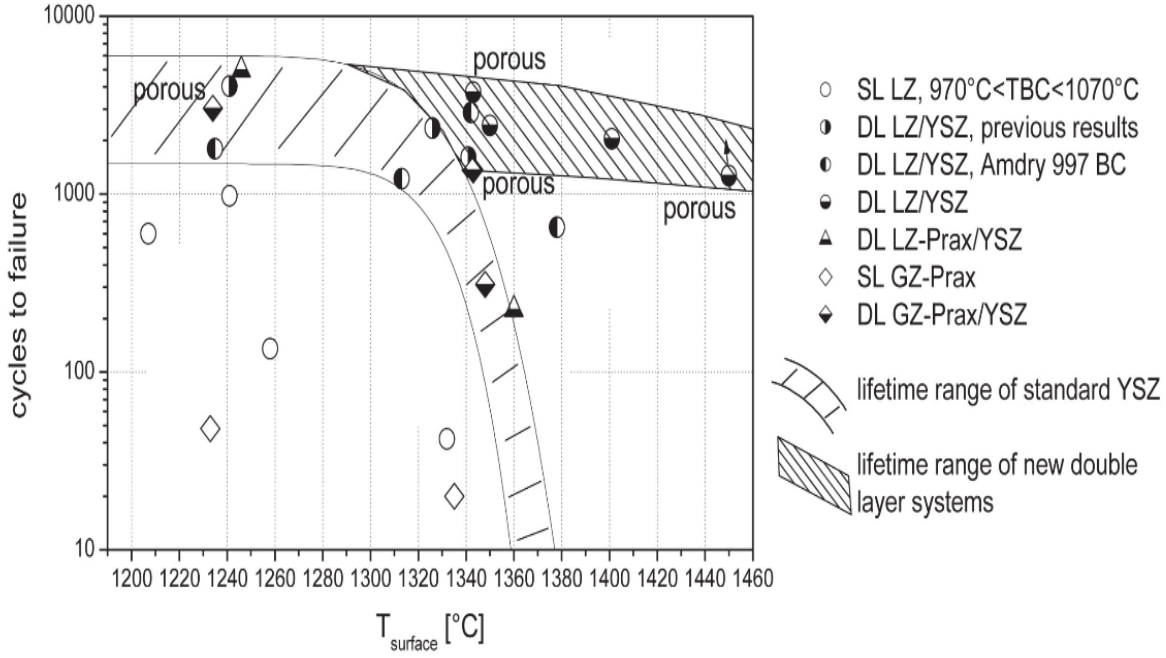

Fig. 2.15: Cyclic lifetime of Ln-zirconate and Gd- zirconate based single and double layer plasma sprayed TBC systems [101].

Superalloy substrate and bond coats have relatively higher thermal-expansion coefficients (about 15 x 10^{-6} K^{-1}) and therefore cracks can easily grow due to the stresses which build up in the TBC close to the bond coat during operation [52, 101, 102]. This could be a possible reason for the lower life time of $La_2Zr_2O_7$ and $Gd_2Zr_2O_7$ based plasma sprayed TBC systems shown in Fig. 2.15. Incompatibility between pyrochlore and TGO has also been reported which results in the formation of perovskite phase causing a reduction in the TBC lifetime [108]. To overcome these problems, a thin layer of 7YSZ is deposited between the bond coat and pyrochlore compositions. This is called double layer structure and has shown a significantly improved lifetime for many pyrochlore TBC systems as shown in Fig. 2.15. In such a structure, 7YSZ provides a better toughness than pyrochlores close to the bond coat and better adhesion with TGO while the pyrochlore material applied on the top provides low sintering and high thermal stability [102]. These systems based on pyrochlore/YSZ double-layers show excellent high-temperature

capability significantly better than the one of YSZ and they are expected to improve the thermal capabilities of gas turbines during application [101].

Some of the pyrochlore compositions are difficult to deposit, especially by EB-PVD technique and some fluctuations in composition have been encountered. For $La_2Zr_2O_7$, it has been observed that doping with yttria, in the range of 3-10 wt% reduces the compositional scatter during evaporation [109, 110]. In case of plasma-spraying for $La_2Zr_2O_7$, loss of La_2O_3 has already been stated [111] which leads to an impurity phase of non-stabilized ZrO_2 which might be detrimental for the coating performance.

2.8.3 Perovskites

Perovskite with ABO_3 crystal structure have a high temperature stability making them an attractive candidate for ceramic top coat applications. $BaZrO_3$ and $SrZrO_3$ have been the early candidate materials for TBC applications. $BaZrO_3$ has a high melting temperature, however, its relatively poor thermal and chemical stability led to early failure of coatings during thermal cycling tests at 1200°C surface temperature [112]. $SrZrO_3$, on the other hand, has shown better performance in thermal cycling test at temperatures higher than 1250°C as both lone ceramic top coat and as a double-layer for 7YSZ in a TBC system [113]. However, $SrZrO_3$, at intermediate temperature of about 730°C undergoes an undesirable phase transformation from orthorhombic to pseudo-tetragonal. It has been observed that such transformation can be suppressed by doping with Gd or Yb, which also improves the thermophysical properties of the coatings at elevated temperatures [114]. $CaZrO_3$ has been the latest material to be considered for TBC applications in this group. The melting point of this material has been found to be lower than that of 7YSZ, however, it has a promising thermal conductivity of ~ 2 W/m K [115].

Some complex perovskites like Ba $(Mg_{1/3}Ta_{2/3})O_3$ (BMT) and $La(Al_{1/4}Mg_{1/2}T_{1/4})O_3$ (LAMT) have also been tested for ceramic top coat application because of their suitable properties [102, 116, 117]. Despite the promising bulk properties, their toughness is still inferior compared to 7YSZ. In addition, some non-stoichiometric phases form during atmospheric plasma spraying due to the differences in vapour pressure of the component oxides [102, 118, 119]. However, recent study suggested that this problem could be minimized by proper optimization of plasma spray parameters to obtain shorter residence time of the particles in the hot plasma plume [120].

2.9 Sintering of ceramic top coat

Sintering can be defined as a thermal treatment which results in bonding of particles into a coherent, predominantly solid structure via mass transport events which often occur at atomic scale. The process of sintering leads to improved strength and lower system energy [121]. Sintering is driven by reduction in free surface energy and interfacial energy acting over curved surfaces. Two adjacent particles with free surfaces have a higher energy and by undergoing

sintering these particles eliminate the free surface energy [122]. Sintering also results in a reduction of surface curvature of particles as surfaces with curvatures have high surface area per unit volume. In case of polycrystalline materials, sintering causes a reduction in grain boundary energy by causing a reduction in grain boundary area [123, 124].

Solid state sintering first involves formation of a sinter bond or neck at the points of contact for particles approaching each other. In the 1st stage of sintering, the number and size of necks between individual particles is quite small [125, 126]. In the 2nd or intermediate stage sintering involves shrinkage, densification, pore rounding and grain growth [127]. In the end the pore structure collapses and spheroidization of pores takes place to complete the sintering process. Sintering is a result of atomic level mass transport which can be the result of surface diffusion, grain boundary diffusion or lattice or volume diffusion [124, 127]. Surface diffusion is thermally activated phenomenon requiring a comparatively lesser activation energy than other mass transport mechanisms and usually involves the motion of atoms from and to surface defect sites. Grain boundary diffusion which takes place at relatively higher temperatures is a bulk transport process and plays an important role in the densification of most material systems. Grain boundary diffusion involves intermediate activation energy between surface diffusion and volume diffusion. However, grain boundary energy could be reduced by impurities or additives that segregate at grain boundaries [128, 129]. In case of volume diffusion, there is motion of atoms from the inter-particle grain boundary through the crystalline structure, to the neck surface, or a reverse vacancy flow, with subsequent shrinkage and densification. The volume diffusion rate depends on temperature, composition and curvature [124].

In case of sintering kinetics in stabilized zirconia, mechanisms are still not clear. It has been stated that the early stage sintering kinetics are dominated by grain boundary and surface diffusion [130, 131] while there are other studies which support that volume diffusion is the dominant mechanism [132, 133]. The rate of volume diffusion is controlled by the cations in zirconia while mechanism of cations diffusion in stabilized zirconia is also not clear [134-137]. The sintering rate of zirconia strongly depends on impurity content like MgO, Fe_2O_3, Al_2O_3, SiO_2 and CuO [138-142]. It can be assumed that the sintering of EB-PVD 7YSZ is comparable to the first stage sintering already explained [59]. The magnitude of the sintering force (Laplace stresses) depends on the number of necks along the length of each sintering body, the interface 7YSZ- pore surface tension and the ratios of the necks [59]. As reduction in the surface energy is the driving force for sintering and induces changes in the surface area of pores, the morphology of pores changes until the lowest surface area is obtained for a corresponding volume resulting in an equilibrium shape [143, 144].

2.10 Failure Mechanisms of TBC systems

Thermal barrier coatings are complex multi-material systems where interplay between several physical phenomena like diffusion, oxidation, phase transformation, elastic and plastic

deformation, thermal expansion, fracture and sintering takes place during their working conditions [5]. Despite the severe conditions in which TBCs are applied, they are expected to last thousands of take-offs and landings in commercial jet engines and up to 30,000 hours of operation in industrial gas-turbine engines [5]. However, due to the combined effect of all the above mentioned phenomena in different layers of a TBC system, premature spallation takes place frequently and is an area of concern for TBC manufacturers. Various mechanisms which affect the lifetime of TBC systems are as follow:

2.10.1 TGO Growth and Residual Stresses:

TGO growth during the working of TBC operation is the most important phenomenon responsible for TBC failure. Residual stresses in the TGO have been documented through piezospectroscopic measurements where the thermal expansion mismatch is the dominant factor [145, 146]. Compressive stresses in the range of 3- 4 GPa, depending upon the coefficient of thermal expansion of substrate have been reported in the literature [147, 148]. These stresses would have been spatially uniform, had the TGO a uniform thickness. However, non-planarities cause the misfit stresses to redistribute which results in normal and shear stresses at various sites along the interface [149, 150]. The growth stresses are compressive and are usually small. It is because the misfit induced by growth is relaxed by rapid creep in the TGO. They are in the range of 0- 1GPa and can be estimated by subtracting the misfit stress from the total stress measured at ambient [145].

2.10.2 Buckling

TGO films usually fail by small scale buckle- driven delamination which first involves formations of separations at imperfections and then buckling; which finally results in the spallation of TBC [145]. Failure is driven by strain energy density in the TGO and is resisted by the fracture toughness of the interface [145]. Due to the differences in coefficients of thermal expansion of different layers of a TBC system, compressive stresses build up in the TGO layer during cooling. These stresses lead to delamination at the TGO- bond coat interface [151, 152]. However, even with an area of decohesion present between the oxide and substrate, buckling may not occur as the size of decohesion must ensure sufficient stress within the coating. This critical stress is given in the equation 2.1 which clearly shows that the decohesion size and oxide thickness are important factors in buckle propagation, assuming the deformation to be only plastic [151, 153, 154].

$$\sigma_c = \frac{1.22E_{ox}}{(1-\nu_{ox}^2)}\left(\frac{\xi}{R^*}\right) \qquad 2.1$$

σ_c = Critical buckle propagation stress

E_{ox} = Young's modulus of the oxide (367GPa for α-alumina)

υ_{ox} = Poison's ration of the oxide (~ 0.3)

ξ = Oxide thickness

R* = Radius of the area of decohesion

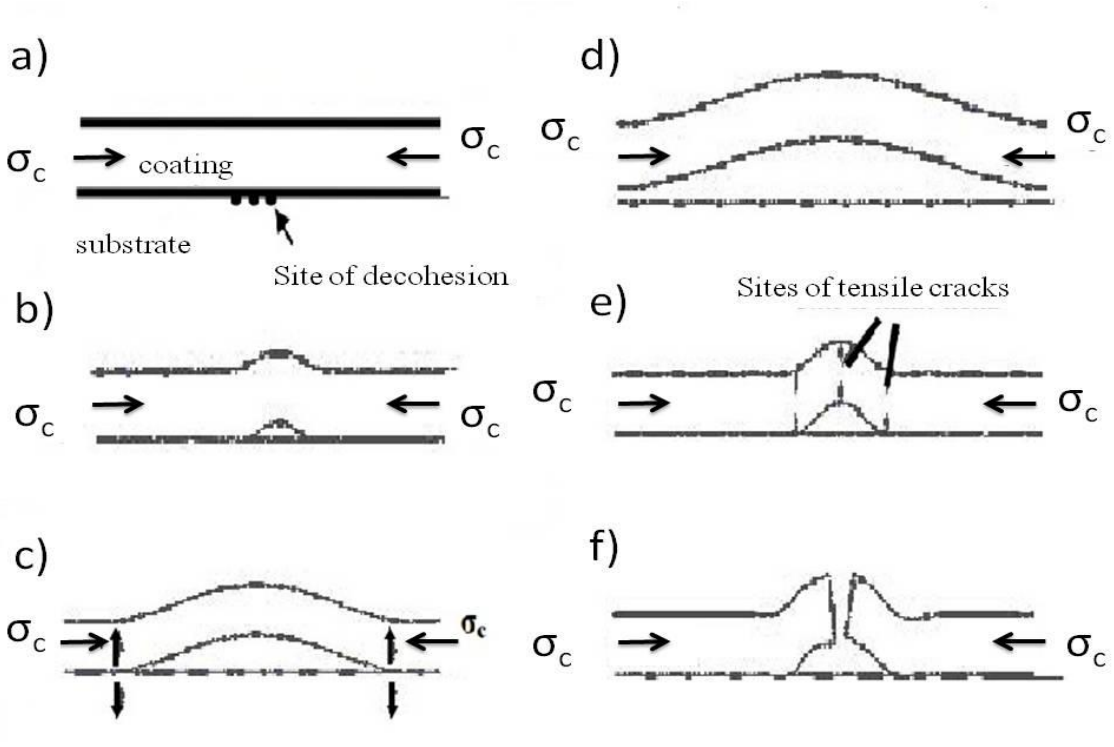

Fig. 2.16: Schematic diagram showing the buckling failure mechanism [151, 153].

As it can be deduced from Eq- 2.1, the critical buckle stress is directly proportional to the TGO thickness. A typical example of buckling is shown in Fig. 2.16. It is now widely accepted that buckling is the failure mechanism for most of the TBCs [153, 155, 156].

2.10.3 Rumpling and Ratcheting:

Under thermal cyclic conditions, instabilities in the morphology of bond coat surfaces in the absence of ceramic top coat have been recognised for some time [157-159]. It has been suggested that these changes are due to the strains associated with phase transformations within the bond coat [157]. However, a recent study showed that surface instabilities can arise even in the absence of phase transformation [160]. The two terms rumpling and ratcheting are sometimes considered to be synonymous but it is important to distinguish between them as the surface displacements involved differ significantly [159]. Rumpling is associated with a displacement of

the bond coat both above and below the original position of the bond coat surface whereas in case of ratcheting, the displacement is only downwards i.e. into the bond coat [159]. It has been shown that rumpling takes place only in thermal cycled specimens and identical specimens which are isothermally tested do not exhibit rumpling [156, 158]. Rumpling could be a result of several factors including thermal coefficient of expansion mismatch between the bond coat, TGO and top coat resulting in the contraction of TGO which is accommodated by creep of the bond coat [161]. Till now, there has been no evidence of this mechanism taking place in typically used coatings and this can be due to the mechanical constraint imposed by outer ceramic layer.

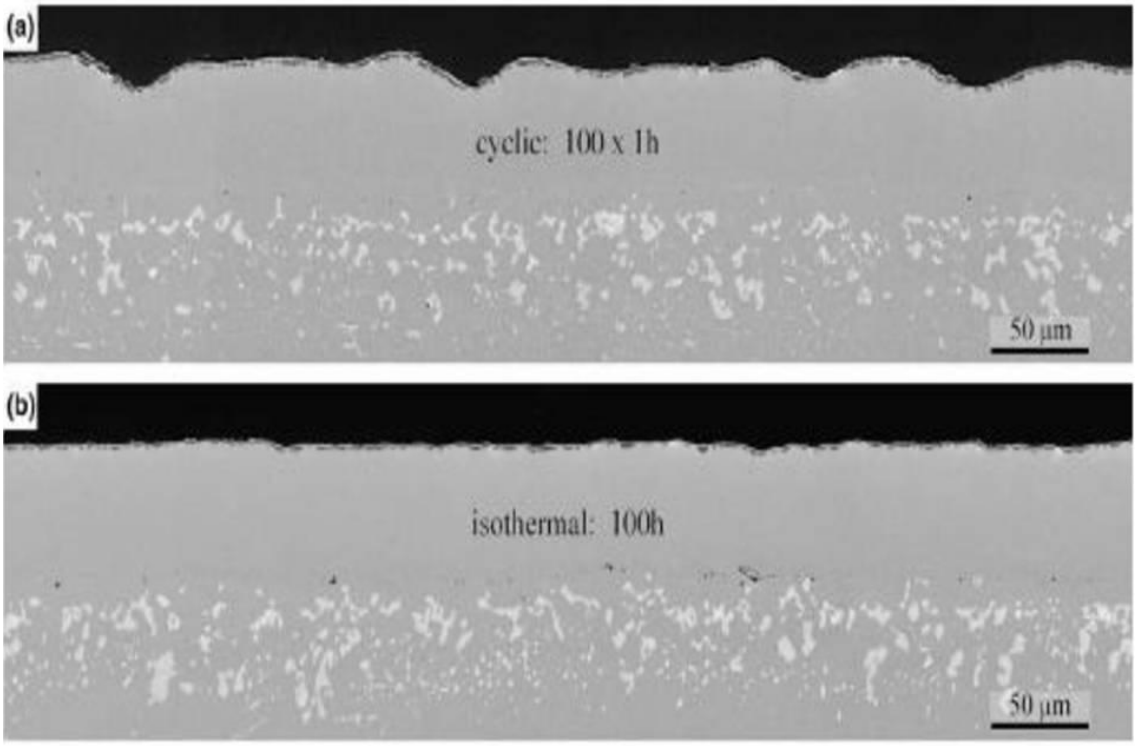

Fig. 2.17: A comparison of two identical diffusion bond coats without bond coat, a) after 100 x 1 h thermal cycles at 1150°C and b) after 100 h isothermal heating at 1150°C [153, 161].

In contrast to rumpling, ratcheting does take place in full TBC systems as well under thermal cycling conditions. Considerable stresses are developed in the TGO upon cooling due to the thermal expansion mismatch with the underlying bond coat. These compressive stresses within the TGO can be relaxed by its inward movement into the bond coat. The extent of inward movement increases with the number of thermal cycles as does the length of the lateral crack in the vicinity of the TGO/ top coat interface [159, 162].

2.10.4 Mud Cracking

As already mentioned, sintering of ceramic top coat takes place at high temperatures. Sintering in the initial stages causes coarsening of pores, rounding off of sharp microstructural features. Afterwards, sintering at the contact points of columns takes place and causes the isolated columns to have the macroscopic response of a layer with finite in-plane stiffness and strength. As a result the strain compliance of columns drops. This intercolumnar sintering can cause mud-cracking upon cooling due to the buildup of tensile stresses within the ceramic top coat layer. It has been calculated by Hutschinson et al. [163] that mud cracking is encouraged by low value of toughness between columns, and by high in-plane and thick TBC layer. The mud-cracking has been found to relieve the stresses in the ceramic top coat, however, it promotes subsequent sintering. As a result of mud-cracking clusters within ceramic top coat are formed and as the columns within each cluster continue to sinter, the opening of each mud-crack increases and this affects the overall integrity of TBC system. The openings between clusters may allow chemical ingress to the TGO and bond coat and may lead to spallation at the base of TBC layer.

2.10.5 Chemical Failure

The composition of bond coat is selected so that alumina is formed as a protective oxide layer between ceramic top coat and the bond coat. However after prolonged exposure to high temperatures, Co- and Ni- rich oxides are also known to develop [164, 165]. Especially in overlay coatings, these oxides can be seen initially at the apex of bond coat protuberances [159, 164]. This change in oxide type is said to be a form of "chemical failure". This failure takes place because the selective oxidation of aluminum to form alumina through much of the coating life depletes the underlying coating of that element. According to literature, a minimum of 2.5 wt% of Aluminum must be there in the bond coat adjacent to the TGO to re-heal alumina layer, once the layer be cracked [159]. The formation of localized fast growing oxides leads to an increased out of plane stresses within the TBC system and large variations in upward displacement rates along the TGO- bond coat interface. Rapid oxidation of other bond coat constituents after the Aluminum is depleted is also termed as mechanically induced chemical failure (MICF) [166]. The situation can be particularly severe at bond coat protuberances since here the Al- diffusion is enhanced due to larger surface- to volume ratio and these regions are expected to experience MICF first. A typical reaction for spinel formation is given below:

$$Na + 2Cr + 2O_2 \rightarrow NiCr_2O_4 \qquad A$$

This reaction is appropriate for MCrAlY coating but the volume expansion for the formation of spinel in reaction A is 105% as calculated from molar volumes [167] and so imposes a marked increase in out-of-plane displacements compared with alumina formation. It is yet to be proven if this mechanism leads to the spallation of EB-PVD coatings, however, it has been shown in overlay coatings as a consequence of the formation of diffusion cells [159].

3- Experimental Procedure

3.1 Different Materials for TBC systems

The whole experimental research for this PhD study has been carried out at the German Aerospace Center (DLR) in Cologne, Germany. Several materials have been tested which form the different constituents of a TBC system. For the superalloy substrate, results from IN100 are compared with those from CMSX-4 superalloy. IN100 is a conventional superalloy with equiaxed microstructure. CMSX-4 is a more advanced, single crystal superalloy with a relatively higher refractory content. The exact composition of both the superalloys is given in Table 3.1.

Table 3.1: Composition of different materials used in this study.

Layer	Material	Composition in wt %
Substrate	IN 100	14 Co, 9 Cr, 5 Al, 2.3 Mo, 5 Ti, 0.18 C, 0.015 B, 0.05 Zr, 1 V, balance Ni
Substrate	CMSX-4	9 Co, 6.5 Cr, 5.6 Al, 0.6 Mo, 6 W, 6.5 Ta, 3 Re, balance Ni
Bond Coat	NiCoCrAlY	47 Ni, 21 Co, 20 Cr, 11 Al, 0.19 Y
Bond Coat	NiCoCrAlY-2	49 Ni, 21 Co, 17 Cr, 12 Al, 0.42 Y
Bond coat	NiCoCrAlY-Hf	47 Ni, 21 Co, 20 Cr, 11 Al, 0.19 Y- 0.6 Hf
Ceramic top coat	7YSZ	7 Y_2O_3 in ZrO_2
Ceramic Top coat	GdZ	60 Gd_2O_3 + 40 Zirconia

The superalloy substrates are used in a cylindrical geometry with a diameter in the range of 6mm and the length of around 60mm. The specimens are thoroughly cleaned before the deposition of bond coats to remove any oxide, dirt or grease present on the surface of specimens. The bond coats tested in this study have been different versions of NiCoCrAlY overlay coatings. The deposition is carried out by Electron beam physical vapor deposition (EB-PVD) technique. To investigate the effect of bond coat composition on the lifetime of TBC system, NiCoCrAlY bond coats are doped with Y or Hf on different substrate materials. The compositions of different NiCoCrAlYs tested in this study are given in Table 3.1. To avoid confusion with the standard NiCoCrAlY bond coat, the NiCoCrAlY version with higher yttrium content is denoted by NiCoCrAlY-2 in this study. After the bond coat deposition, peening of the specimens is done

which is followed by vacuum annealing at 1080°C for 4h. The purpose of this annealing is to form a thin dense α- Al_2O_3 film (TGO) so that the ceramic top coat is deposited on this TGO and not directly on the bond coat. To investigate the effect of ceramic top coats on the lifetime of TBC systems, GdZ is deposited as single and double layers and the results are then compared with those of standard 7YSZ. The deposition parameters for both 7YSZ and GdZ are identical and will be discussed in the upcoming section. The compositions of GdZ and 7YSZ are given in Table 3.1.

3.2 Bond coat deposition

Deposition of NiCoCrAlY bond coats has been done by modified LEYBOLD ESC equipment with the maximum EB-power of 60kW shown in Fig. 3.1.

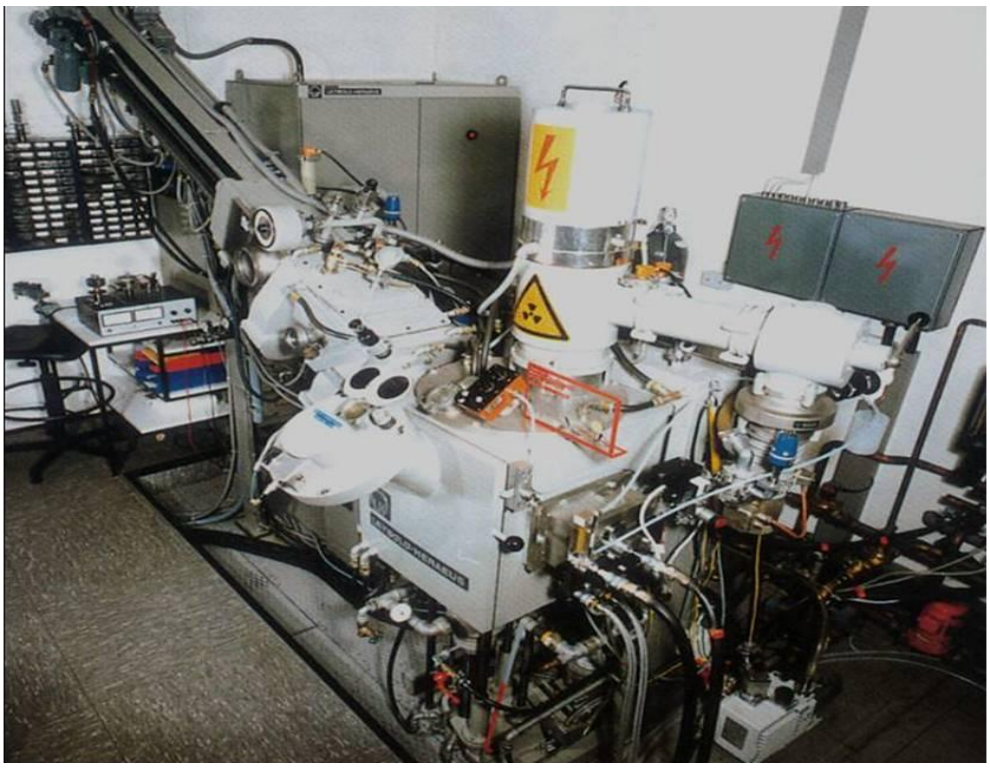

Fig. 3.1: 60 kW LEYBOLD ESC equipment for EV-PVD deposition.

This equipment consists of three chambers; to load, to pre-heat and to deposit. The substrates are polished and subsequently cleaned in an ultrasonic bath of alcohol In order to achieve a clean, impurity- free surface to be coated. After cleaning, the substrates are fixed in a rotating holder within the loading- chamber and deposition is done at a pressure of around 10^{-5} mbar. The evaporation source is a 50mm ingot with chemical composition to be deposited. The bond coat deposited in this way has a light columnar structure containing some irregularities (inter-columnar gaps), which need to be closed in order to achieve a compact surface required for a

homogenous deposition of ceramic cop coat. As a result, peening is done where the specimen is bombarded by ceramic particles. However internal stresses are developed due to the compacting process and these stresses are eliminated by the subsequent annealing process. Annealing is done at 1080°C for 4h which results in re-crystallization of the bond coat microstructure along with the formation of an oxide film on top of the bond coat. Subsequent deposition of ceramic top coat is done on this TGO layer rather than the bond coat to improve the lifetime of TBC systems. This equipment is capable of evaporation from a single source, hence for bond coats which required a more complicated evaporation, two-source evaporation equipment is used which will be discussed in the next section.

3.3 Ceramic top coat deposition

The deposition of ceramic top coat materials and the bond coats with Y or Hf- doping has been done by a "von Ardenne Anlagentechnik GmbH" 150kW EB-PVD plant which is shown in Fig. 3.2.

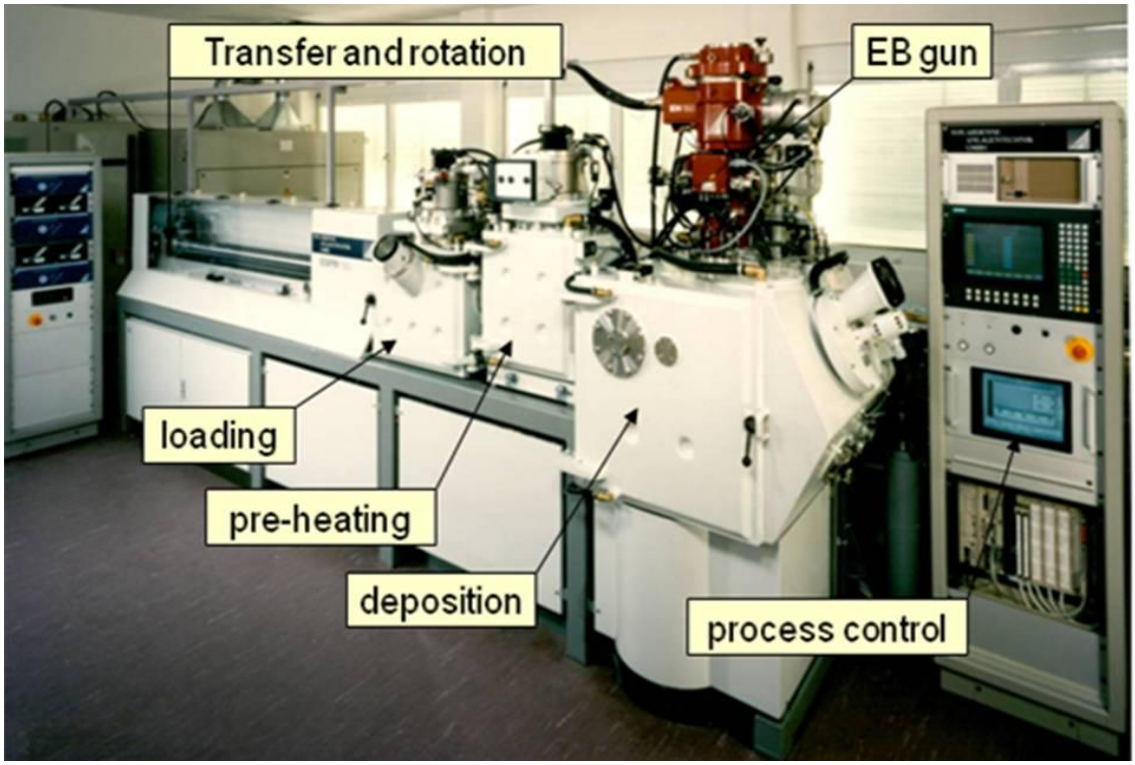

Fig.3.2: 150 kW EB-PVD plant with 2-beam evaporation source.

The sample to be deposited is fed into the 1st chamber. The samples are pre-heated in the 2nd chamber to a temperature of about 920-1000°C at a pressure in the range of 10^{-5} mbar. In the deposition chamber, the ingot is melted and evaporated with the help of an electron beam which is focused on to the ingot of around 62.5mm diameter. This equipment has the capability of

deposition from two ingot sources. In this study, the deposition of Hf- doped NiCoCrAlY and NiCoCrAlY-2 bond coats has also been done on this equipment. The vaporization of ingot surface is controlled by the physical properties of the vaporizing source and the different process parameters such as electron-beam scanning pattern, focus, electron gun power etc., hence a refined know-how of the established coating conditions during the EB-PVD process is very important. During the deposition, the specimens are rotated about their axis and the speed of rotation plays an important role in the determination of the resulting microstructure. In this study, the deposition of both 7YSZ and GdZ has been done at 12rpm.

3.4 Furnace cyclic Testing

Furnace cyclic testing (FCT) of the TBC samples has been done by holding them in a pre-heated furnace at 1100°C for 50min and then cooling them to room temperature by forced air cooling for 10mins. In this study, there has been no thermal gradient across the thickness of the samples. The FCT setup is shown in Fig. 3.3.

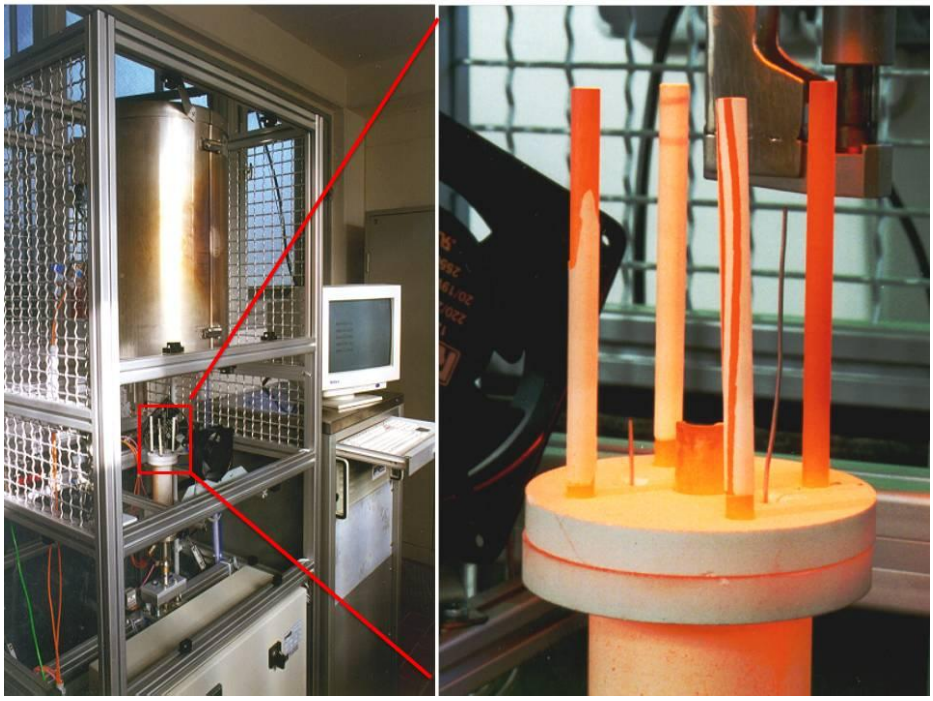

Fig.3.3: Furnace cyclic testing set up.

The temperature at the sample stage is measured with the help of two thermo-couples of different lengths which can be seen in Fig. 3.3. The failure of TBC systems has been defined as coating spallation of an area with one of the dimensions greater than 5mm. There are two thermo-couples on the sample stage with different heights to keep an accurate control over the temperature in the furnace.

3.5 Metallographic Preparation

TBC specimens in the as-coated condition and after thermal cycling are prepared by standard metallographic techniques for the subsequent microscopic investigations of the sample cross-sections. Mechanical cutting is performed under water cooling conditions, so that the temperature doesn't increase too much during the cutting process. After cutting, the slices of TBC specimens are hot mounted at a temperature of 180°C. Grinding and polishing steps are also carried out on Struers CCTV machine where grinding is performed on SiC discs while polishing is done with OPS solution.

3.6 Scanning Electron Microscopy and Energy Dispersive X-ray spectroscopy

The microstructural analysis has been done on an analytical SEM (LEO Gemini 982) equipped with EDS (energy dispersive x-ray spectroscopy) system. As TBC is a multi-layer system, SEM micrographs are taken in such a way that the ceramic top coat is always shown on the top and substrate is at the bottom so that symmetry is maintained among the SEM micrographs. SEM microscopy has been done to obtain the thickness of different TBC layers esp. the TGO, to investigate any chemical reactions which take place during the thermal cycling and to observe any changes in the morphological features of the TBC systems. Excitation voltage of 3-5kV has been selected to take the SEM images by secondary electron (SE) sources so that the interaction volume is not very large and the image obtained is sharp enough at higher magnifications. For the non-conducting materials, a very thin layer (~nm) of Pt is deposited on top so that SEM micrographs are obtained without any difficulty. EDX, however, has been done at much higher exciting voltage of 15- 20kV mainly to excite the atoms from the individual elements.

3.7 X-ray Diffraction

X-ray diffraction (XRD) has been used to investigate the phase changes in TBC systems which take place as a result of thermal cycling. Most of the times the sample is ground to form a very fine powder in order to obtain information for all the phases present. For this purpose Siemens D5000 powder diffractometer with Ni filtered Cu-K_α radiation equipped with a secondary graphite mono-chromator and by using the EVA/ Topas software package of Bruker AXS has been employed. However, a few coatings have also been investigated to study the phase changes which take place during the furnace cyclic testing.

4- Results:

4.1 IN100 based TBC systems

In this section, the effect of different bond coats on the lifetime and microstructure with 7YSZ as the ceramic top coat are given.

4.1.1 IN100-NiCoCrAlY-7YSZ system

Fig. 4.1 shows the SEM micrograph of as-coated IN100- NiCoCrAlY- 7YSZ system. It can be seen that the microstructure consists of standard EB-PVD columns with a thin TGO layer with a thickness of around 1µm. This TGO layer starts to develop at the bond coat surface during the annealing step even before the deposition of ceramic top coat. Ceramic top coat in the as-coated condition consists of inter and intra- columnar porosity which not only reduces thermal conductivity but also improves the capability of the system to accommodate stresses. Column tips of as-coated 7YSZ have been highlighted in Fig. 4.1 where the different microstructural features of EB-PVD columns, like feather arms, inter- and intra- columnar porosity, can be seen.

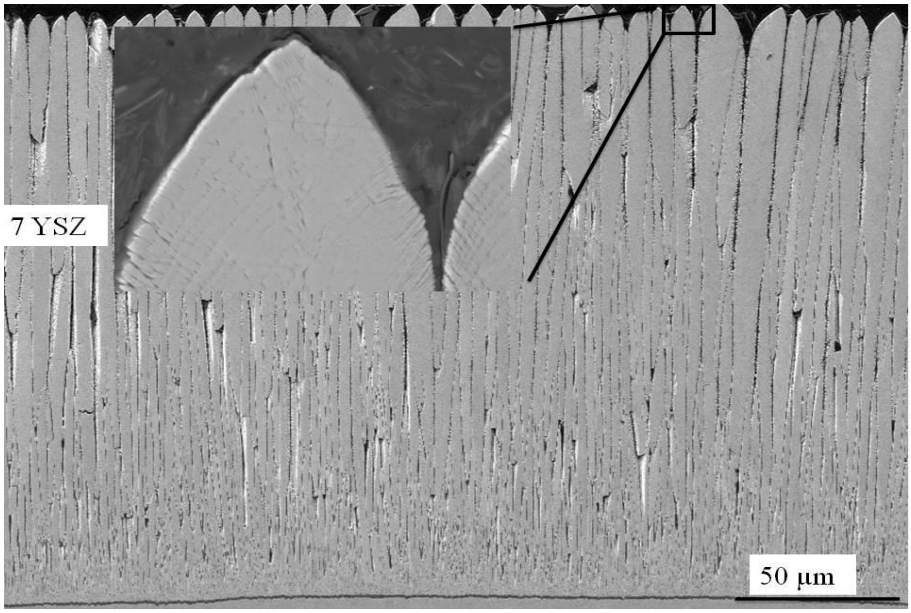

Fig 4.1: Morphology of as-coated EB-PVD columns of 7YSZ.

4.1.1.1 TGO Microstructure

The TGO in IN100- NiCoCrAlY- 7YSZ system and all other TBC systems investigated in this study consists mainly of alumina. It has been observed that yttrium is the most reactive element in the NiCoCrAlY system and is the first element to be oxidized. In the as- coated condition, yttria exists in the form of islands and the alumina layer looks to have been pushed downwards

locally by these islands (Fig. 4.2a). These yttria islands are present frequently at the TBC-TGO interface. Adjacent to the island is the common mixed zone containing zirconia particles embedded in alumina. The TGO microstructure after thermal cycling is shown in Fig. 4.2b. It can be seen that the as-coated TGO after thermal cycling forms the mixed zone with the further TGO growth taking place by inward diffusion of oxygen forming columnar alumina grains underneath the mixed zone. Yttria islands present in the as-coated condition remain unchanged after thermal cycling and can be seen after thermal cycling.

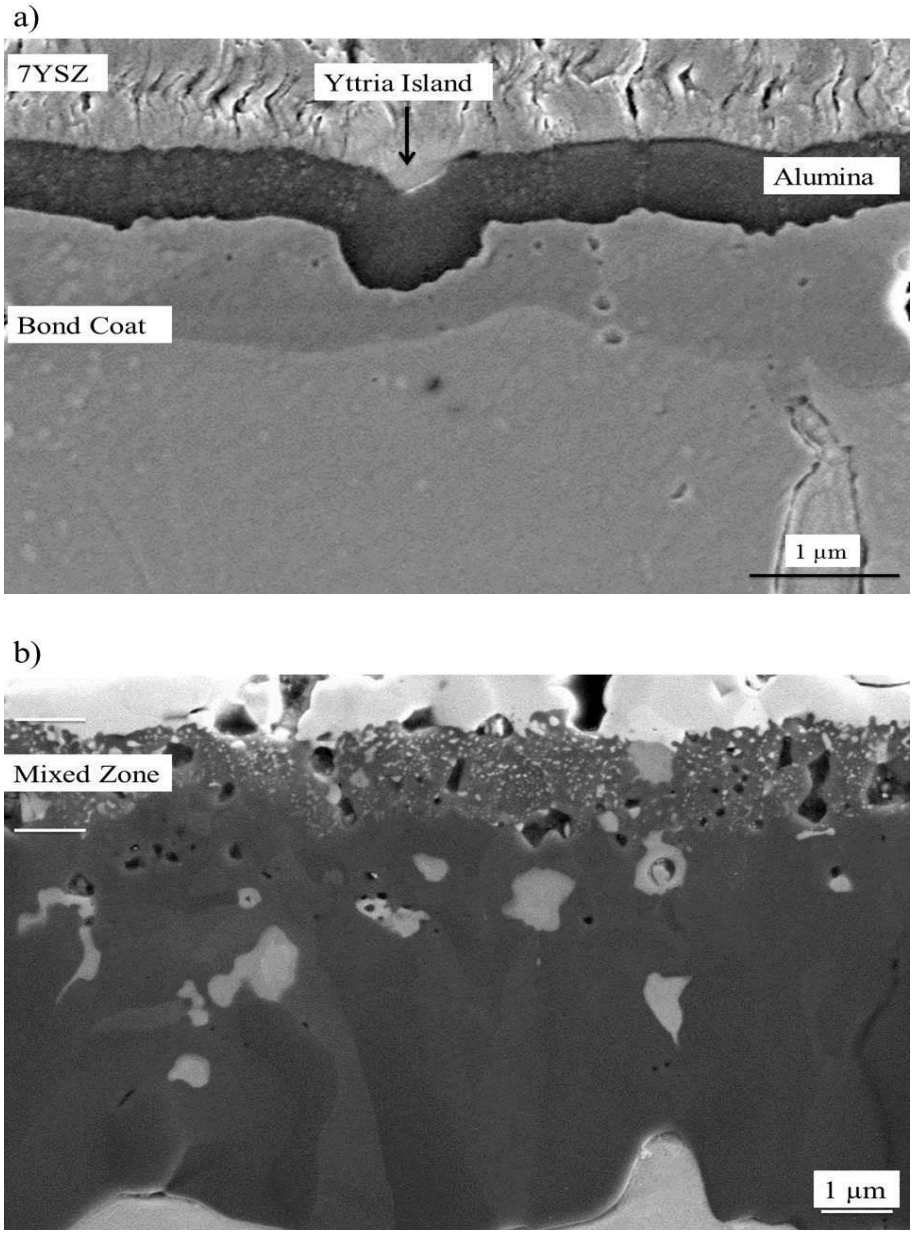

Fig 4.2: TGO microstructure of 7YSZ-NiCoCrAlY- IN100 system in a) as-coated condition [67] and b) after 2000 cycles.

4.1.2 IN100- NiCoCrAlY-2-7YSZ System

To investigate the effect of bond coat composition on the microstructure and lifetime of IN100 based TBC systems, NiCoCrAlY bond coat was doped with slightly higher yttrium content. The exact composition has been given in Table 3.1 (Experimental Procedure).

4.1.2.1 Lifetime results

It has been observed that IN100 based TBC systems with NiCoCrAlY-2 bond coat show a slightly lower lifetime than those with NiCoCrAlY bond coat with 7YSZ as the top coat material. In this study, the lifetime values for NiCoCrAlY- based systems have been taken from the DLR-database where more than 10 samples have been tested to obtain the average lifetime value. However, for NiCoCrAlY-2- based TBC systems, 4 samples were tested which showed lifetimes of 730, 1354, 197 and 767 and the average lifetime is shown in Fig. 4.3.

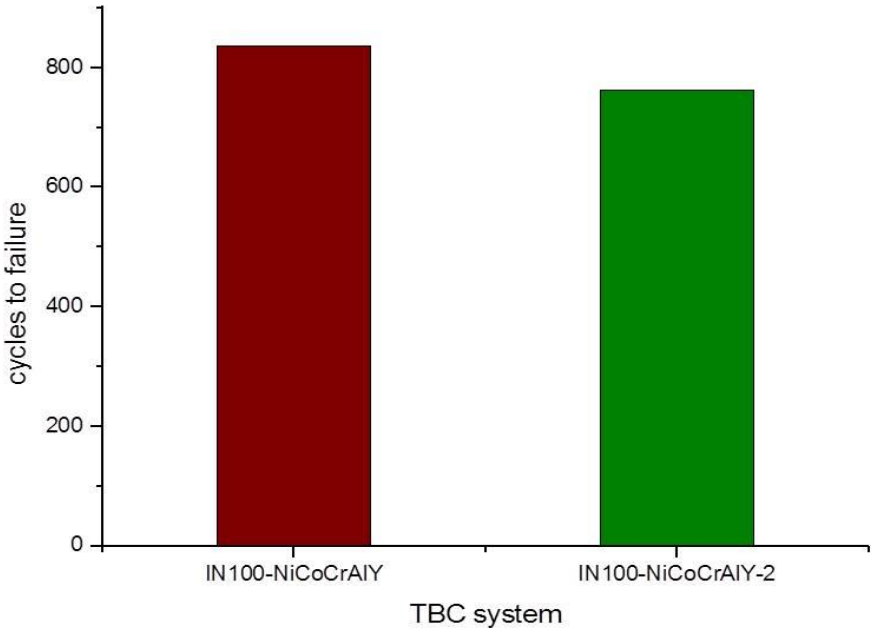

Fig. 4.3: Average lifetime values of NiCoCrAlY and NiCoCrAlY-2 based TBC systems with IN100 as the substrate and 7YSZ as the top coat material.

4.1.2.2- TGO Microstructure

It has been already mentioned that yttrium is the 1st element to oxidize in NiCoCrAlY system. In NiCoCrAlY-2 bond coats, where there is higher yttrium, yttria doesn't form in the form of islands but in the form of a flatter phase which is present almost continuously at TBC-TGO

interface (Fig. 4.4a). A similar yttria rich phase is present at the TBC- TGO interface after thermal cycling as well (Fig. 4.4b) which proves that yttria does not get dissolved in TGO during thermal cycling, however, it might react with alumina to form Y-Aluminates.

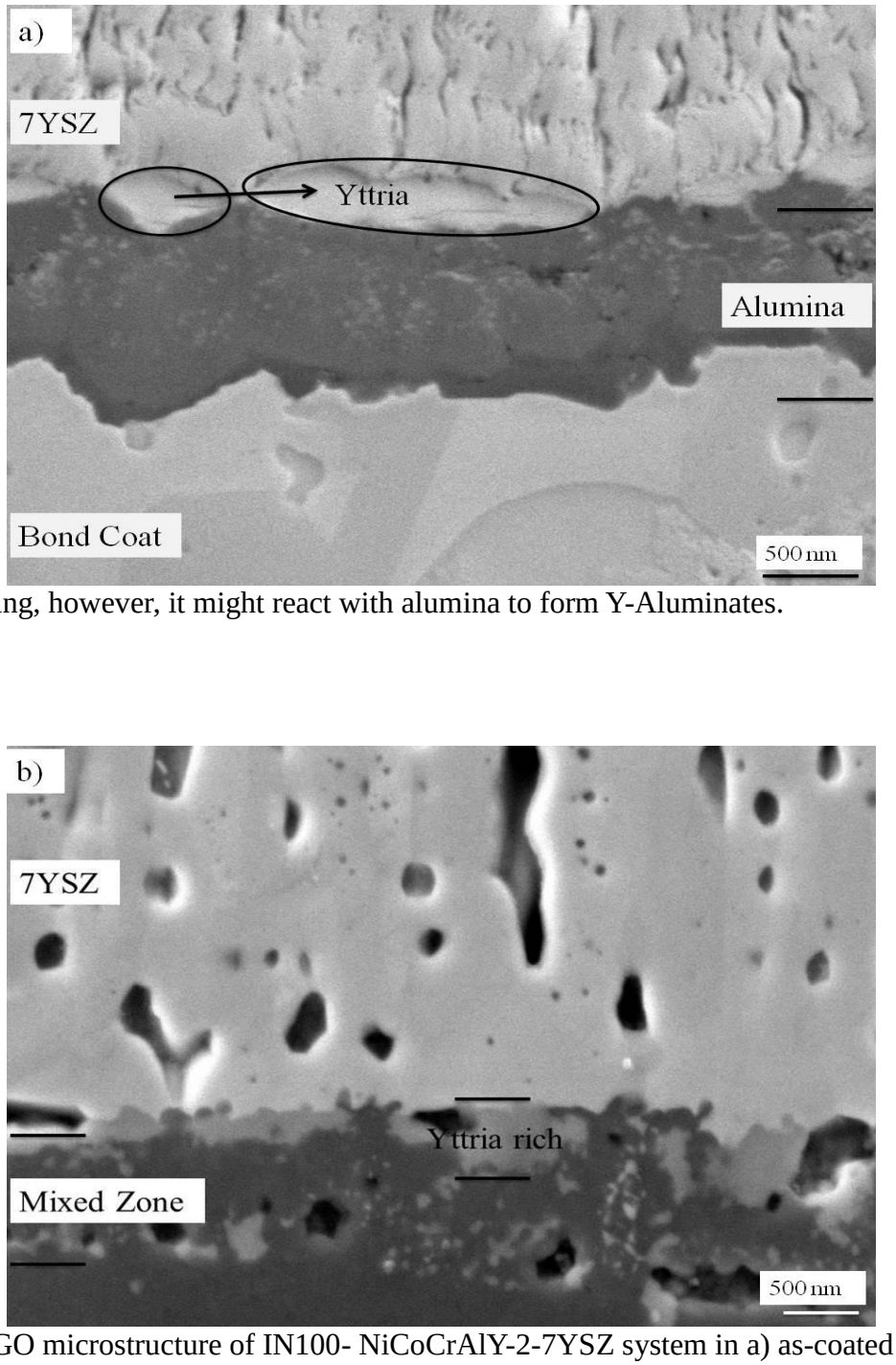

Fig. 4.4: TGO microstructure of IN100- NiCoCrAlY-2-7YSZ system in a) as-coated condition and b) after 1300 cycles.

4.2 CMSX-4 based TBC Systems

The effect of different bond coat compositions on the microstructure and lifetime of CMSX-4 based TBC systems with 7YSZ ceramic top coat material is given as below:

4.2.1 CMSX-4- NiCoCrAlY- 7YSZ System

Microstructure of CMSX-4- NiCoCrAlY- 7YSZ system in the as-coated condition is very similar to that of IN100 based system which has been explained earlier. The TGO thickness of CMSX-4 based system in the as-coated condition and its microstructure has been found to be very similar to that of IN100 based system. Similarly, 7YSZ columns for both the systems have the same microstructure as already been explained in 4.1.1. However, CMSX-4 contains a significant amount of refractory elements which can diffuse towards the TGO upon exposure to high temperature. This diffusion of elements in the CMSX-4 based TBC system has been explained in the upcoming section.

4.2.1.1 Diffusion of Elements

CMSX- 4 superalloy contains several refractory elements which are added to the superalloy to improve its high temperature properties. It has been observed that these refractory elements diffuse towards the TGO as a result of thermal cycling. This diffusion of refractory elements has been investigated by using EDX and is shown in Fig. 4.5. Fig. 4.5a shows roughly the location where EDX measurement is done. Point no. 1 on the line measurement is the one closest to the TGO while the point no. 5 is the one farthest from the TGO. Fig. 4.5b shows the sum of refractory elements Ta, W and Re while in Fig. 4.6c the amount of individual refractory elements has been given after 569 cycles. It has been observed that at most of locations near TGO, W is present in a higher quantity than other refractory elements which shows its faster diffusion towards the TGO. Some of the diffusion results have already been published [187].

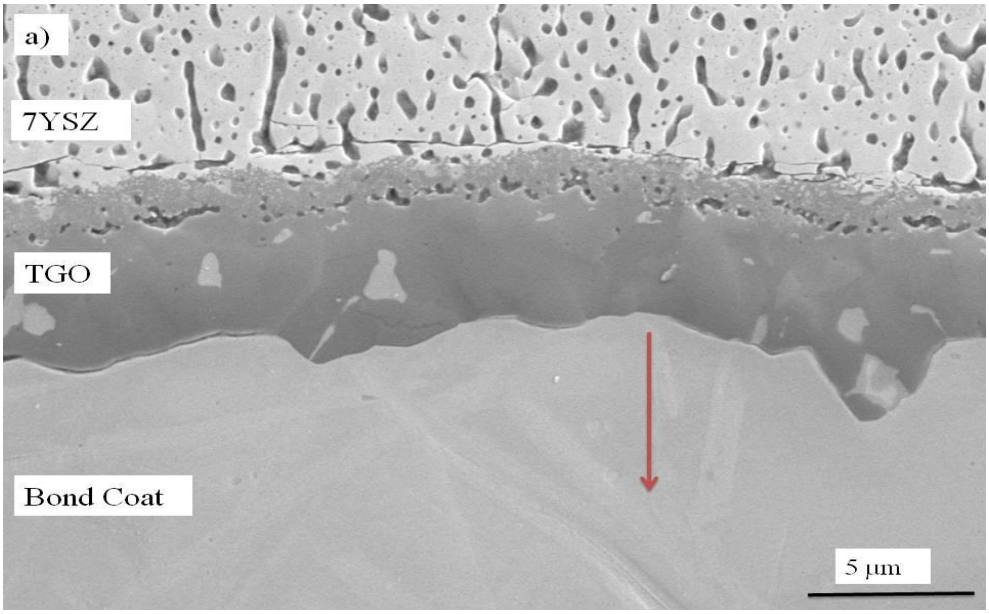

b)

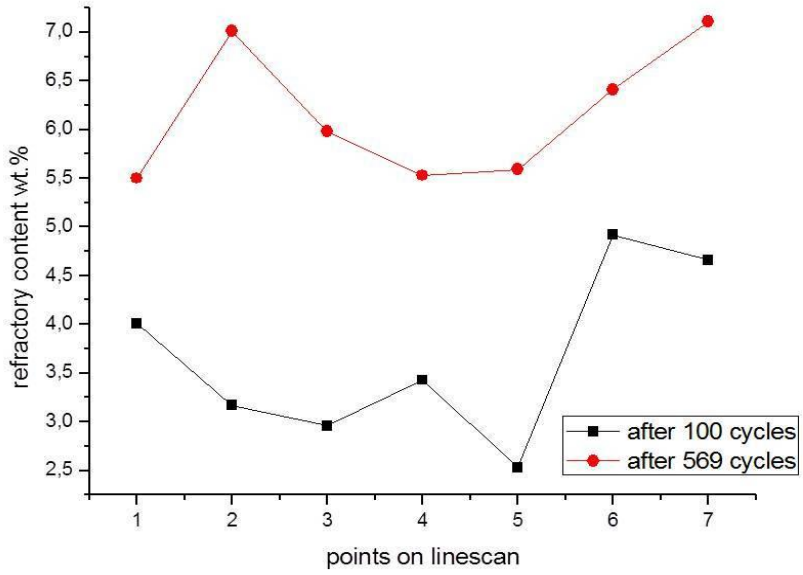

c)

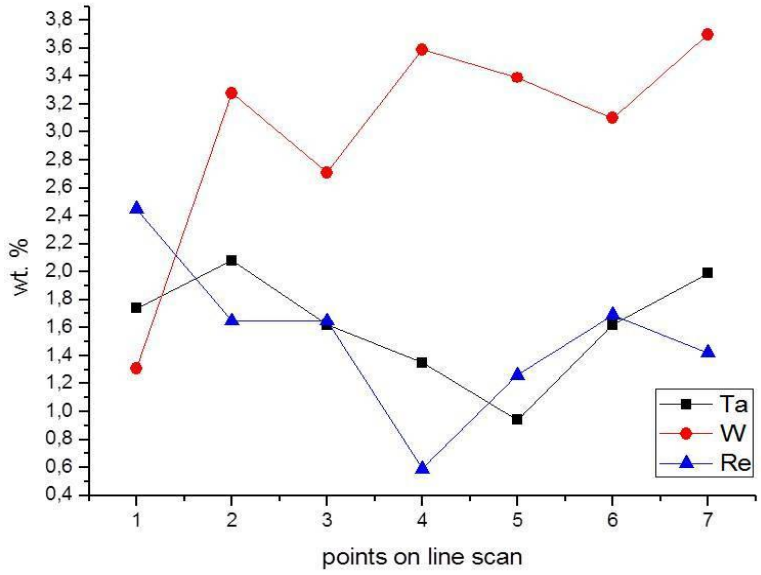

Fig. 4.5: EDX measurement showing a) the location where EDX measurement is done, b) total refractory content after different thermal cycles and c) individual refractory elements present in the bond coat after 569 cycles [187].

To confirm the presence of refractory elements in the bond coat, x-ray fluorescence (XRF) measurements have been done on the TBC samples after spallation. The measurements were

performed at locations where TBC has been spalled to find out the elements present beneath the point of failure.

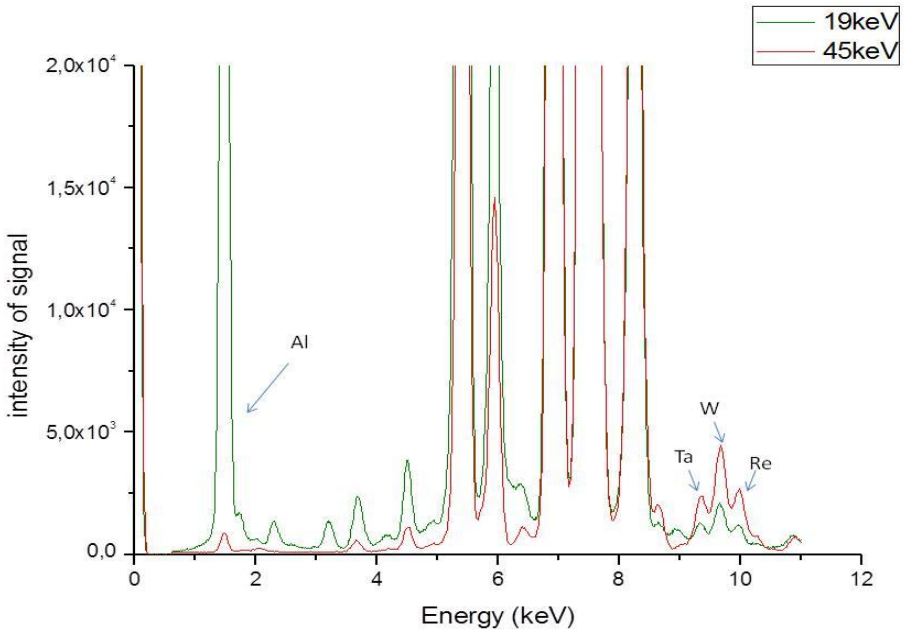

Fig. 4.6: XRF result highlighting the major peaks of Ta, W, Re and Al in CMSX-4 and 7YSZ based TBC system spalled after 569 cycles [187].

These measurements also revealed the presence of refractory elements in the bond coats where the TBC has been spalled off. However, as XRF measurements give the surface composition with around 20- 30µm depth, a relatively higher amount of aluminum was observed revealing the presence of TGO on the spalled surface. In Fig. 4.6, only the peaks for Ta, W, Re and Al are highlighted, where XRF measurement is done at x-ray energies of 19 and 45keV.

4.2.2 CMSX-4- NiCoCrAlY-Hf- 7YSZ system

4.2.2.1 Lifetime results

To study the bond coat effect on microstructure and lifetime of TBC systems, a small amount of Hf (0.6%) has been added in the NiCoCrAlY bond coat. It was observed that the Hf- doped NiCoCrAlY bond coat improves the lifetime of CMSX-4 based TBCs to around 10times when 7YSZ has been used as the top coat material. Fig. 4.7 shows the comparison of lifetimes when Hf- doped NiCoCrAlY system is compared with the standard NiCoCrAlY system, while the substrate and top coat materials remain the same. The lifetime of the standard CMSX-4/ NiCoCrAlY/7YSZ has been determined by testing more than 10 samples while the lifetime of Hf- added system has been determined by testing two samples where the lifetime values obtained are 2929 and 3039.

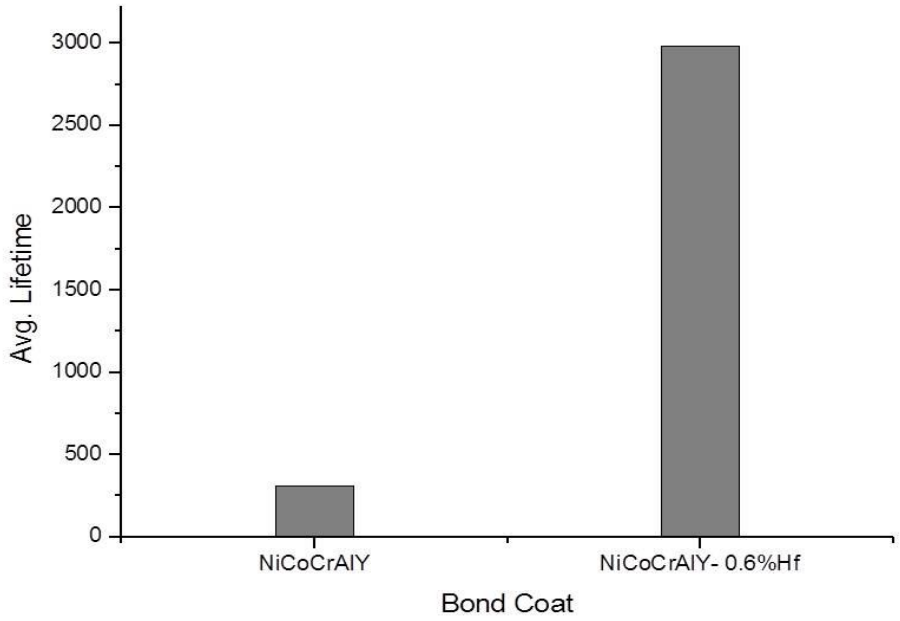

Fig. 4.7: Lifetime comparison of NiCoCrAlY bond coat system with NiCoCrAlY-Hf system when CMSX-4 has been used as substrate and 7YSZ has been used as top coat material.

4.2.2.2 Microstructural Analysis

Fig. 4.8 shows the TGO microstructure of Hf- doped NiCoCrAlY in the as-coated condition. Some hafnium oxide can be seen at TBC-TGO interface which show that Hafnium is the 1st element to oxidize in the NiCoCrAlY-Hf system. Hafnium oxide can also be seen within the bond coat confirming a strong oxygen affinity of Hafnium. The TGO thickness in the as-coated condition has been found to be around 1µm. At locations, where the as-coated TGO has slightly higher thickness, hafnium oxide can be seen at the bottom which shows that hafnium results in a faster oxidation of bond coat. There are also alumina and hafnia present within the bond coat which is not connected to the TGO. This can be due to the faster diffusion of oxygen towards Hafnium present within the bond coat or can be due to the residual oxygen (if any) present in the bond coat.

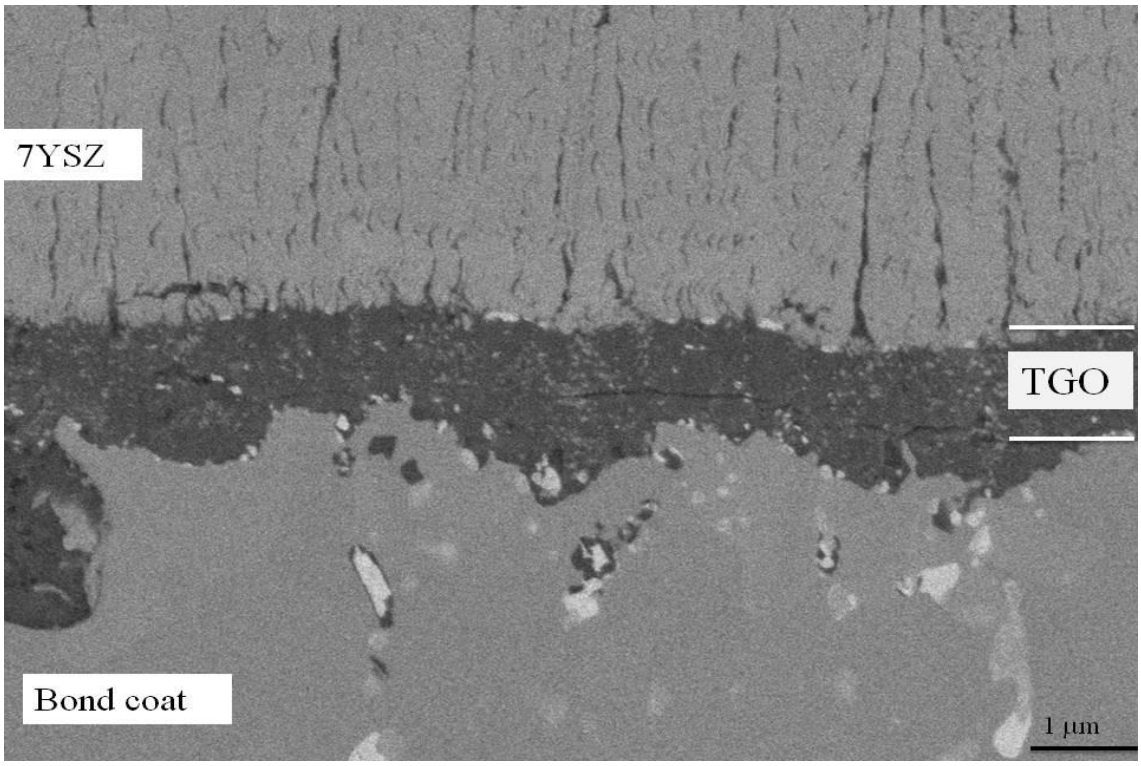

Fig. 4.8: TGO microstructure of NiCoCrAlY-Hf system in the as-coated condition.

To understand the evolution of TGO microstructure, Hf- doped systems were thermally cycled for 100, 200, 500 and 1000 cycles. It was observed that the Hf- stringers run very deep into the bond coat in a very short time. The comparison of TGO microstructure after 100 cycles on standard NiCoCrAlY bond coat and NiCoCrAlY-Hf bond coat is given in Fig. 4.9, where Hf-stringers have a depth of around 20µm while the TGO thickness is close to 10µm. In case of TGO on standard NiCoCrAlY bond coat, the thickness of TGO is also close to 10µm, however, the yttria pegs have a very limited depth compared to the Hf- stringers.

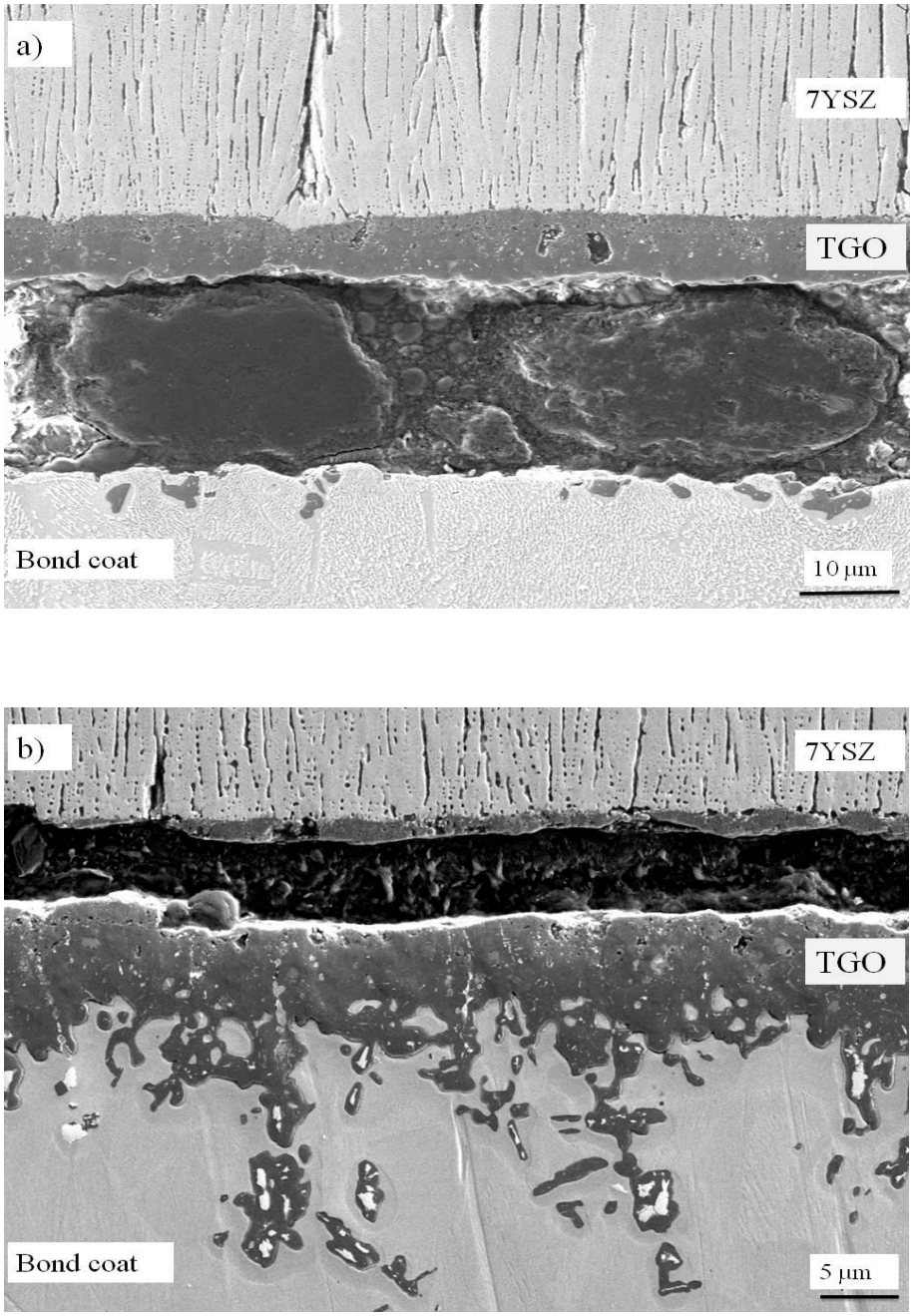

Fig. 4.9: TGO microstructure after 100 cycles on a) standard NiCoCrAlY bond coat and b) NiCoCrAlY-Hf bond coat.

Hafnium seems to be the main driving force for the diffusion of oxygen as Hafnium present deeper in the bond coat is also oxidized in a very short time, along with the aluminum around it. Due to this preferred growth of TGO towards Hafnium, the bond coat is "entrapped" in the TGO at several places as shown in Fig. 4.10a. Oxidation of this entrapped bond coat, in the later stages of thermal cycling, results in the formation of spinels which are shown in Fig. 4.10b.

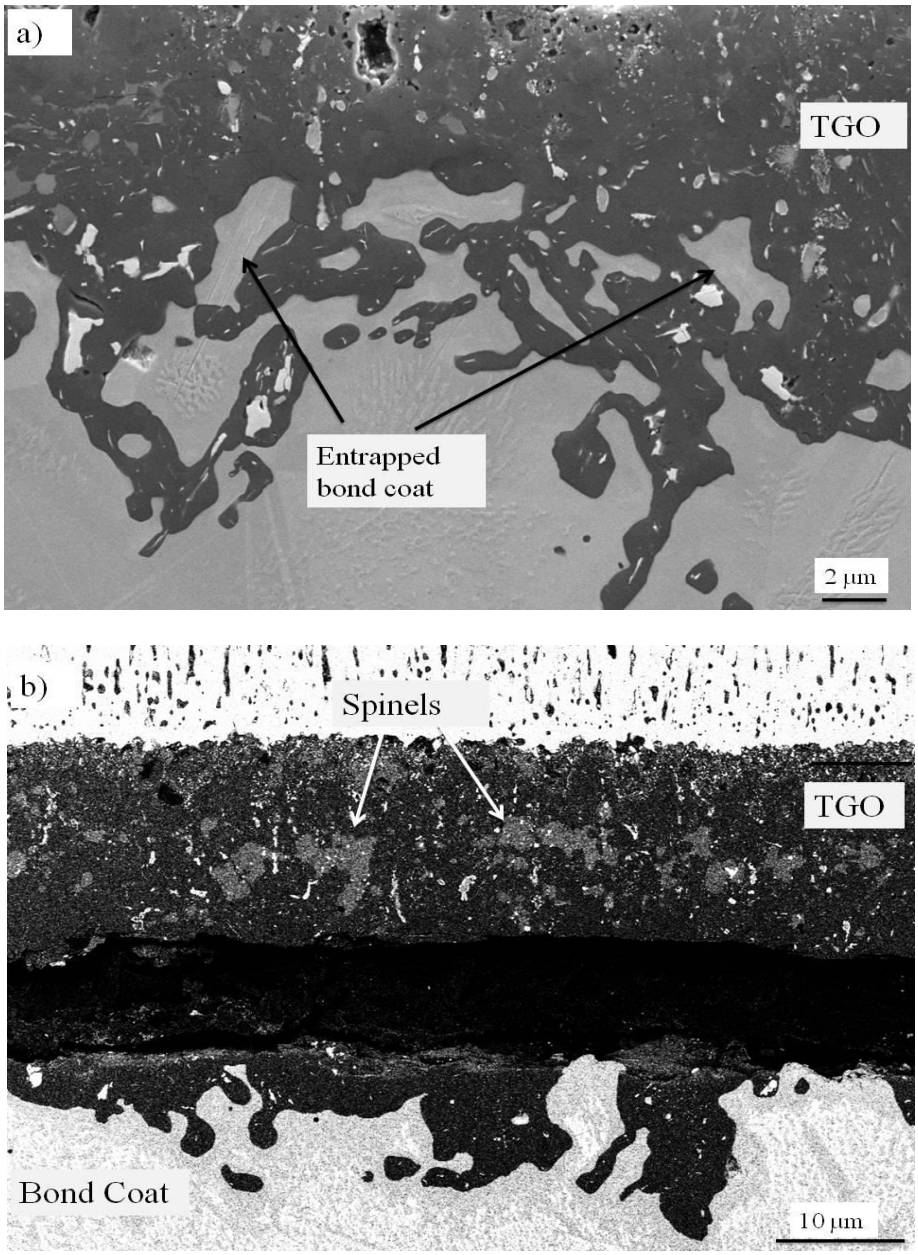

Fig. 4.10: TGO microstructure of Hf-added system after thermal cycling for a) 200 cycles and b) 2500 cycles.

After 500 cycles, the difference in the thickness of Hf- stringers and the bulk of TGO has been reduced. However, a new phase appears right beneath the TGO. In Fig. 4.11, it can be seen that this new phase has a thickness or around 1μm and it is present underneath the TGO and around alumina at all places in the bond coat. As thermal cycling is continued, it has been observed that this new phase grows in thickness while the difference between depth of Hf- stringers and TGO thickness reduces further. Careful EDX measurements indicated that this new phase contains

very little or no Hafnium and has a higher amount of refractory elements. After 3000 cycles, the thickness of this new phase has been found to be in the range of 4µm as shown in Fig. 4.11b.

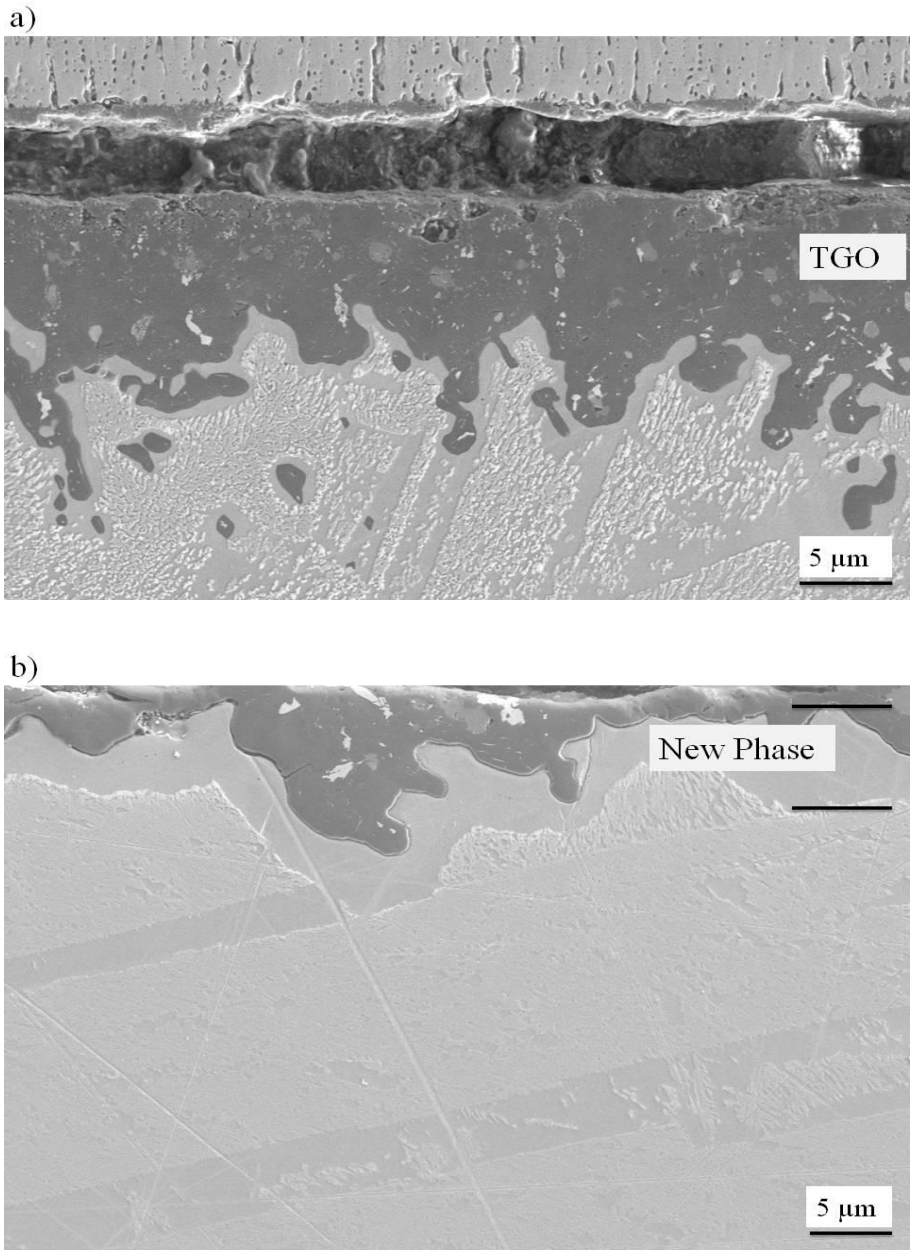

Fig. 4.11: TGO microstructure of Hf- added NiCoCrAlY system after a) 500 cycles and b) after 3000 cycles.

4.2.2.3 Diffusion of elements in NiCoCrAlY-Hf system

In the standard CMSX-4- NiCoCrAlY- 7YSZ system, diffusion of refractory elements from the substrate towards the TGO has already been mentioned in section 4.2.1.1. To investigate the diffusion of elements in the Hf- added system, EDX was performed after thermal cycling of 100, 200, 500, and 1000 and after spallation as well. It has been observed that the refractory elements diffuse continuously towards the TGO which has been observed by a continuous increase in the refractory content in the bond coat. The composition of bond coat after 100 cycles and 3000 cycles is shown in Fig. 4.12. It has been observed that the diffusion in the beginning of thermal cycling is faster and with more thermal cycling it becomes slower.

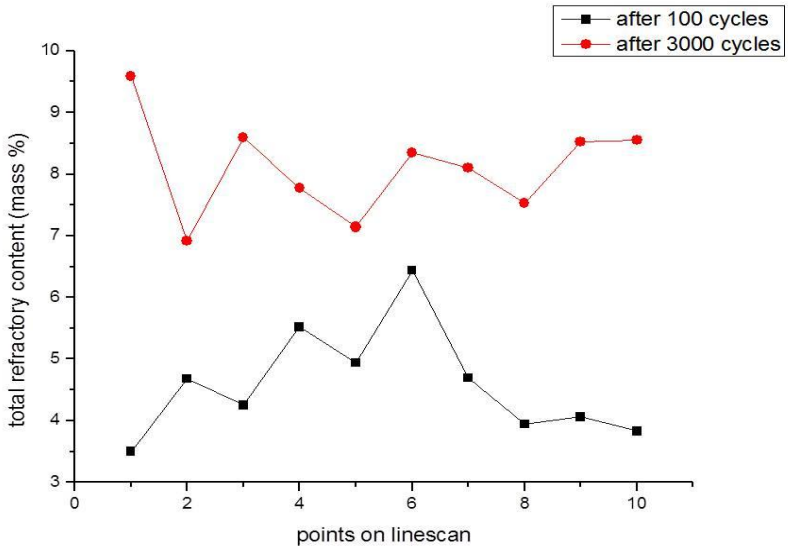

Fig. 4.12: Refractory content in the bond coat near to the TGO after 100 cycles and after 3000 cycles.

4.3 Gadolinium Zirconate as Ceramic top coat Material

In this study, Gadolinium Zirconate has been deposited on different bond coat and substrate materials and the effect on microstructure and lifetime has been investigated. It has been observed that GdZ, in the as-coated condition, consists of EB-PVD columnar structure; however, the columns are not straight but are tilted in one direction. The direction of bending of GdZ columns has been found to be the same as the direction of rotation during deposition. It has been observed that by changing the direction of rotation of GdZ samples during deposition, the direction of column bending is also changed. Further, the columns don't have a uniform diameter across the length but the diameter is larger at the tip of the columns than their bottom. GdZ columns in the as-coated condition are shown in Fig. 4.13a. GdZ columns also differ to 7YSZ columns in that they have more column branching at their tips and moreover the feather arms run deeper into the columns that in 7YSZ columns.

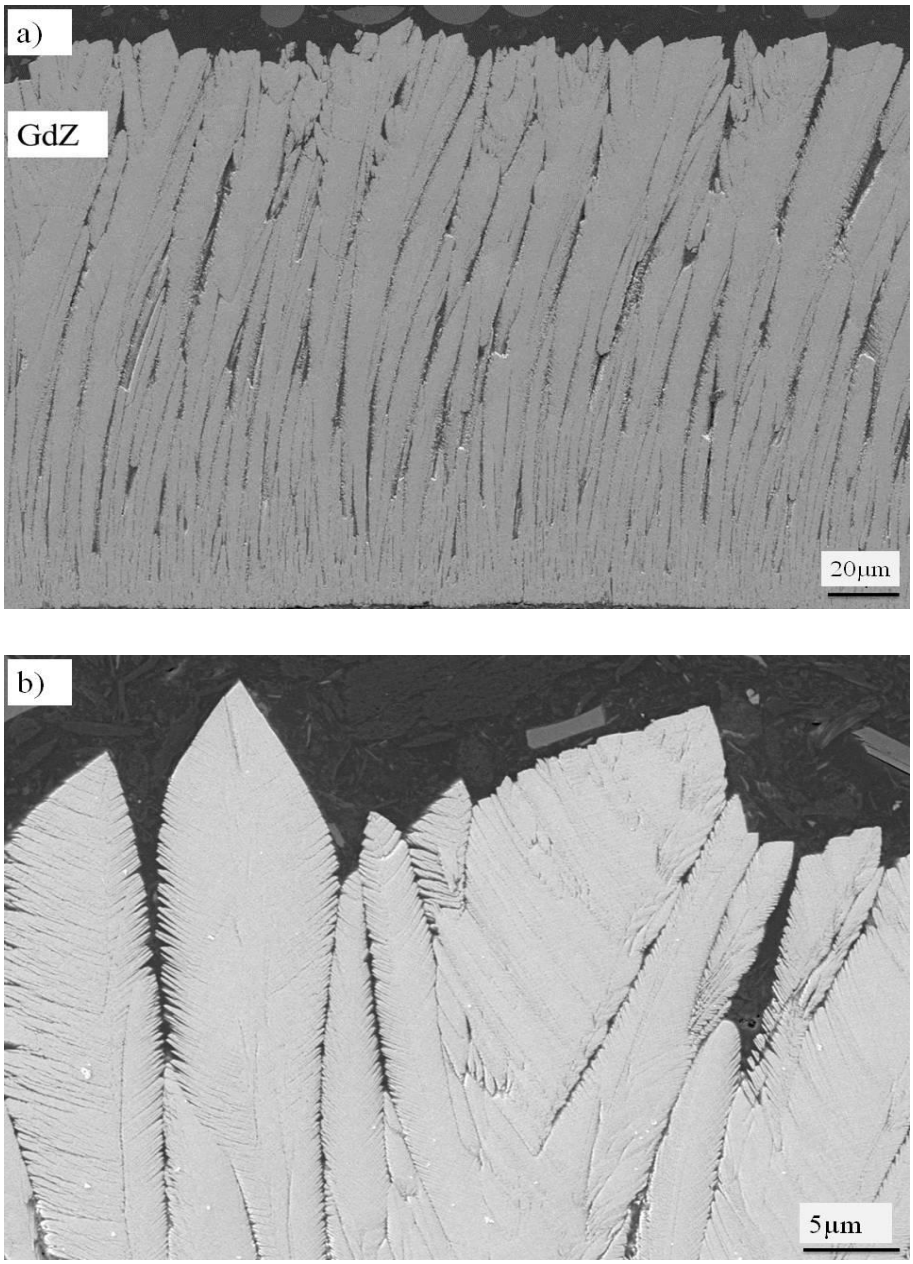

Fig. 4.13: a) GdZ columns in the as-coated condition and b) column tips of GdZ columns in the as-coated condition.

4.3.1 Phase Change during Thermal Cycling

Fig. 4.14 shows the diffraction patterns of GdZ after different thermal treatments. Arrow heads are used to highlight the pyrochlore peaks as the cubic to pyrochlore ordering has been the main focus of this XRD study. It can be clearly seen that GdZ doesn't have the pyrochlore structure in the as-coated state. Even after annealing at 1260°C for 2 h, pyrochlore peaks were not observed

but are visible after 2850 cycles. This means that GdZ undergoes the expected phase ordering during the thermal cycling process.

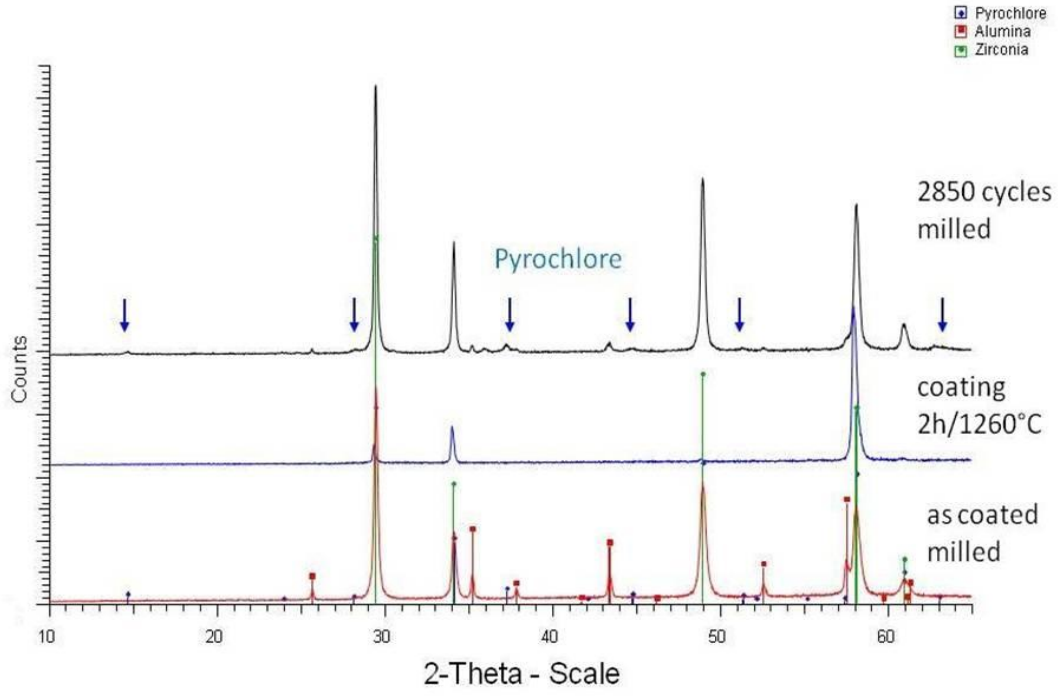

Fig. 4.14: XRD plot of as-coated GdZ (milled), sintered for 2hrs at 1260°C (coating) and after 2850 cycles (milled).

4.3.2 Double layer GdZ TBC

Double layer TBCs of GdZ have been investigated by depositing GdZ on top of 25µm 7YSZ with NiCoCrAlY as bond coat and IN100 as the substrate material. This double layer GdZ TBC is then compared with its single layer counterpart for lifetime and microstructure. The as-coated columns of GdZ grow on already existing 7YSZ columns such that the continuity of the columns is not disturbed. From a performance point of view, such a structure will be more strain-tolerant than forming of new columns in the second ceramic layer. It has been observed that column morphology of double layer GdZ is similar to the single layer GdZ. The columns of GdZ are bent in one direction and have a different diameter at their tips than their bottom, as shown in Fig. 4.15a. However, the lifetime of double layer GdZ TBCs has been found to be longer than standard 7YSZ TBCs but shorter than single layer GdZ TBCs, as shown in Fig. 4.15b.

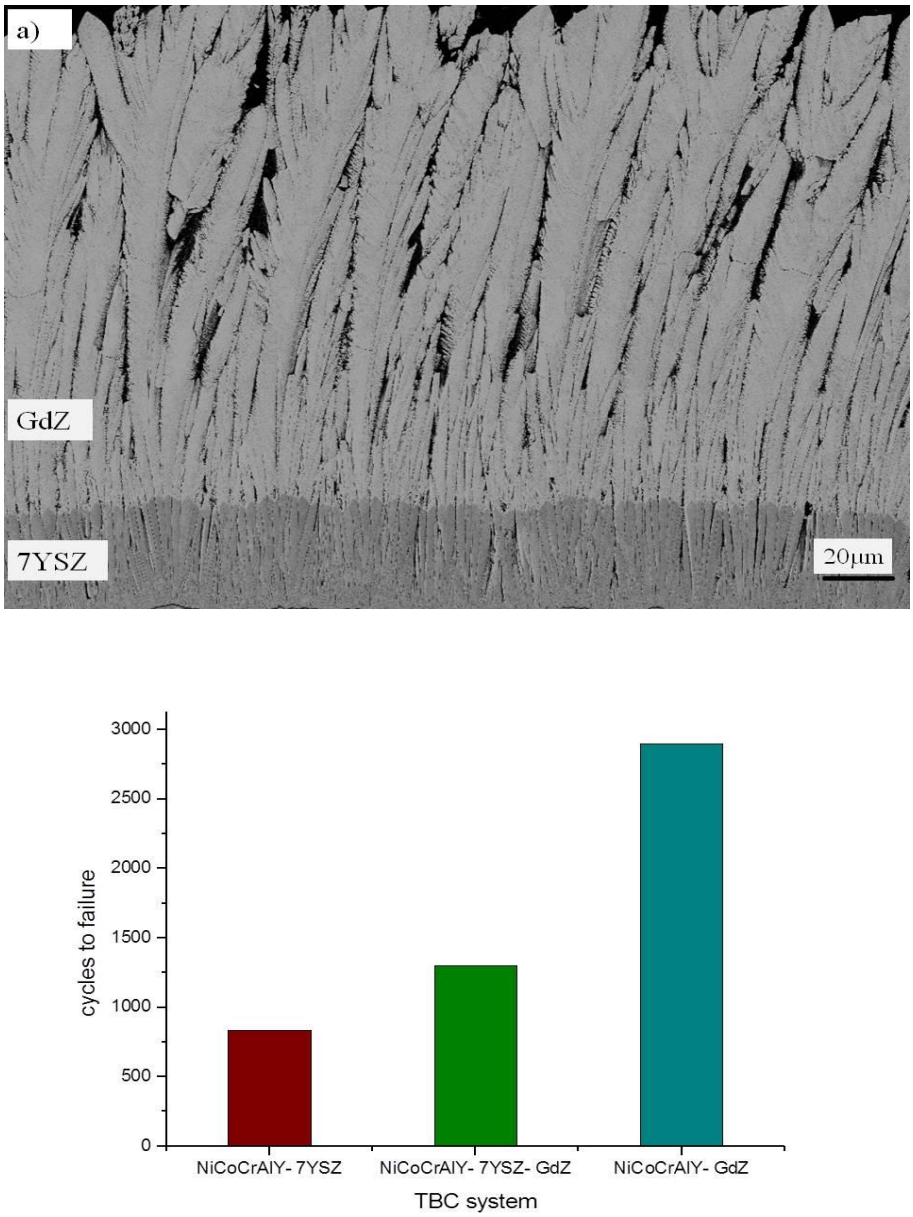

Fig. 4.15: a) SEM Micrograph of a double layer GdZ TBC in the as-coated condition and b) lifetime values of single and double layer GdZ TBC compared with standard 7YSZ system.

4.3.3 Sintering of Gadolinium Zirconate

Sintering of the ceramic layers leads to the coarsening of intra-columnar pores, disappearing of inter-columnar pores and by a reduction in the sharpness of the feather-arms. To compare the sintering in 7YSZ and GdZ, the interface of 7YSZ-GdZ double layer TBC can be helpful. In Fig. 4.16, such an interface is shown in the as-coated as well as after thermal cycling state. Microstructural features like inter-columnar porosity, intra-columnar porosity and feather-arms are marked. It can be seen in Fig. 4.16a that inter and intra-columnar porosity is very similar in

both ceramic layers in the as-coated condition and feather arms are also present in both 7YSZ and GdZ layers. After thermal cycling, the inter-columnar porosity disappears to a greater extent in the 7YSZ layer (Fig. 4.16b). Similarly, feather arms have also been rounded in both layers due to sintering. It can be seen that the feather arms in 7YSZ layer are almost vanished after thermal cycling while in the GdZ layer; the feather arms are not completely disappeared. Instead, they form a structure which is similar to steps at the column boundaries. There is a remarkable variation in the contrast which can be seen in between the 7YSZ columns, marked in Fig. 4.16b. Careful measurements by EDX reveal presence of some gadolinium in between the 7YSZ column boundaries, however, no upward diffusion of yttrium into GDZ is found. The results on the sintering of GdZ have already been published [174].

a)

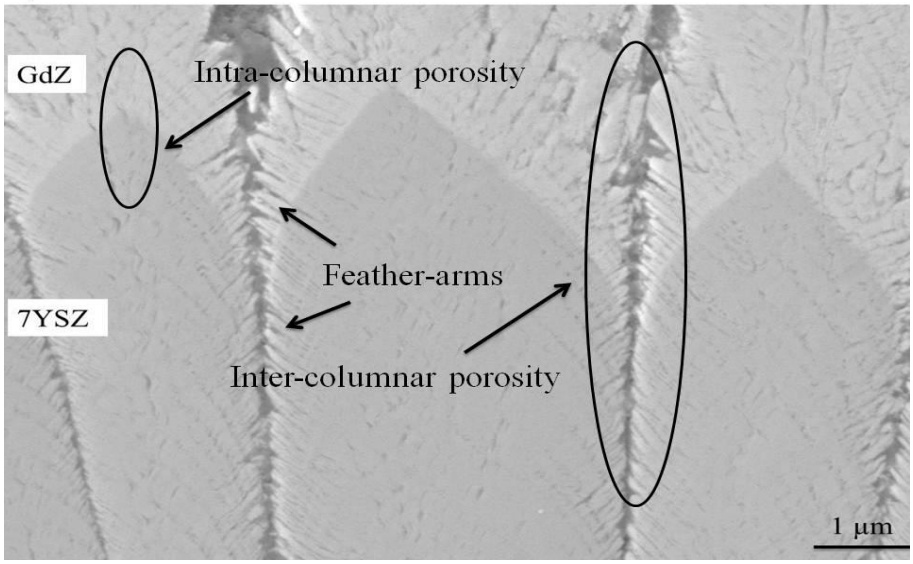

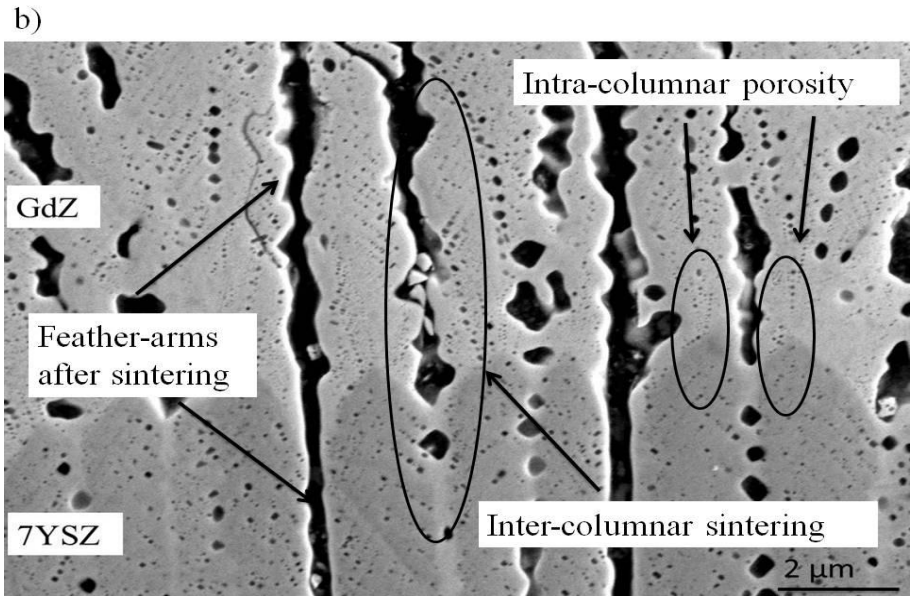

Fig. 4.16: GdZ- 7YSZ columns interface in a) the as-coated condition and b) after thermal cycling for 635 cycles [174].

As the microstructure changes of GdZ after thermal cycling are compared with those of 7YSZ, it has been observed that the sintering of GdZ at column tips is more than that at 7YSZ column tips. It can be seen in Fig. 4.17 that the feather-arms and inter-columnar boundaries which are present in the as-coated condition have been disappeared after 2000 cycles while in case of 7YSZ these features are not much changed. This different extent of sintering at the middle and tip of the columns can also be due to the different column morphology of GdZ columns in the as-coated condition.

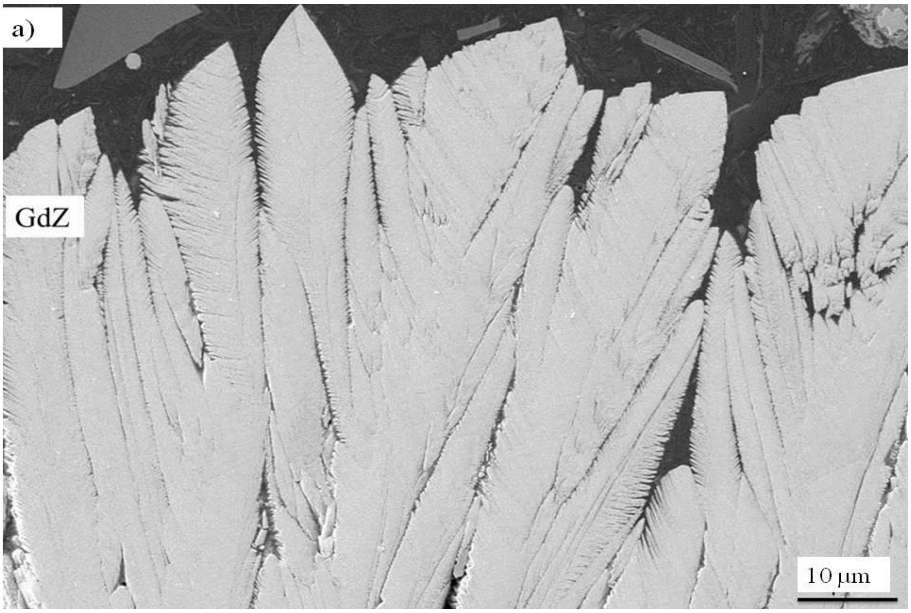

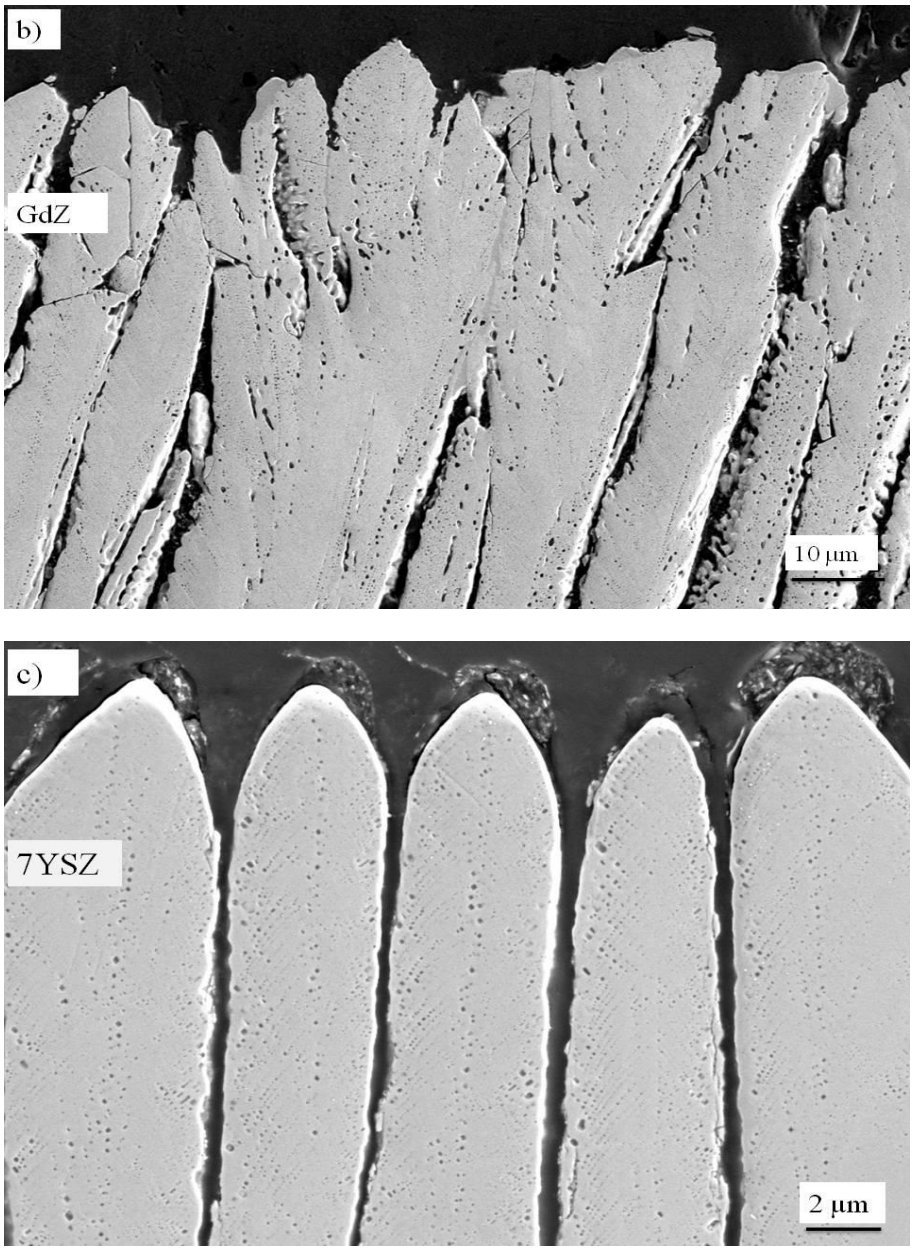

Fig. 4.17: SEM micrograph showing the tip of the columns a) as-coated GdZ columns tip, b) GdZ after 2000 cycles and c) 7YSZ after 3000 cycles [174].

Effect of sintering can also be observed in Fig. 4.18, where as-coated GdZ columns are compared with GdZ columns after 5000 cycles. It can be seen that in the as-coated samples the microstructural features like feather-arms and inter-columnar porosity look very sharp whereas in case of cycled sample the features are not sharp anymore. Further, the edges after thermal cycling are rounded and at some locations sintering necks can also be seen.

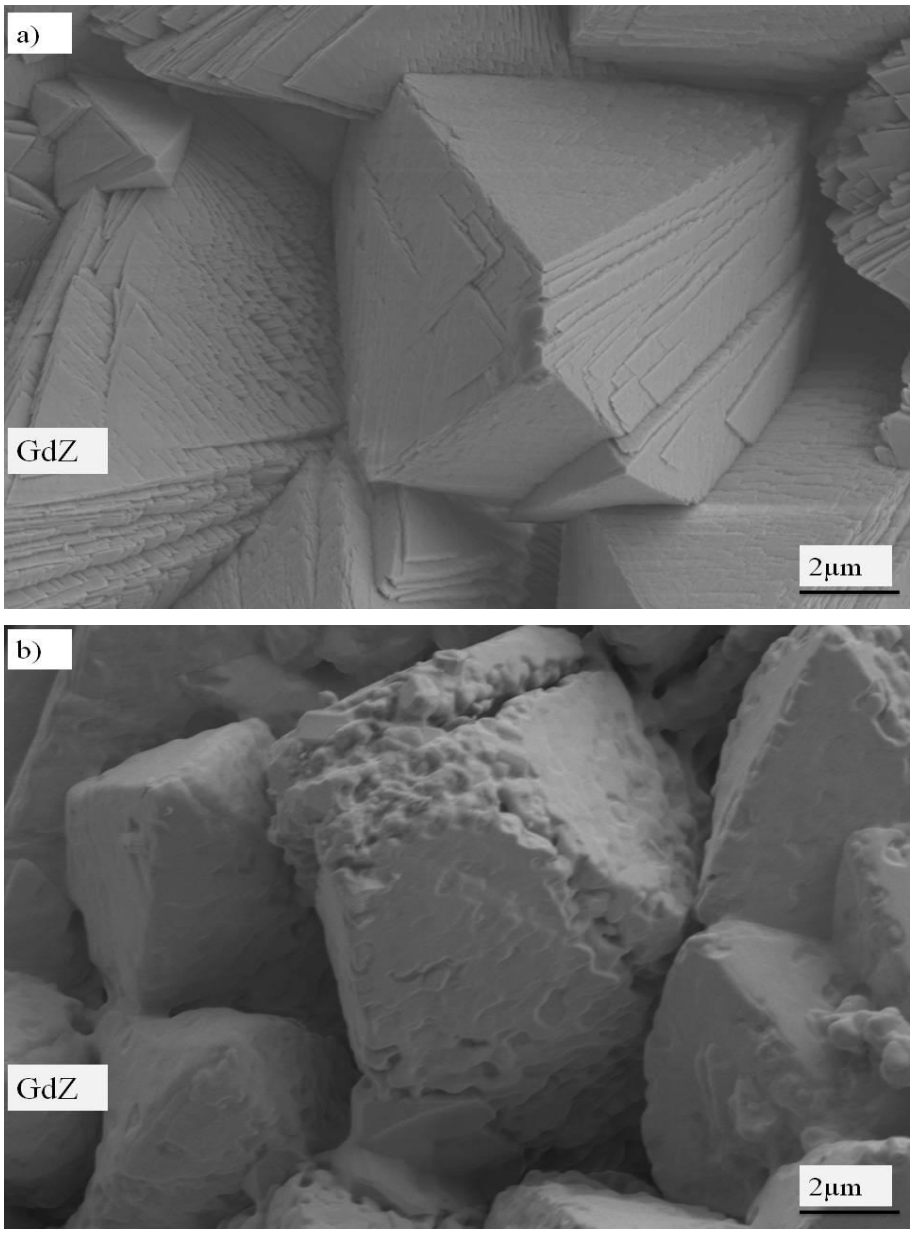

Fig. 4.18: Top-view of a) as-coated GdZ columns and b) GdZ columns after 5000 cycles [174].

4.4 GdZ on different TBC systems

The effect of different bond coat compositions and different substrate materials on the lifetime and microstructure of TBC systems has already been discussed when 7YSZ is deposited as the ceramic top coat material. To investigate the ceramic top coat effect, 7YSZ has been replaced by GdZ on all the previously described TBC systems and effect on microstructure and lifetime has been investigated.

4.4.1 Effect on Lifetime

Fig. 4.19 shows the ceramic top coat effect on different TBC systems investigated in this study. It has been already mentioned in the literature that CMSX-4- NiCoCrAlY system with 7YSZ as top coat shows a lower lifetime than the IN100 based counterpart. However, it has been observed that GdZ improves the lifetime of both NiCoCrAlY based systems by a factor of around 4. The maximum improvement has been observed in the lifetime of NiCoCrAlY-2 based TBC systems where replacement of 7YSZ by GdZ caused an almost 5-fold improvement in the lifetime. However, in case of CMSX-4 based system with Hf- doped NiCoCrAlY, GdZ has not made any significant change in the lifetime values.

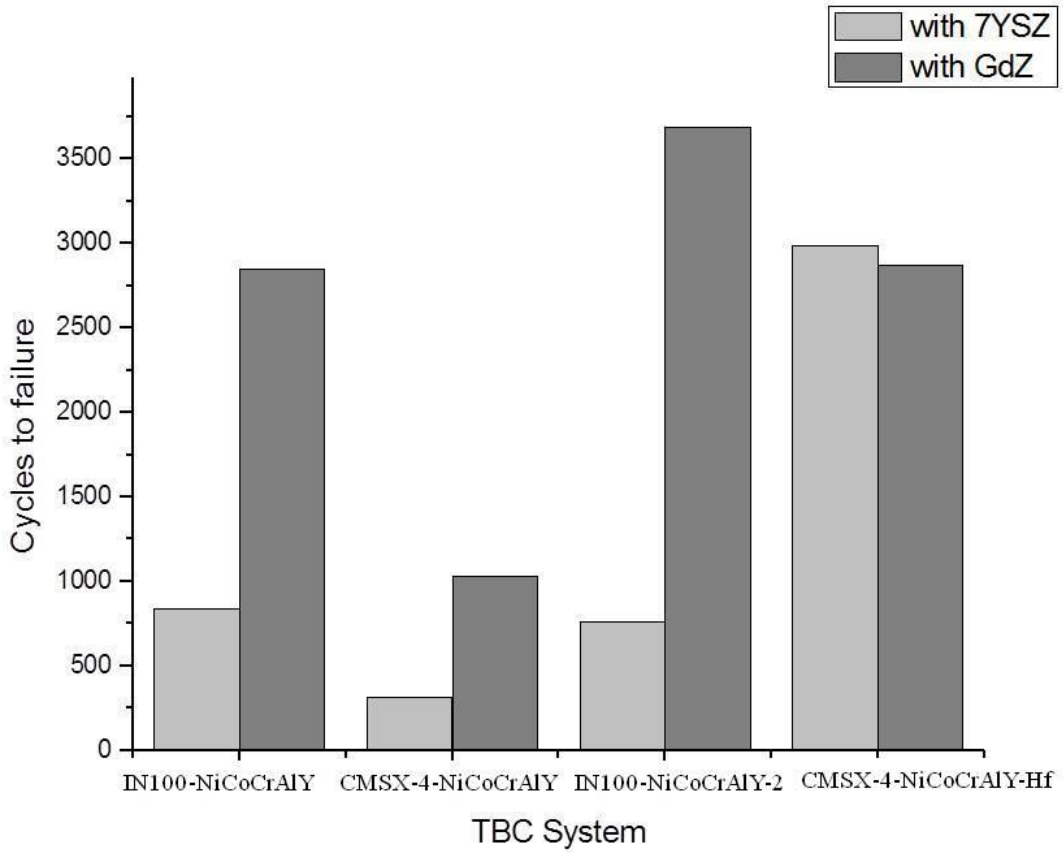

Fig. 4.19: Lifetime comparison of GdZ vs. 7YSZ on NiCoCrAlY-Hf and CMSX-4.

4.4.2 Effect on TGO Microstructure

On NiCoCrAlY bond coat with IN100 as the substrate material, the as-coated TGO for GdZ based system has been found very similar to that of 7YSZ based system (Fig. 4.2a). However, an interaction between GdZ and TGO has been observed as a result of thermal cycling. Fig. 4.20a shows the TGO of GdZ-NiCoCrAlY system with IN100 as substrate material, where a new phase has started to form after 685 cycles. It has been observed that this new phase becomes more and

more continuous with thermal cycling and after 5000 cycles, it is present continuously at TBC-TGO interface with a thickness of around 300nm (Fig. 4.20b).

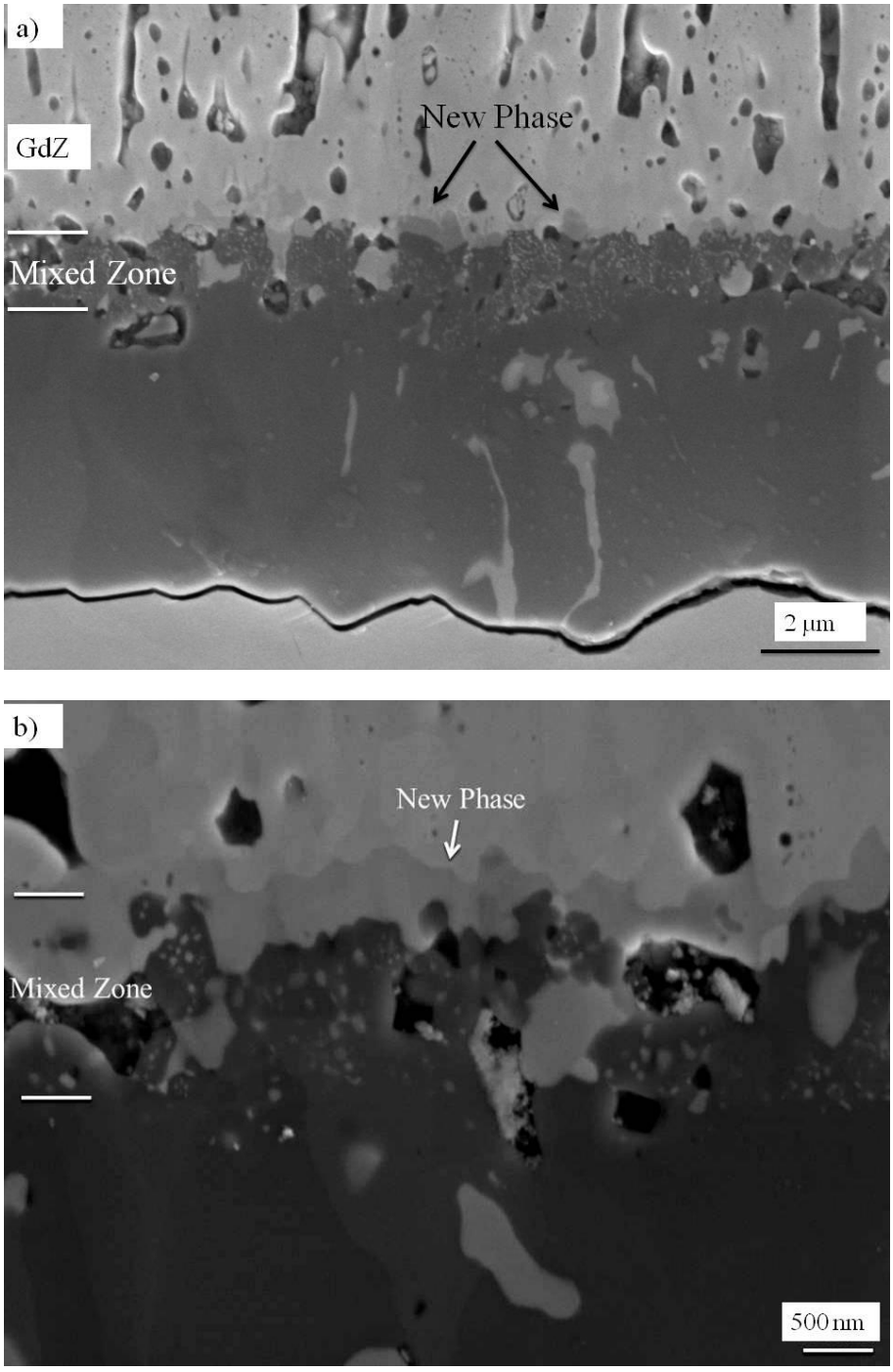

Fig. 4.20: TBC- TGO interface of IN100-NiCoCrAlY-GdZ TBC system after thermal cycling for a) 685 cycles and b) after 5000 cycles.

GdZ on top of NiCoCrAlY bond coat with CMSX-4 as the substrate material undergoes a similar TBC-TGO interaction that has been mentioned for IN100 based systems.

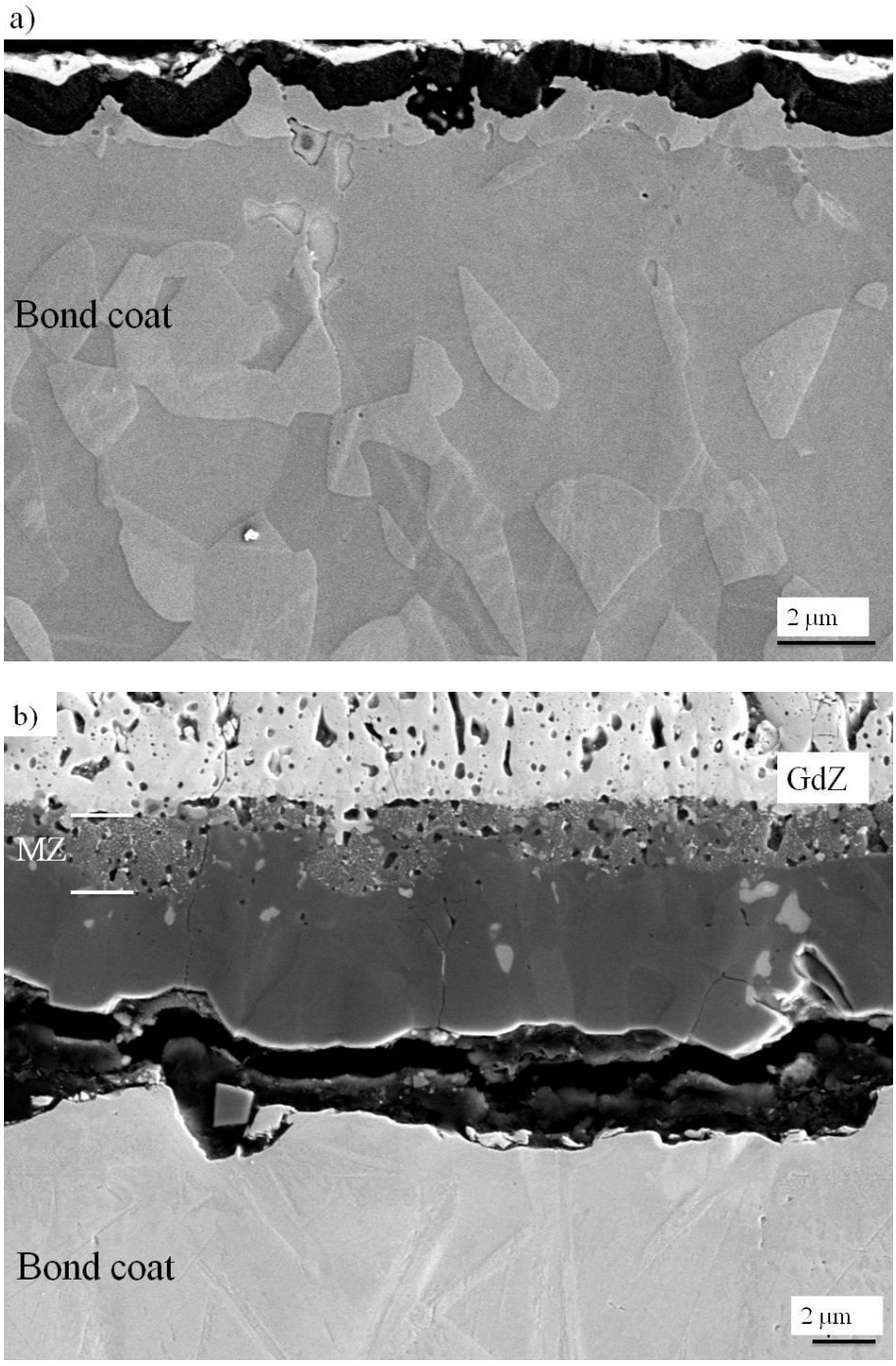

Fig. 4.21: TGO microstructure of GdZ-NiCoCrAlY-CMSX-4 TBC system in a) the as-coated condition and b) after thermal cycling for 980 cycles.

However, in CMSX-4 based system, the TGO in the as-coated condition has been found to be wavier than in IN100 based system. This wavy TGO in the as-coated condition resulted in the formation of a wavy mixed zone as shown in Fig. 4.21b, where it can be seen that the mixed zone at some locations has a thickness of around 2µm while at other locations the thickness is in the range of 0.5µm. Such a wavy mixed zone has not been found for other TBC systems.

In GdZ- NiCoCrAlY TBCs on both CMSX-4 and IN100 substrates, some diffusion of Al has been observed from the TGO towards the TBC as a result of thermal cycling. However, the diffusion was in the range of a few microns and it was observed that the depth of diffusion didn't change much with the number of cycles. Fig. 4.22 shows exemplarily an EDX line scan of the GdZ-NiCoCrAlY TBC system where the aluminum diffusion can be seen from the TGO towards the ceramic top coat.

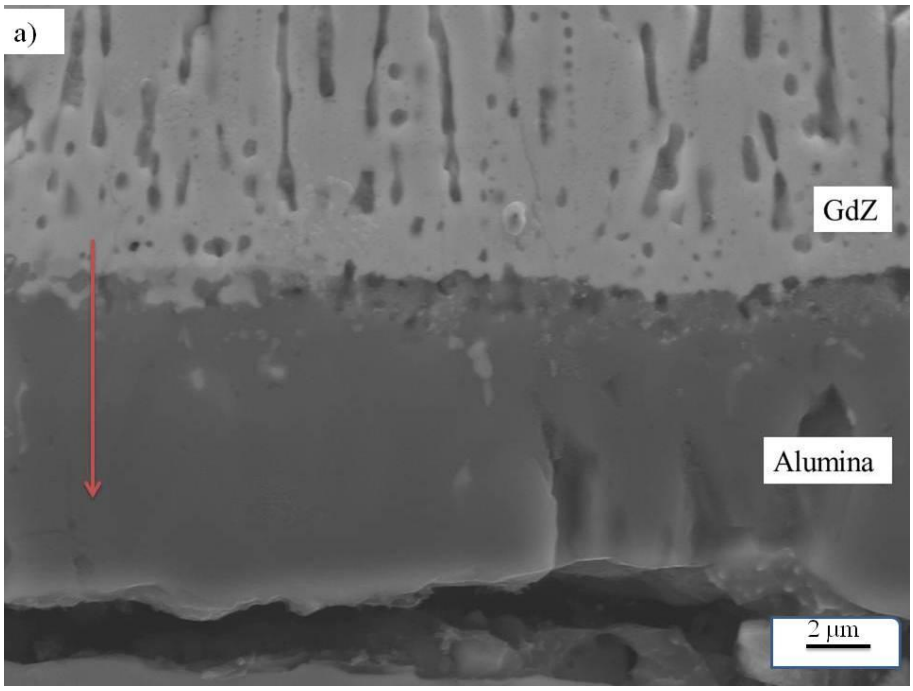

b)

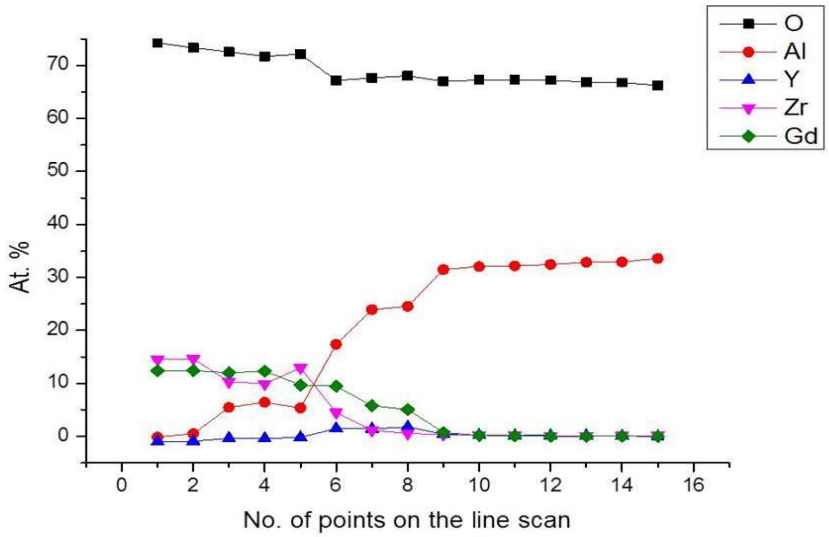

Fig. 4.22: Al diffusion in GdZ- NiCoCrAlY TBCs after thermal cycling for 685 cycles.

For the TBC system with GdZ on NiCoCrAlY-2 bond coat, the chemical reaction at the TBC-TGO interface results in the formation of a reaction zone with alternating phases. Careful EDX results revealed that the composition with lighter contrast is rich in Gd while the composition with darker contrast is rich in Y. As the dimensions of these phases are quite small, exact compositions could not be derived in SEM analysis. SEM micrograph of TBC-TGO interface, thermally cycled for 2000 cycles, with the alternating phases is shown in Fig. 4.23.

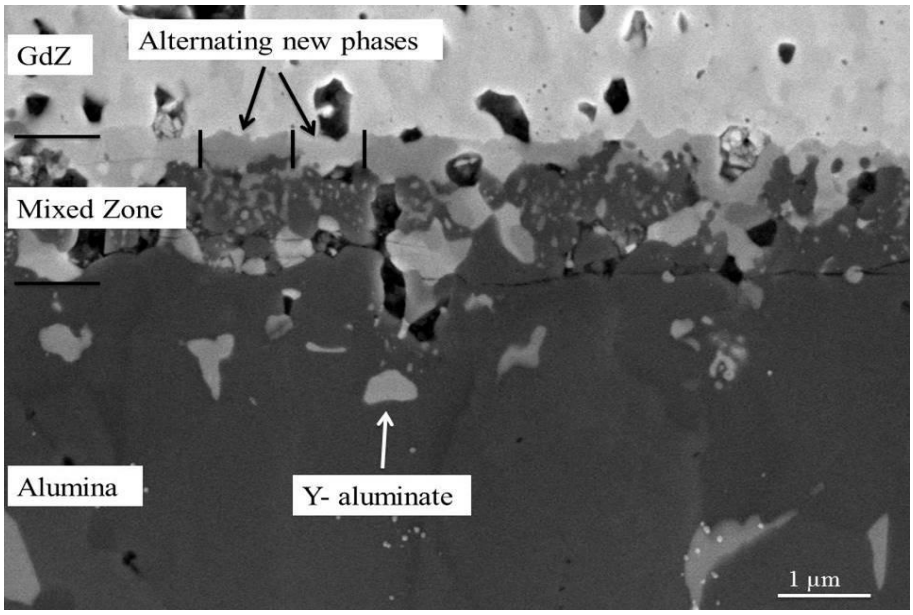

Fig. 4.23: TBC-TGO microstructure for GdZ- NiCoCrAlY-2 TBC system on IN100 substrate.

In case of NiCoCrAlY-Hf based system, the TGO in the as-coated condition has been found to be very similar to its 7YSZ counterpart. However, after thermal cycling no interaction has been observed between GdZ and TGO even after 3000 cycles which has been the case for other GdZ-NiCoCrAlY systems. TBC- TGO interface for GdZ- NiCoCrAlY-Hf TBC is shown in Fig. 4.24.

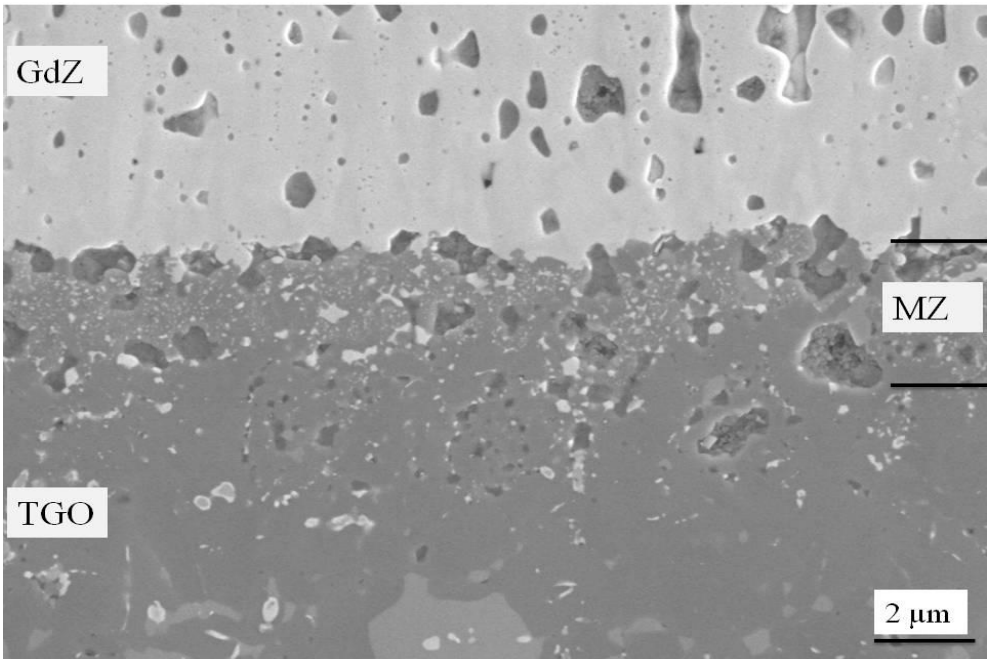

Fig. 4.24: TBC-TGO microstructure for GdZ- NiCoCrAlY- Hf TBC system on CMSX-4 substrate after 3000 cycles.

4.4.3 Failure mechanism and Failure location

The spallation patterns of different TBC systems on IN100 substrate are shown in Fig. 4.25

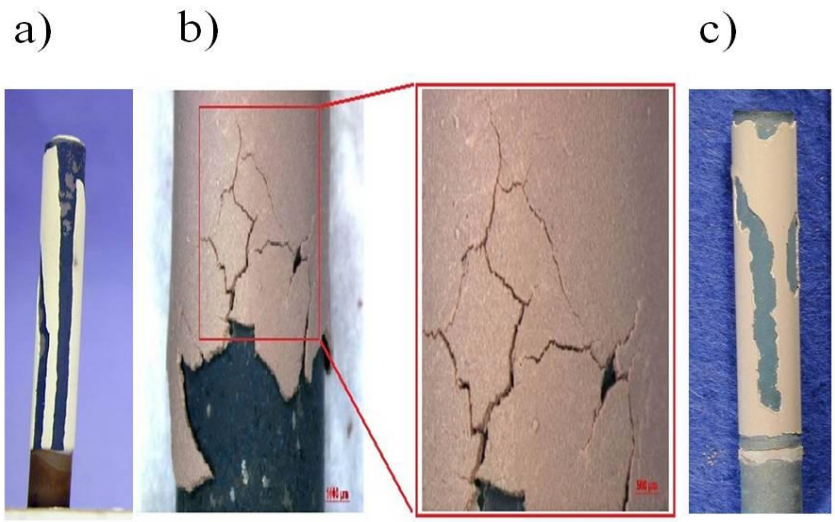

Fig. 4.25: Macroscopic failure pattern of a) 7YSZ- NiCoCrAlY system, b) GdZ- NiCoCrAlY system and c) GdZ- 7YSZ- NiCoCrAlY system

It has been observed that 7YSZ TBCs on IN100 substrate show the standard buckling strip- like failure (Fig. 4.25a) whereas for the single layer GdZ TBCs, a mud-crack failure pattern has been observed (Fig. 4.25b). The GDZ thereby spalled in small pieces accompanied by a typical crack pattern that slowly progressed along the length of the samples. In the double layer GdZ TBC (Fig. 4.25c), a combination of both mud-crack failure and buckling has been observed although buckling seems to be the dominant factor for spallation. In all these systems with IN100 substrate, failure location was mostly found at TGO- BC interface. However out of the three GdZ-NiCoCrAlY-2 samples which failed during thermal cycling, one sample had failure location within the ceramic top coat as shown in Fig. 4.26. This sample showed a lifetime of about 3700 cycles and after the TBC failure, it was observed that a small layer of GdZ coating is always sticking to the TGO.

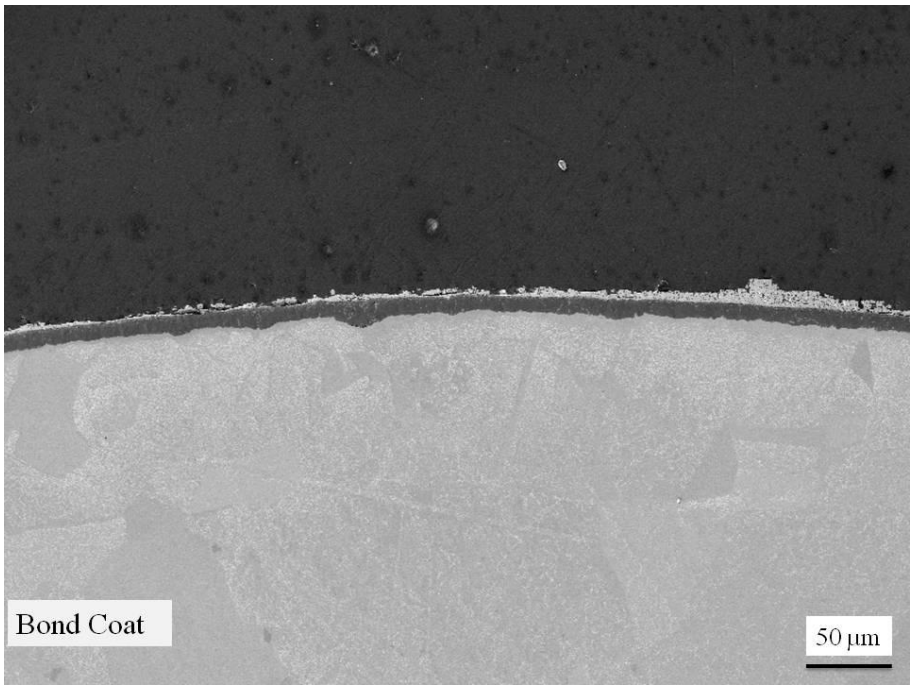

Fig. 4.26: Failure location of a GdZ- NiCoCrAlY-2 system where a thin TBC layer remains intact with the TGO after TBC failure.

For the GdZ- NiCoCrAlY system, one of the samples showed a lifetime of above 5000 cycles. It was taken out of the furnace as the length had been considerably reduced due to the oxidation of the substrate material. When this sample was mechanically cut, TBC spallation took place. However, it was interesting to see that the failure location, which represents the weakest location in the system, was not at TBC-TGO or TGO- bond coat interface. Instead it was found to be within the GdZ coating very similar to the one shown in Fig. 4.26.

In case of CMSX-4 based systems, different failure mechanisms have been observed compared to IN100 based ones. As shown in Fig. 4.27, large scale spallation of TBC has been observed for NiCoCrAlY based systems when either 7YSZ or GdZ is used as the ceramic top coat material Fig. (4.27 a, c- d). In case of CMSX-4- 7YSZ TBC system with NiCoCrAlY-Hf bond coat, failure pattern where buckling seems to be the dominating mechanism, has been observed (4.27b).

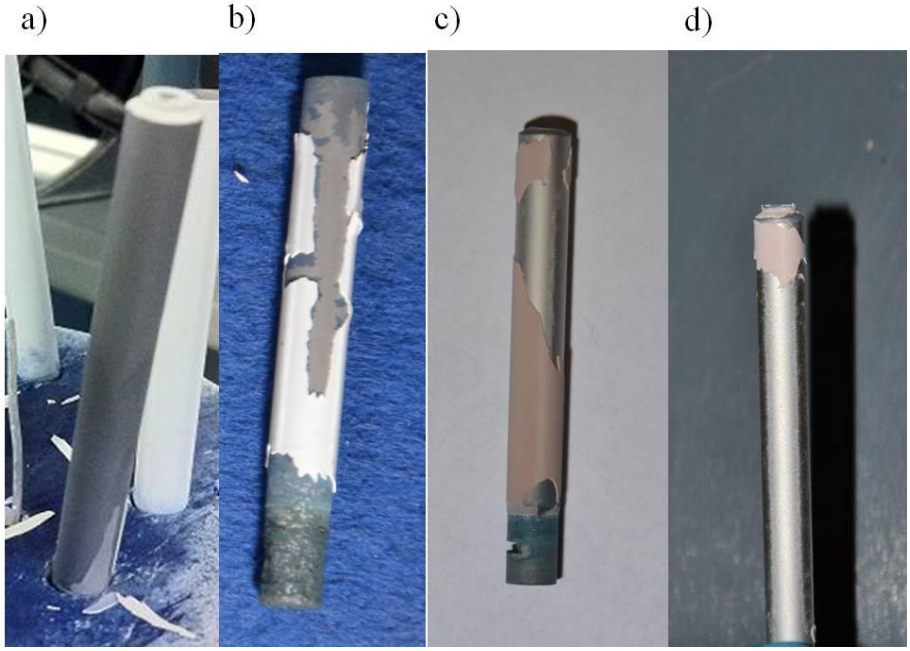

Fig. 4.27: Failure pattern of a) CMSX-4-NiCoCrAlY-7YSZ system, b) CMSX-4-NiCoCrAlY-Hf-7YSZ system and c & d) CMSX-4-NiCoCrAlY-GdZ system.

For GdZ on NiCoCrAlY-Hf bond coat systems, macroscopic failure patterns seem to be predominantly buckling although the spallation takes place by piece by piece spallation as in case of mud-cracking (Fig. 4.28a). Also, the direction of mud-cracking has not been found irregular as it was in Fig. 4.25b. Fig. 4.28b shows that the failure location in case of GdZ-NiCoCrAlY-Hf TBCs has been at the TBC- TGO interface which has never been the case in other TBC systems.

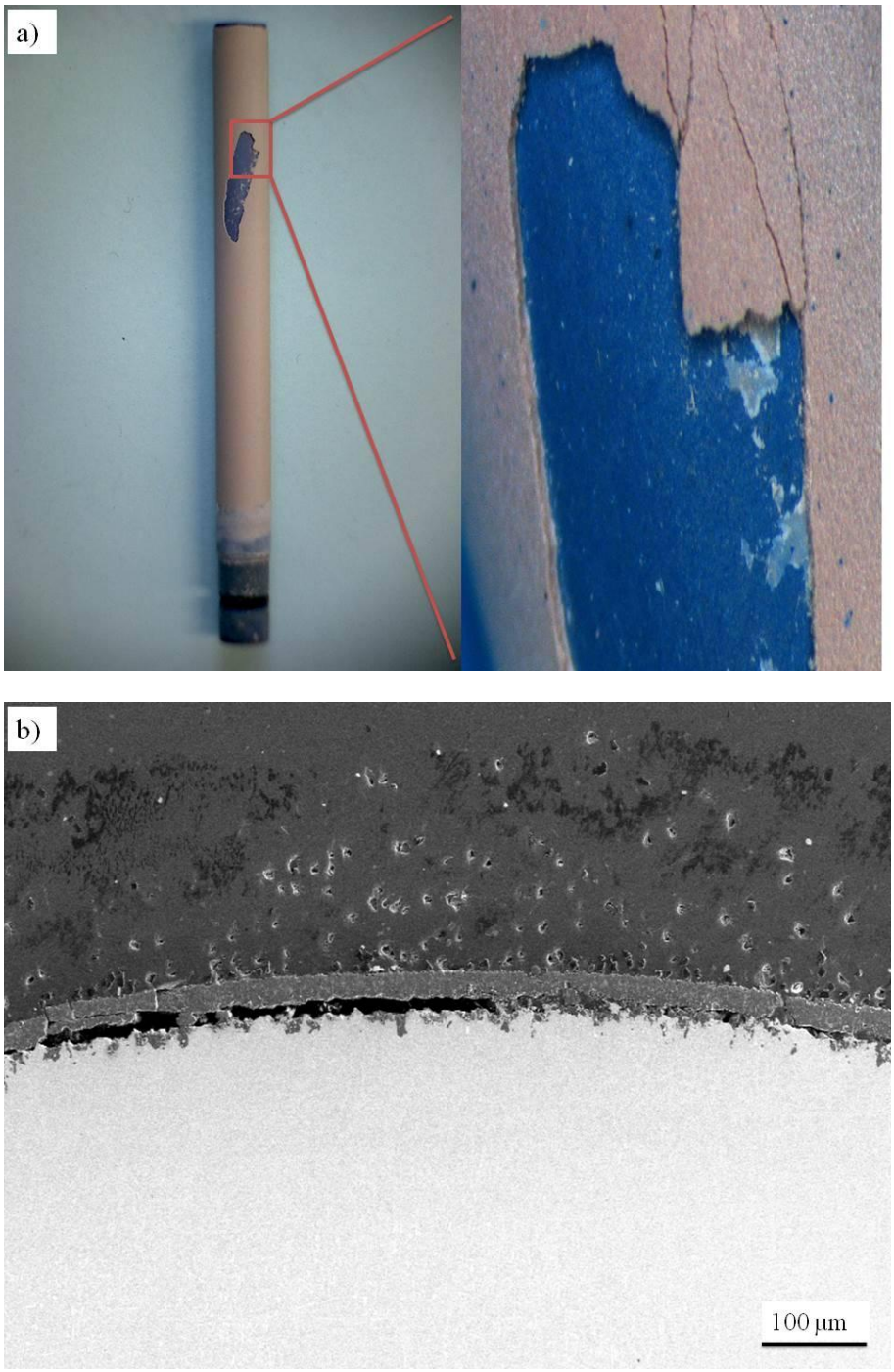

Fig. 4.28: a) Macroscopic failure pattern of GdZ- NiCoCrAlY-Hf system and b) failure location of GdZ- NiCoCrAlY-Hf TBC.

4.4.4 TGO Growth

TGO thickness for TBC systems has been shown in Fig. 4.29. Continuous line shows the TGO growth for standard 7YSZ- NiCoCrAlY- IN100 which has been taken from DLR data-base consisting of measurement from more than 10 samples. For other TBC systems, limited number of samples has been tested. TGO thickness has been measured at minimum of three different locations for each TBC system and three measurements have been taken for each location making it a minimum of nine measurements for each sample. As GdZ based TBCs on IN100 substrate have shown relatively longer lifetimes and TGO thicknesses have been measurement mostly after their spallation, TGO thicknesses for smaller number of cycles are not available. However, when each point on TGO thickness curve for single layer GdZ TBCs is considered, it can be seen that the TGO growth is slightly slower for single layer GdZ TBCs. For double layer GdZ TBC, TGO growth has been found to be very similar to that of standard 7YSZ TBC. In case of TGO thickness for GdZ- NiCoCrAlY-2 system, the growth rate appears to be very similar to that of GdZ- NiCoCrAlY system. Similarly the TGO growth for 7YSZ- NiCoCrAlY- 2 system (not shown in the Fig.) has been found to be very similar to that of 7YSZ- NiCoCrAlY system.

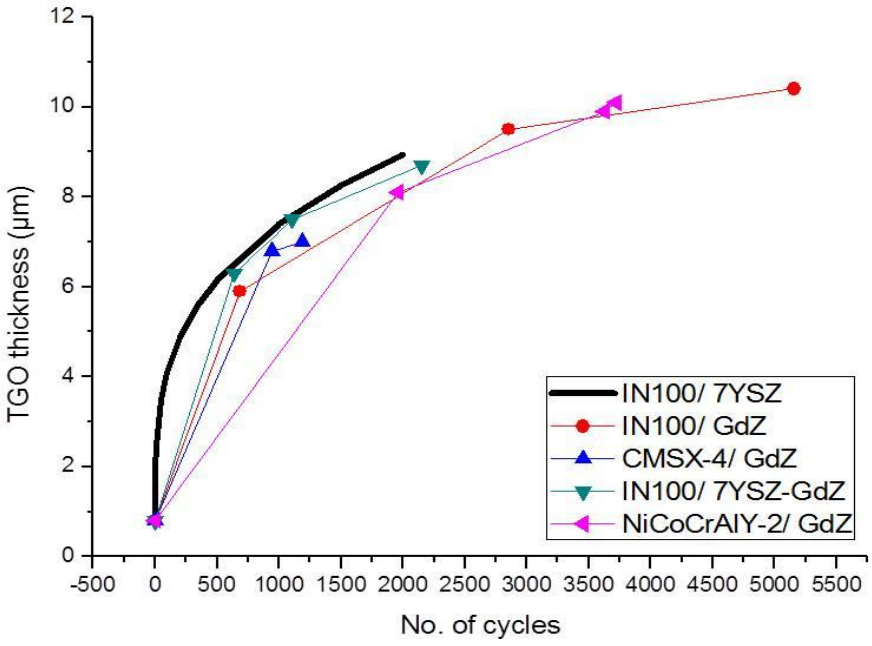

Fig. 4.29: TGO growth for different TBC systems tested in this study.

It has been observed that Hf increases the TGO growth rate for TBC systems. However, when the effect of GdZ on the TGO growth for NiCoCrAlY-Hf based systems has been investigated, it was observed that TGO growth rate is higher for GdZ based TBC system than their 7YSZ

counterpart. TGO growth rate for NiCoCrAlY-Hf TBCs is shown in Fig. 4.30b. The TGO growth for GdZ- NiCoCrAlY-Hf TBC system is not shown in the form of parabolic curve as the TGO thickness values for lesser thermal cycles are not available. As already mentioned, TGO growth in case of NiCoCrAlY-Hf based systems is not uniform and Hf- oxide stringers grow very quickly and deep into the bond coat. Fig. 4.30 shows the schematically the TGO thickness measured for this study. The Hf- oxide stringers are not included in the TGO thickness for the TGO growth study as the depth of Hf- oxide stringers varies significantly.

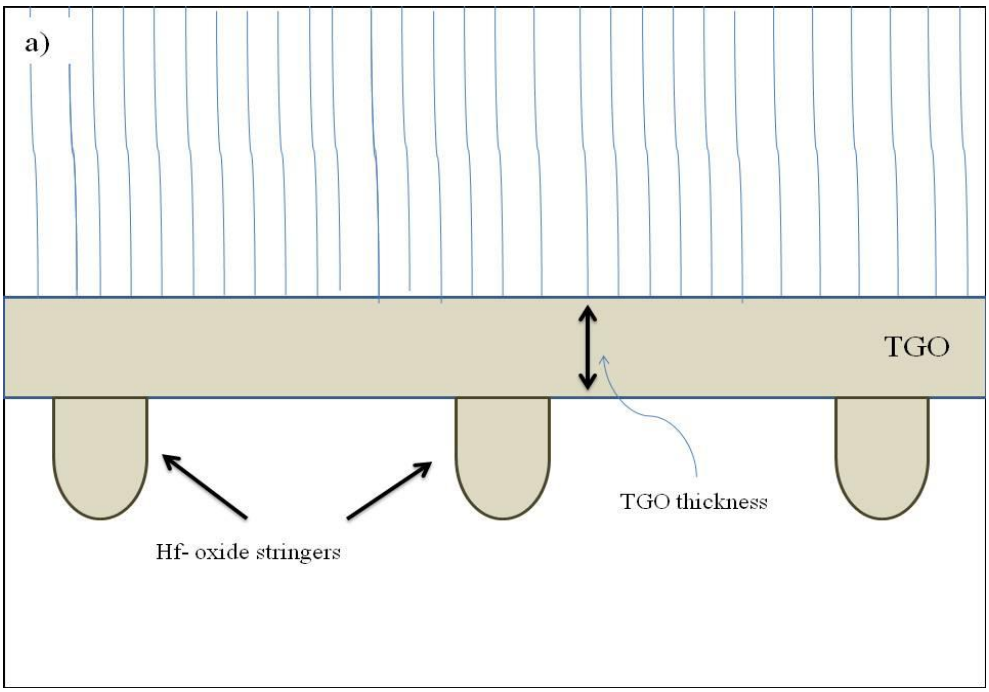

b)

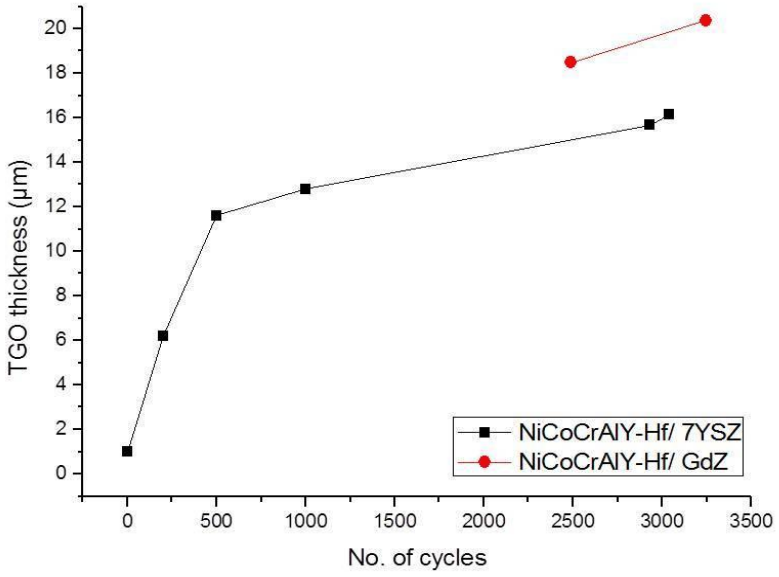

Fig. 4.30: a) TGO thickness measurement for the NiCoCrAlY-Hf based TBC systems and b) TGO growth of NiCoCrAlY-Hf based TBC systems with 7YSZ and GdZ as top coat materials.

5- Discussion

In this study, the effects of different bond coat and ceramic top coat compositions on IN100 and CMSX-4 based standard TBC systems have been investigated. The standard TBC systems refer to 7YSZ and NiCoCrAlY based TBC systems with IN100 or CMSX-4 superalloy substrate. The deposition parameters adopted for this study have been the same for all the bond coat and top coat compositions so that the effect of each and every material on the lifetime of TBC systems and the resulting failure mechanisms can be compared.

5.1 Lifetime investigations

The results from the previous section clearly indicate that TBC is a very complicated system and interplay between substrate, bond coat, TGO and ceramic top coat and all manufacturing steps affect the lifetime of a TBC system. There are several factors which effect the lifetime of a TBC system.

5.1.1 Ceramic top coat effect

It is clear from Fig. 4.19 that GdZ as top coat material improves the lifetime of IN100 and CMSX-4 based TBC systems with NiCoCrAlY as the bond coat material. In this study, single layer GdZ showed better lifetime than the double layer GdZ on IN100 based TBCs. This is contrary to the investigations done on PS systems where double layer GdZ TBCs showed a better lifetime than the single layer ones [101, 168]. Shorter lifetime results for plasma-sprayed TBC systems have been explained by a lower fracture toughness of GdZ in comparison to 7YSZ. Lower value of toughness allows a crack to grow even with lower stress levels. As the stresses at the TGO-TBC and TGO-BC interfaces are higher than in the bulk of the coatings, 7YSZ has been used as a buffer layer between GdZ and TGO to accommodate the higher stresses at TBC-TGO interface. Furthermore, in [168] the failure location in the double layer TBC systems has been found to be very close to the interface between the two ceramic layers which has never been the case in the present study with the double layer systems. This clearly indicates that in the PS systems, the failure is mainly governed by the difference in the physical properties. The EB-PVD columnar structure is more strain-tolerant, which implies that the difference in the coefficient of thermal expansion (CTE) might not cause a big problem and columnar structure has the capability to accommodate more stresses. This has been proposed in [50] that for EB-PVD systems, chemical aspects of failure and TGO formation could dominate over thermo-mechanical effects. This seems to be the case in the present study where GdZ showed better lifetime despite its lower fracture toughness and slightly lower co-efficient of thermal expansion. This is important to mention here that the current results are based on cyclic furnace test while some other results on similar PS TBCs were obtained in a gas flame thermal shock testing arrangement [101, 169]. The samples used in gas flame heating arrangements are usually disc shaped substrates which are coated from one side and are cooled from the other. In these

samples, delamination may start from the edge of the sample. However, in the present study, the samples are cylindrical rods where the top corners are rounded to avoid sharp edges. Further, in case of gas flame heating arrangement, a temperature gradient results in a reduction of temperature at the bond coat- top coat interface. In this study, there has been no temperature gradient across the sample thickness which means the temperature is the same throughout the TBC thickness and this results in severe oxidation of the bond coat. Because of these differences, the failure mechanisms under gas flame testing arrangement may be different and could be an additional reason for the opposite finding of the current work, i.e. longer lifetime for single layer TBCs. Lanthanum zirconate (LnZ) is another pyrochlore material, where double-layer PS TBCs showed a longer lifetime than the single-layer PS TBCs [101]. Results on double layer EB-PVD new TBC compositions are rather limited in literature, but they also indicate a longer life of double layers compared to single layers of new top coat compositions. W. Ma et al. reported a slightly longer lifetime for double layer $La_2Ce_2O_7$ compared to both the single layer system and the standard 7YSZ material, and a very short lifetime of the single layer $La_2Ce_2O_7$ [169]. However, the failure location for the double layer system was found to be at the interface between $La_2Ce_2O_7$ and 7YSZ layers. This has been explained by a temperature difference between the two ceramic layers during testing in a temperature gradient, resulting in different sintering effects rates and hence resulting in parallel contraction of the $La_2Ce_2O_7$ coating surface [169]. In one other study, Zhao et al. reported a higher lifetime for double layer samarium zirconate (SZO) TBCs than the single layer SZO TBCs. The main reason for a lower lifetime in single layer SZO TBC systems has been found to be a chemical reaction between SZO and TGO [170]. In case of double layer system, the chemical reaction was avoided and hence the lifetime of the double layer SZO TBCs was found to be longer. The results shown in the present study reveal a good adhesion between 7YSZ and the new ceramic top layer, which has been the result of clean interfaces and proper pre-heating during EB-PVD processing that lead to columns which nearly grow through (see Fig. 4.15a and Fig. 4.16). There has been no notable interruption of column morphology from the 7YSZ layer to the GdZ top layer despite the fact that deposition of the latter was done with interruptions of several days and samples had been stored outside the vacuum. After thermal cycling, Gd has been observed in between the 7YSZ columns close to the double layer interface. Due to this diffusion of Gd towards the column gaps of the 7YSZ layer, the inter-columnar porosity in the 7YSZ layer close to the interface totally disappears.

5.1.2 Bond Coat effect

Different bond coats have been tested on different substrate materials in this study. It has been already mentioned in [171, 172] that CMSX-4 based TBC systems with 7YSZ ceramic top coat material show a longer lifetime when the bond coat is PtAl based diffusion coating than NiCoCrAlY based overlay coating. In this study, however, NiCoCrAlY is deposited as the standard bond coat material on both IN100 and CMSX-4. Further, different bond coat pre-treatments also play an important role in the lifetime of TBC systems. In this study, the samples

are annealed for 4 h at 1080C in vacuum which is also a finding from previous work where annealing at lower temperatures or in other environment showed a lower lifetime [67, 173]. As expected, the lifetime for CMSX-4 based systems with NiCoCrAlY bond coat has been lower as compared to its IN100 counterparts. However, it has been demonstrated in a previous study that addition of 1.0 wt % SiHf in NiCoCrAlY bond coat causes a significant improvement in the lifetime of CMSX-4 based TBC systems [33]. However, Si was not found in the TBC system in that study and it is considered that the lifetime improvement has been caused by the beneficial effect of Hf. Such an improvement in the lifetime for IN100 based systems was not observed when NiCoCrAlY was doped with Hf [33]. Therefore, in this study Hf- doping for NiCoCrAlY bond coat is not done for IN100 based system. However, doping of NiCoCrAlY with 0.6 wt % of Hf has shown an improvement of more than 10 times for CMSX-4 based TBCs. When the effect of Hf- content in NiCoCrAlY for CMSX-4 based system with 7YSZ ceramic top coat is plotted against the lifetime from this and previous studies, an almost linear relationship is obtained, shown in Fig. 5.1. However, it remains to further research that what is the longest lifetime possible by Hf- doping of NiCoCrAlY bond coat for CMSX-4 systems.

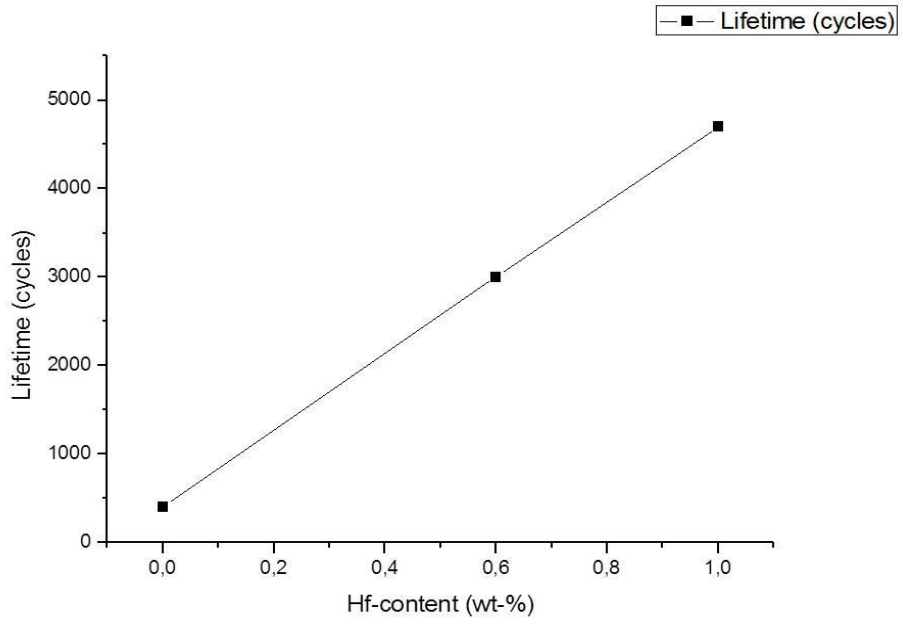

Fig. 5.1: Lifetime vs Hf- content in NiCoCrAlY bond coat on CMSX-4 substrate.

On the NiCoCrAlY bond coats for both IN100 and CMSX-4 based systems, replacement of 7YSZ by GdZ causes an increase in the lifetime by almost a factor of 4. However, such an improvement in lifetime has not been seen for NiCoCrAlY-Hf based system and a similar lifetime is observed when 7YSZ is replaced by GdZ on NiCoCrAlY-Hf based systems. It is important to mention here that the lifetime of CMSX-4- NiCoCrAlY-Hf-7YSZ is already very

long and is comparable to the one obtained for IN100- NiCoCrAlY-GdZ system. It cannot be ruled out that the maximum lifetime obtained with GdZ ceramic top coat after equilibrium is reached between sintering, stress accumulation and stored interfacial energy etc. is in the range of 3000 cycles. Other TBC systems where GdZ doesn't improve the lifetime of TBC systems have been IN100 and PtAl based systems where GdZ is deposited as single and double layer [174]. On PtAl bond coats, double layer GdZ TBCs show better lifetime than the single layer TBCs, although the lifetime for both single and double layer GdZ TBCs has been quite low. The lifetime of double layer GdZ TBC has been found to be very similar to the standard 7YSZ system [174].

In this study, NiCoCrAlY bond coat on IN100 substrates has been doped with an additional amount of yttrium and the impact on the lifetime and microstructure has been investigated. It has been shown in Fig. 4.3 that increasing the amount of yttrium in NiCoCrAlY from 0.19 wt % to 0.42 wt % doesn't improve the lifetime of TBC systems with 7YSZ the ceramic top coat. In fact, the lifetime has been slightly decreased by this additional doping of yttrium. However, TBC systems with the same NiCoCrAlY-2 bond coat show an increase in the lifetime when GdZ is deposited as the top coat material. The lifetime comparison between NiCoCrAlY and NiCoCrAlY-2 based TBC systems with GdZ as the top coat material show that the lifetime for NiCoCrAlY-2 based TBC system is not only higher but the scatter in lifetime results is also lower. However, as the number of specimens is limited, these results still indicate preliminary findings on the lifetime investigations.

5.1.3 Substrate Effect

A part of the following discussion has already been published [187]. Singe crystal superalloys offer very high creep strength at elevated temperatures. However, in this study single crystal superalloy has shown a lower lifetime as compared to a polycrystalline superalloy when the bond coat and ceramic top coat are kept the same. This confirms that compatibility between the different components of a TBC system is very important in order to achieve a longer lifetime. Effect of substrate material on the lifetime of TBC systems has been investigated in several studies before. It has already been reported that CMSX-4 based systems show a lower lifetime than IN100 based ones when NiCoCrAlY and 7YSZ are the other constituents of a TBC system. Same results have been obtained during this study as well. In addition, the same trend has been observed when 7YSZ is replaced by GdZ. This main difference is most likely caused by the difference in alloying elements present in CMSX-4 and IN100. The single crystal structure of CMSX-4 could not be the problem since absence of grain boundaries should be advantageous by avoiding the faster diffusion at the grain boundaries. It has been argued earlier that carbon which ties up the diffusion of detrimental elements in polycrystalline and DS alloys is not present in CMSX-4 which may allow detrimental elements to diffuse to the TGO through the bond coat.

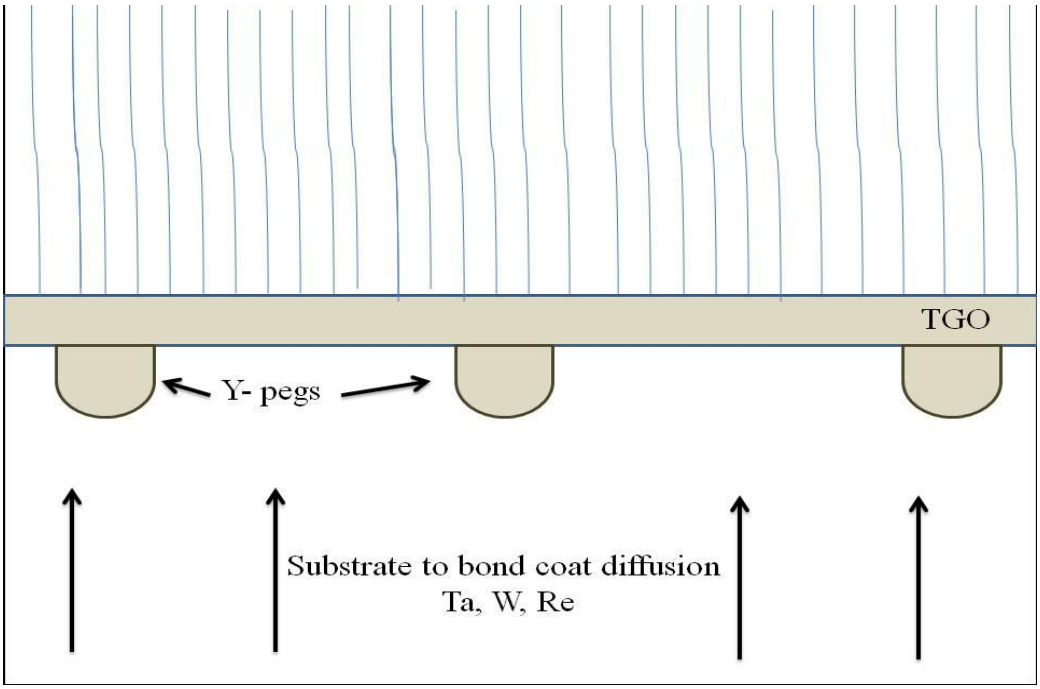

Fig. 5.2: Diffusion of refractory elements from the substrate towards the bond coat.

One of the previous studies also showed a similar result where TBC systems with directionally solidified superalloys showed a better lifetime than the ones with single-crystal superalloys [175]. The main reason reported for this lower lifetime is the difference in CTE value between the substrate and the bond coat. As single-crystal superalloys have a lower CTE value [175, 176], the stresses accumulate due to a relatively higher CTE of the bond coat. In the same study, micro-porosity has been observed at the bond coat- substrate interface which clearly indicates differences in the CTE values of the bond coat and the substrate [175]. Such a micro porosity has not been observed at the substrate- bond coat interface for this study. However, diffusion of refractory elements Ta, W and Re has been observed from CMSX-4 substrate towards the TGO in this study. Diffusion of elements from the substrate towards the TGO has been observed in a previous study as well. Schulz et al. reported diffusion of Hf from the directionally solidified substrates towards the TGO. Hf has been reported to improve the lifetime of both TBC systems with directionally solidified substrates [176]. It is important to understand the effect of each diffusing elements on the lifetime of TBC systems. In one of the previous studies, an attempt has been made to understand the effect of each refractory element present in the CMSX-4 superalloy on the lifetime of TBC systems with NiCoCrAlY as the bond coat [177]. In that study, NiCoCrAlY bond coat is doped with different refractory elements and this doped version of NiCoCrAlY is used as the substrate material. In addition to doping NiCoCrAlY with Ta, W or Re, it was doped with all Ta, W and Re together as well to understand the effect on the lifetime. Furnace cyclic testing was performed for each system and it was observed that the shortest lifetime is observed when NiCoCrAlY is doped with Ta. A longer lifetime was observed even

when NiCoCrAlY was doped with all three refractory elements Ta, W and Re together [177]. This shows that Ta is the most harmful element present in CMSX-4 substrate. Since a longer lifetime is obtained when NiCoCrAlY is doped with all three Ta, W and Re, it can be argued that W and Re reduce the harmful effect of Ta. Conversely, it can be said that in the absence of W and Re, Ta reduces lifetime of the TBC systems more. There is a possibility that Ta might have a higher diffusion rate, had W and Re not present in the substrate. In this study, however, it has been observed that W diffuses faster than Ta and is mostly present in a greater amount than the other two refractory elements at most of the locations in the bond coat. Re has been found to diffuse the least. Inter-diffusion of W, Ta and Re in γ-Ni has been reported in the literature [178, 179]. It has been mentioned that among W, Ta and Re, Ta has the highest diffusivity in γ-Ni, while Re has the lowest diffusivity. These diffusivity measurements have been conducted at the temperature range of 900-1300°C. In another study with different versions of Rene N5 alloy, it has been reported that Ta segregates at the TGO- bond coat interface [180]. It has been reported that elements like Ta, Co, Cr and W are enriched in the grain boundaries of the bond coat and lead to the formation of less protective, less adherent oxides at these regions [180]. Diffusion of different elements from the substrate towards the bond coat has been reported in previous studies [176, 181, 182]. For example, diffusion of Hf has been observed from the substrate towards TGO in [176, 182] while in [181] diffusion of Ta, Ti and W has been observed from the substrate towards the bond coat. However, diffusion of Hf towards TGO has resulted in longer lifetimes while the diffusion of Ta and W has been found to result in shorter lifetimes [177, 180], as is also the case in the present study.

5.2 Morphology of Ceramic top coat materials

EB-PVD ceramic top coats consist of columnar microstructure, which is also evident in this study for both 7YSZ and GdZ. The morphology of EB-PVD columns depends on the process parameters like the substrate temperature, rotation speed chamber pressure etc., adopted during the EB-PVD deposition [54]. Various microstructural features like inter and intra-columnar porosity and feather arms are strongly influenced by the rotation speed during EB-PVD deposition. Similarly, the substrate temperature affects the number of nucleated primary columns and the activation of surface diffusion that influences the continuity of the nucleated intra-columnar pores and the voids between feather arms. Effect of process parameters on the microstructure of EB-PVD columns has been discussed in detail in literature. Schulz [54] reported the creation of microstructure analogous to “fine”, “intermediate” and “parallel” which can be obtained by using similar process parameters. Out of the above mentioned microstructures, the “intermediate” EB-PVD coatings show one of the highest total porosity values and are obtained by rotation the specimens at 12rpm during ceramic top coat deposition and pre-heating the substrate to a temperature of around 950- 1000°C [59]. The same process parameters have been used in this study to achieve the “intermediate” microstructure, however, the microstructure obtained for 7YSZ and GdZ are still different to each other. GdZ columns

have been found to be curved in one direction and also the diameter changes significantly over the length of the columns. The direction of curvature of GdZ columns has been found to be the same as the direction of rotation during EB-PVD deposition. By changing the direction of rotation during deposition, direction of curvature can also be changed. Further, there is excessive column branching at the tips of the columns which also weaken the texture of GdZ coatings as compared to zirconia-based TBCs. In one of the studies, pole figures for 7YSZ showed a strong alignment of columns in <100> growth direction, however, for GdZ broader peaks and lower pole density has been observed [174]. Since the measurement depth of the used Cu radiation is in the order of a few ten microns, the pole figures represent mainly the top region of the TBC which is for GdZ characterized by column branching and a variety of column orientation with respect to the perpendicular of the sample. Consequently, this special mode of growth for GdZ is reflected in the pole figures. Curvature of the columns towards the rotational direction as clearly found in SEM cross sections does not translate into a peak shift in the pole figures since this shift should occur in horizontal direction. Further experiments and additional investigations are required to understand the reason for column curvature and additional column branching at the tip of the columns. A similar weaker texture has been observed for directed-vapor deposited samarium zirconate that also possessed some column branching. However, it can be assumed that the sharpness of the texture does not play a major role for the lifetime of the coatings.

5.3 Sintering and Phase changes during thermal cycling

It can be seen in Fig. 4.14 that GdZ does not have the pyrochlore structure in the as-coated condition. Even after 2 h annealing at 1260°C, the cubic pyrochlore peaks are not observed and the GdZ has a “disordered” cubic fluorite structure. However, when GdZ is investigated after 2850 cycles, pyrochlore peaks are observed indicating a cubic-pyrochlore ordering during thermal cycling. The result is very similar to the fluorite- pyrochlore ordering in samarium zirconate which also took place during thermal cycling [170]. In case of 7YSZ, long term exposure at high temperature causes diffusion of yttrium to form yttria-rich and yttria-depleted regions and upon cooling the latter transforms into monoclinic phase. This transformation has been found to be detrimental for the lifetime of TBC systems as there is a large volume change associated with such a transformation. However, as the GdZ based TBCs in the present study show a long lifetime, it is clear that the cubic to pyrochlore ordering during thermal cycling is not detrimental to the lifetime of GdZ-based TBCs. The discussion on phase changes and sintering of GdZ has also been published [174, 183].

The phenomenon of sintering is not desirable in the TBC systems as it causes an increase in thermal conductivity and stiffness of the ceramic top coat. As a result of an increase in stiffness, the ability of the system to accommodate stresses decreases and eventually the TBCs fail. Sintering can be observed in the TBCs by coarsening of pores, rounding off the microstructural features and also by merging of columns in inter-columnar sintering. It has been reported in

different studies that GdZ sinters less than 7YSZ when parallel columns are considered [174, 183]. Sintering in 7YSZ and GdZ can be compared by looking at the GdZ- 7YSZ interface closely in double- layer TBCs. It can be clearly seen in Fig. 4.16a and 4.16b that inter and intra-columnar pores disappear much more in 7YSZ than GdZ. Further, the feather arms in case of 7YSZ are also totally disappeared while in GdZ layer the feather arms are not totally disappeared but have taken a new step- like shape. However, the disappearing of feather arms in 7YSZ columns can also be due to the diffusion of Gd towards the column boundaries in 7YSZ layer. This is also evident from the difference in the contrast between the 7YSZ columns and also the EDX results, in this study, revealed the presence of Gd in between the 7YSZ columns. However, this diffusion of Gd towards the column boundaries of 7YSZ is limited to a certain depth and also no Gd has been observed in the bulk of 7YSZ columns. Further, no diffusion of yttrium from 7YSZ towards the GdZ layer has been observed. In a similar study with double layer samarium zirconate, Sm has been found to diffuse into the 7YSZ in a limited thickness region already during directed vapor deposition with no yttrium upward diffusion into the pyrochlore SZO [170]. This is in accordance with the present findings and suggests a faster diffusion coefficient of the gadolinium cations out of the pyrochlore than that of yttrium out of the tetragonal phase along the inter-columnar grain boundaries. In case of SZO, a continuous diffusion of Sm was found with increasing time which is not clearly evident in the current results since the presence of Gd is restricted towards the column boundaries within 7YSZ and is limited to a few microns underneath the 7YSZ- GdZ interface.

It has been observed that sintering at the tips of the columns in case of GdZ is higher when compared with the middle of the columns. GdZ column tips, in the as-coated condition, contain inter- and intra-columnar porosity, a high number of large and thin feather arms and they show considerable column branching. However, as a result of thermal cycling, the column tips seem to have undergone heavy sintering as the inter-columnar porosity (column boundaries) disappears considerably. When a comparison is made with the column tips of 7YSZ (Fig. 4.17c), inter-columnar porosity (column boundaries) can be easily seen. This can also be due to a different morphology of GdZ columns. Due to significant column branching at the columns tips, the distance between the adjacent columns decrease, however, at the middle of the columns the distance between the adjacent columns is higher. In a previous study, difference in the column diameter at the tips and middle of the columns for 7YSZ has been reported [185]. However, it has been observed that sintering is higher for 7YSZ at the bottom of the columns where the column-diameter is smaller than the tips where the diameter is slightly larger [185]. This is contrary to the findings of the current study where a higher sintering has been observed for GdZ columns tips, where the diameter is larger.

5.4 TGO Microstructure

The microstructure and composition of TGO depends on the bond coat. Yttria stabilized zirconia is a fully oxidized material and provide easy transport for oxygen by ionic transportation through the lattice and by gaseous diffusion through the networks of inter-connected micro-cracks and pores. In this study, the TGO for all the bond coats mainly consisted of alumina with some minor addition of other elements. The chemical reaction for the formation of alumina is given below:

$$2Al + 3/2\ O_2 \rightarrow Al_2O_3 \qquad 5.1$$

For any oxide to form on a metal, following equation is applicable from thermodynamic standpoint:

$$\Delta G = -RT \left(\frac{a_{oxide}}{a_{metal}^{a} \times P_{O_2}^{b}} \right) \qquad 5.2$$

ΔG = Free energy of formation of the oxide

R = Universal gas constant

T = Temperature (K)

a_{oxide} = activity of the oxide

a_{metal} = activity of the metal

P_{O2} = partial pressure of oxygen at equilibrium

For oxidation of a metal to take place, the oxygen partial pressure must be greater than this equilibrium value and G must be less than 0. This can also help to predict the expected composition of an oxide scale by plotting the activities of an oxide at various temperatures to form an Ellingham diagram which is shown in Fig. 5.3.

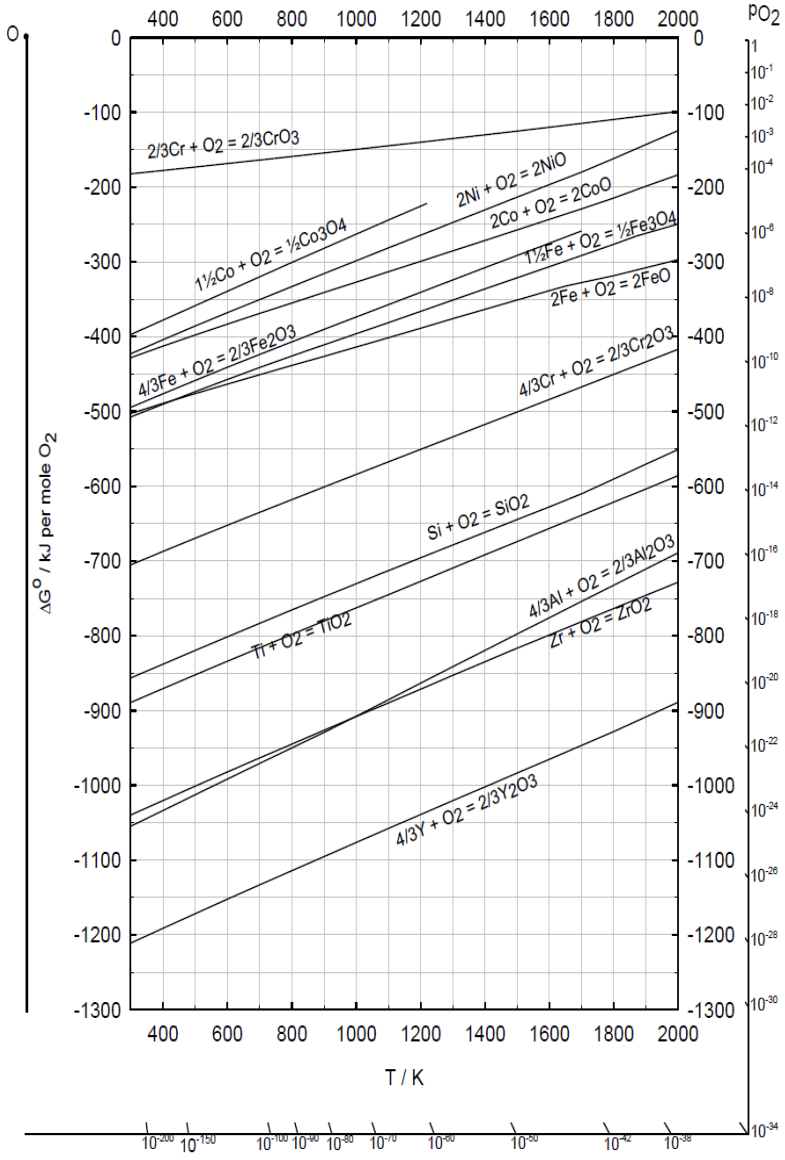

Fig. 5.3: Ellingham diagram of some oxides modified from Birks and Meier [17].

It is clear from Fig. 5.3 that yttria forms an oxide more readily than Aluminum. This is also evident from the formation of yttria islands at the TBC-TGO interface in case of NiCoCrAlY bond coats.

5.4.1 IN100 based system

In case of NiCoCrAlY2 bond coats, where the amount of yttrium is relatively higher, the effect of yttria on the TGO microstructure is even more evident.

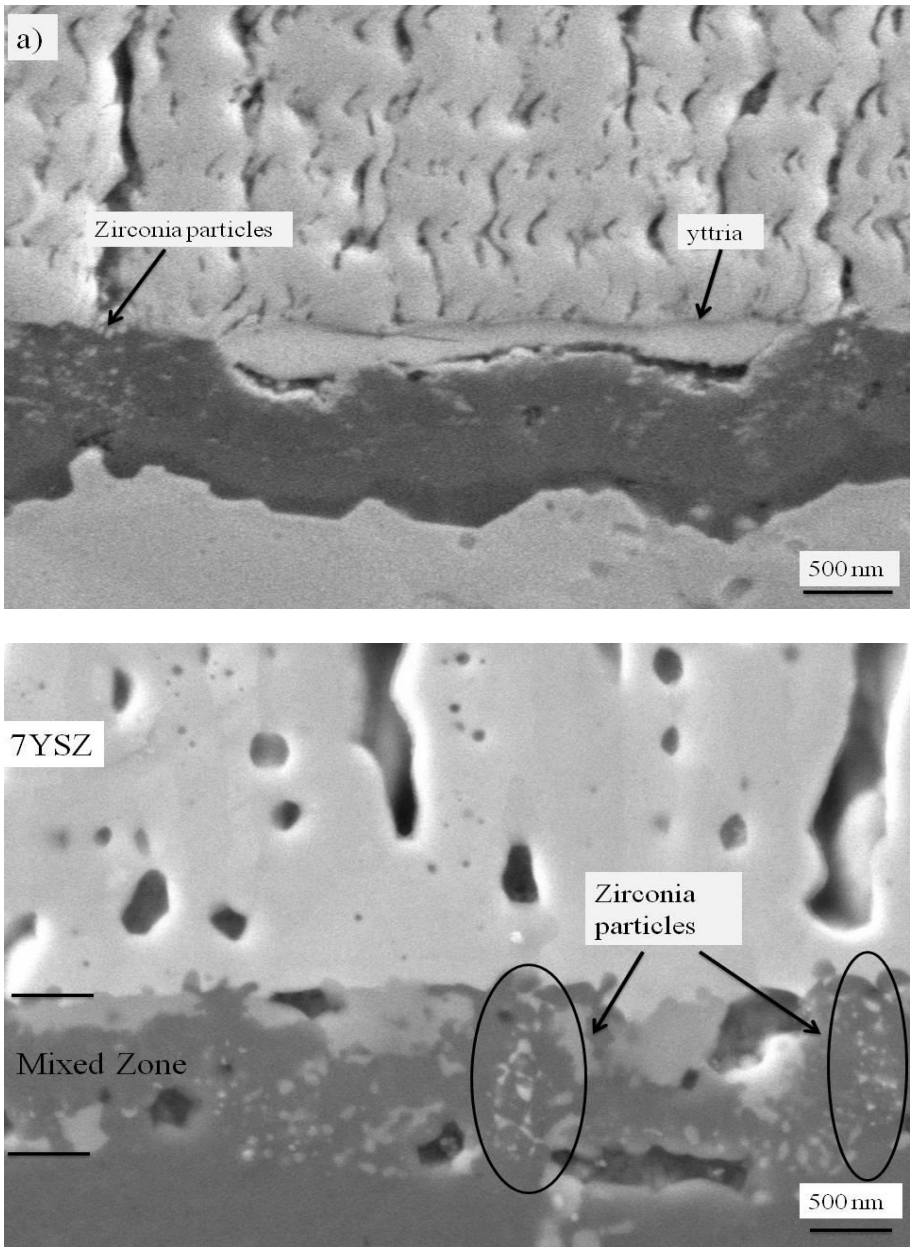

Fig. 5.4: Formation of the mixed zone for NiCoCrAlY-2 bond coat system with 7YSZ ceramic top coat.

Due to a higher amount of yttrium in the bond coat, the yttria doesn't exist in the form of islands but forms more continuous phase. This yttrium rich phase is also present after thermal cycling as shown in Fig. 5.4. The chemical reaction for the oxidation of yttrium is given below:

$$2Y + 3/2\ O_2 \rightarrow Y_2O_3 \qquad 5.3$$

It has been mentioned in literature that yttria doesn't allow zirconia to pass through it and interact with the underlying alumina. It can be seen in Fig. 5.4a that bright zirconia particles are present

in the as-coated TGO where yttria barrier is not there. However after thermal cycling, some precipitates are present with a slightly low contrast also below the yttrium rich phase. They are clearly not the zirconia particles as the contrast for zirconia particles is relatively higher. According to literature, yttria can react with alumina to form different compounds given by the following reactions.

$$Y_2O_3 + Al_2O_3 \rightarrow YAlO_3 \qquad 5.4$$

$$YAlO_3 + Al_2O_3 \rightarrow Y_3Al_5O_{12} \qquad 5.5$$

The chemical compatibility at TBC-TGO interface in case of IN100-NiCoCrAlY2-7YSZ system can also be understood from the $YO_{1.5}$, $AlO_{1.5}$ and ZrO_2 phase diagram, calculated at 1250°C.

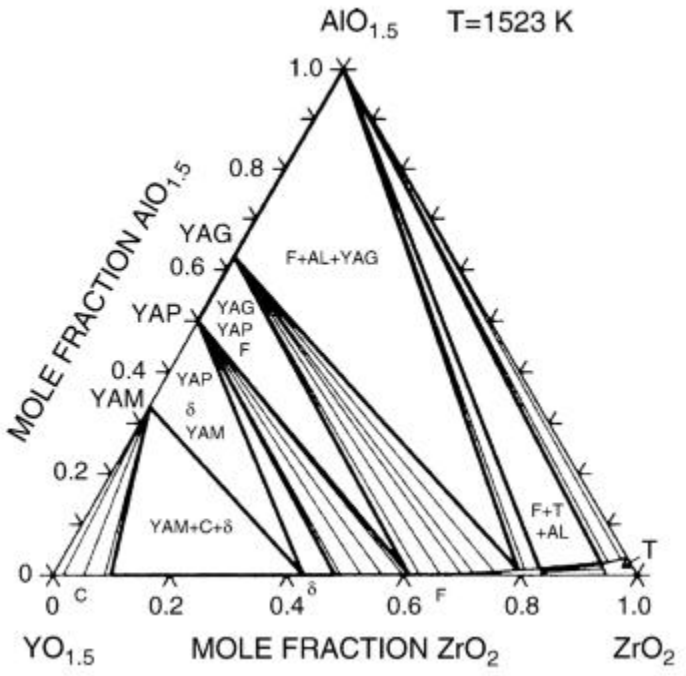

Fig. 5.5: Ternary phase diagram of $YO_{1.5}$, $AlO_{1.5}$ and ZrO_2.

The different compounds formed between Y_2O_3 and Al_2O_3 according to Fig. 5.5 are mentioned as YAG ($Y_3Al_5O_{12}$), YAP ($YAlO_3$) and YAM ($Y_4Al_2O_9$). Another possibility mentioned in the literature is that during the ceramic top coat deposition, an approximately 0.25µm thick continuous intermediate spinel layer is present below the reactive element islands (in the case of NiCOCrAlY2 bond coat, an almost continuous yttria layer). This spinel layer is formed due to a relatively higher oxygen partial pressure during the EB-PVD deposition of ceramic top coat and a steady temperature ramp from room temperature to 1000°C. These spinels also react with yttria during the thermal cycling of TBC systems and the chemical reaction is given below:

$$(Ni, Co)(Al, Cr)_2O_4 + Y_2O_3 \rightarrow 2YAlO_3 + MeO \ (M = Cr, Co, Ni) \qquad 5.6$$

The spinels may contain any of the above mentioned metals depending upon the availability at that particular location, however, the order of oxide forming tendency for each metal will still be governed by the Ellingham diagram shown in Fig. 5.3.

5.4.2 CMSX-4 based systems

In case of standard CMSX-4 based system, the TGO doesn't show a uniform mixed zone. This has not been the case for IN100 based systems where the mixed zone has been found to be more or less uniform for the standard systems. For CMSX-4 based systems, the mixed zone after thermal cycling has been found to be quite thick at some locations. In the as-coated condition, however, the thickness of the TGO has not been found to be that much. This means there has been an increase in the thickness during thermal cycling which could be the result of diffusion of elements from the substrate or the bond coat. In some EDX measurements, very small amount of refractory elements has been observed. However, it is not clear if these elements are actually present there or this is just a noise in the EDX signals. Also, the mechanism of refractory elements diffusion through the TGO to reach the mixed zone is not clear when the refractory elements have not been found in the bulk TGO.

In case of NiCoCrAlY-Hf bond coat systems with 7YSZ as the ceramic top coat, a different TGO growth has been observed when compared with the standard NiCoCrAlY systems. It has been observed that Hf diffuses very quickly towards the TGO and forms oxides on both sides of the TGO even during the ceramic top coat deposition. Such quick diffusion of Hf is not observed in those cases where Hf is present only in the substrate material and not in the bond coats . Also when Hf diffuses from the substrate towards the TGO, it is mostly found in the lower parts of the TGO. However in this study and the previous one where Hf is present in the NiCoCrAlY bond coat, it is also present at the TBC-TGO interface. Diffusion in case of MCrAlY-Hf is faster than for Y, and consequently the tendency for surface enrichment is higher for Hf as compared to Y as shown in [33]. Due to this strong affinity of Hf towards oxygen, Hf- stringers are formed very quickly and they run very deep into the bond coat. Even after only 100 cycles, the depth of Hf-stringers has been found to be as deep as 20µm. These Hf- stringers may act as crack stoppers as an interface crack has to change its propagation direction repeatedly if it follows intimately the TGO- bond coat interface that possesses the lowest interface toughness. Due to this abnormal growth of TGO, the bond coat is entrapped within the TGO at several locations and this bond coat later oxidizes to form spinel according to following reaction:

$$Me + 2Cr + 2O_2 \rightarrow MeCr_2O_4 \ (\text{where } Me = Ni, Co, Cr) \qquad 5.7$$

According to literature, a volume expansion of around 105% is associated with the formation of spinels which usually imposes a marked increase in out-of-plane displacements compared with alumina formation [167]. However in this study, the formation of spinels has not been found

detrimental for lifetime of NiCoCrAlY-Hf based TBC systems. This can be due to the formation of Hf- stringers which plan an anchoring role for the TGO in the bond coat. It has also been mentioned in the literature that Hf improves adhesion between TGO and bond coat which is explained by shortening of metal- oxide distance due to strong bond formation between Hf and the neighboring oxygen atoms in Al_2O_3. Hf has an open d-shell structure which allows it to form a mixture of ionic, covalent and donor-accepter character, which increases the bond density by 25% and as a result makes the bonds particularly strong [186].

The lower lifetime of CMSX-4 and NiCoCrAlY based TBC systems has been reported to be due to the diffusion of "undesirable" elements from the superalloy substrate towards the TGO. In this study, diffusion of Ta, W and Re has been already mentioned. These refractory elements diffuse continuously from the substrate towards the TGO and there is a continuous increase in their amount along with thermal cycling. As NiCoCrAlY-Hf systems have shown longer lifetimes, the continuous diffusion of refractory elements creates a region at the TGO- bond coat interface which is rich in refractory elements. This refractory rich region is termed in this study as "Hf-depleted" region as no Hf is found in this region. It looks like these refractory elements reduce the adhesion between the TGO and the bond coat so much that at some stage Hf- stringers also don't provide enough strength. It has been observed that addition of Hf to the NiCoCrAlY does not influence the diffusion of refractory elements. After 100 cycles, a very similar amount of refractory elements has been found for both NiCoCrAlY and NiCoCrAlY-Hf bond coats. The improvement of lifetime is mainly due to the Hf- stringers which are not present in the standard NiCoCrAlY bond coat and due to the improved adhesion which Hf imparts at the TGO- bond coat interface [36, 37,186].

5.4.3 Ceramic top coat effect on the TGO

The TGO microstructure for different bond coats with 7YSZ as the ceramic top coat has been discussed in the previous sections. In case of single layer GdZ- TBC on NiCoCrAlY bond coats, some interaction between TGO and TBC is observed. As it can be seen in the Fig. 4.20a, a new phase starts to form in the early stages of thermal cycling and then become more and more continuous with thermal cycling. After 685 cycles, the reaction phase is visible in small patches and is not continuous, however after 5000 cycles, the reaction phase becomes continuous as can be seen in Fig. 4.20b. The thickness of this reaction phase after 5000 cycles has been found to be between 200-500nm which shows that the growth of this phase is not very fast.

To understand the interaction between GdZ and alumina, a ternary phase diagram between $AlO_{1.5}$-$GdO_{1.5}$-ZrO_2 $YAlO_3$ is shown in Fig. 5.6. This phase diagram has been developed at 1200°C, which is taken as an upper bound for the temperature of the TBC-TGO interface in TBC systems. As already mentioned, zirconia and alumina are thermo-chemically compatible; which means they do not form inter-phases and their mutual solubility is very limited. The $AlO_{1.5}$-$GdO_{1.5}$ system also doesn't show any significant mutual solubility of the terminal oxide,

however, shows two line compounds of orthorhombic perovskite and monoclinic structure. These two compounds are $GdAlO_3$ and $Gd_4Al_2O_9$ which are represented in the phase diagram by symbols GAP and GAM respectively.

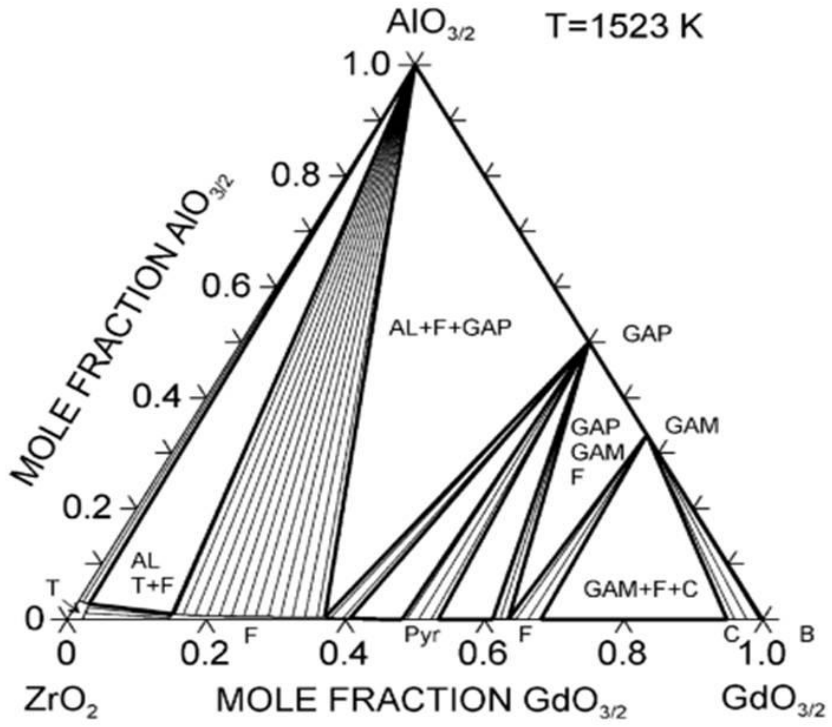

Fig. 5.6: Isothermal sections at 1250°C for $AlO_{1.5}$-$GdO_{1.5}$-ZrO_2 system [108].

The chemical reaction between GdZ and alumina has been mentioned in the literature where GdZ is deposited on sapphire (alumina) substrate and isothermal treatment is performed at 1100 and 1200°C. It was observed that $GdAlO_3$ forms as a result of the chemical reaction according to the following chemical reaction [107]:

$$Gd_2Zr_2O_7 + Al_2O_3 \rightarrow 2GdAlO_3 + 2ZrO_2 \qquad 5.8$$

This also seems to be the case in the present study where careful EDX indications revealed the elements of Gd, Al and O in the interaction zone. In a study with samarium zirconate on NiCoCrAlY bond coat, the chemical reaction between TBC and TGO leads to the formation of $SmAlO_3$ [170]. It has been mentioned in [107] that isothermal treatments at different temperatures lead to different reaction rates. As expected, the thickness of the interaction zone is reduced as the temperature of treatment is lowered from 1200°C to 1100°C. It was observed that

after 100 h treatment at 1200°C, the interaction zone is 700nm while after the same duration a treatment at 1100°C leads to an interaction zone of 100nm. The perovskite $GdAlO_3$ phase formed in the study [107] has been found to contain porosity towards its interface with the substrate which is detrimental for TBC adherence. However in the present study, no such porosity has been observed which reduces the TBC adherence. Instead, very long lifetimes have been obtained for GdZ- NiCoCrAlY TBCs where such a chemical reaction has been observed. The difference in the findings in the present study can be due to the fact that there is a mixed zone at the TBC- TGO interface which contains zirconia particles with some yttrium aluminates along with traces of Ni, Co or Cr. In a recent study, where GdZ was deposited on PtAl bond coat, no chemical reaction was observed between the GdZ and alumina [174]. It can be due to very short lifetimes of GdZ- PtAl TBCs which shows that GdZ- alumina chemical reaction is facilitated by higher temperatures with longer time durations. This trend is also consistent with the absence of any interaction between GdZ- alumina during the EB-PVD deposition as the temperature is low (~ 1000°C) and the exposure time is also very short (~1 h) [107] which is the case in the present study as well, although deposition time has been less than 1 h in the present study.

In case of GdZ on NiCoCrAlY2 bond coat, the situation becomes more complicated since yttria is also present almost continuously at the TBC-TGO interface. Database for ZrO_2-$GdO_{1.5}$-$YO_{1.5}$-$AlO_{1.5}$ system has been reported in the literature [184]. The thermodynamic data base has been based on an assumption that ideal solubility exists between perovskite, garnet and monoclinic phases namely LnAP, LnAG and LnAM respectively [184]. The ternary phase diagrams of ZrO_2-$AlO_{1.5}$-$YO_{1.5}$ and ZrO_2-$GdO_{1.5}$-$AlO_{1.5}$ have already been shown and discussed. A ternary phase diagram on $AlO_{1.5}$-$GdO_{1.5}$-$YO_{1.5}$ here would complete the story and is shown in Fig. 5.7.

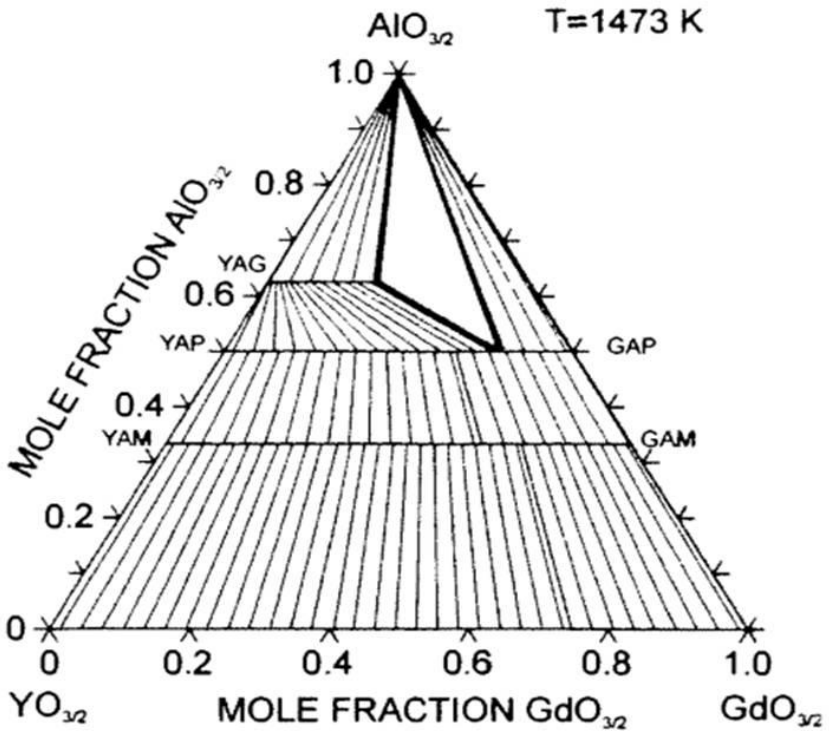

Fig. 5.7: Isothermal sections of $AlO_{1.5}$-$GdO_{1.5}$-$YO_{1.5}$ system at 1200°C [184].

As can be seen in Fig. 5.7, the garnet phase on the Y- side is destabilized by the addition of Gd which is expected from its absence in $AlO_{1.5}$-$GdO_{1.5}$ binary. Further, both the maximum Gd content in the LnAG phase and the minimum Gd content to reach direct equilibrium between the LnAP and corundum phase decrease with increasing temperature [184]. In the present study, a reaction zone with alternating phases forms at the TBC-TGO interface as a result of thermal cycling of GdZ- NiCoCrAlY2 system. EDX results show that the light and dark compositions are aluminates with higher Gd and Y- content respectively. As the ZrO_2-$GdO_{1.5}$-$YO_{1.5}$-$AlO_{1.5}$ data base doesn't show any additional new complex phases containing both Y and Gd, it can be assumed that the two perovskite phases of different Y and Gd content exist next to each other. It is possible that the locally high yttrium contents in the islands have triggered the formation of the yttrium-rich phase while the reaction between alumina and GdZ results in the Gd-rich phase [174]. These alternating phase are almost continuously present at the TBC-TGO interface, even after thermal cycling for 1960 cycles. It means that the chemical reaction is faster in case of NiCoCrAlY2 bond coat than that of standard NiCoCrAlY bond coat where even after 2800 cycles, the interaction zone is not so continuous. To have an exact identification of these phases present at the TBC-TGO interface for GdZ-NiCoCrAlY-2 system and to identify the position of the excess Zr that is left over in the reaction, transmission electron microscopy (TEM) is needed which is the topic of ongoing research.

Along with the chemical reaction between GdZ and TGO, some diffusion of aluminum is also observed from the TGO towards the TBC as shown in Fig. 4.22. This diffusion of Al for single layer GdZ TBCs has been found in both IN100 and CMSX-4 systems with NiCoCrAlY being the bond coat. However, the diffusion of Al has been found till a very limited depth inside the GdZ layer and this depth doesn't change much with thermal cycling. In previous studies with GdZ on alumina, no such diffusion has been reported [101, 107]. The difference in the findings can be due to the fact that in the present study, GdZ is not in contact with pure alumina but there is a mixed zone at the TBC-TGO interface which consists of a variety of phases and elements. However, despite this diffusion single layer GdZ on NiCoCrAlY bond coats have shown excellent lifetimes which means that this diffusion is not detrimental for the TBC lifetimes.

In case of GdZ on NiCoCrAlY-Hf bond coat, no significant chemical reaction between GdZ and TGO has been observed after thermal cycling despite thermal cycling for a very long time. This can be due to the fact that Hf diffuses towards the TGO at the early stages of ceramic top coat deposition and oxidizes over there. Even during the thermal cycling, Hf continuously oxidizes in the growing TGO. The composition of TGO in contact with GdZ plays an important role in the chemical reaction between GdZ and TGO. In case of the previous study where GdZ on pure alumina have been isothermally treated, 100 h isothermal heating resulted in an interaction zone of 100nm. However in this study, thermal cycling of GdZ on NiCoCrAlY for 5000 cycles results in an interaction zone of only 200-500nm. Similarly, a different reaction rate has been observed for GdZ on NiCoCrAlY2 bond coat. However in case of NiCoCrAlY-Hf bond coat, no chemical reaction between GdZ and TGO has been observed even after 3000 cycles. This can be due to the fact that regions of pure alumina are very seldom in contact with GdZ and consequently the reaction cannot take place.

5.5 Failure Mechanisms and Locations

Macroscopic failure patterns for different TBC systems on IN100 substrate have been shown in Fig. 4.25. It can be seen that single layer GdZ on NiCoCrAlY with IN100 substrate material show mud- cracking type failure. According to literature, such failure pattern arises from the inter-columnar sintering of the ceramic top coat material. It has been already mentioned that GdZ undergoes heavy sintering at the column tips which can be considered as the starting point of such crack initiation and propagation which ultimately results in the failure of GdZ-NiCoCrAlY TBCs. Due to the inter-columnar sintering, the lateral compliance of TBC layer decreases. The columns cannot accommodate the different thermal expansion from the underlying TGO and the bond coat and this leads to in-plane tensile stresses build up in the TBC system, as shown in Fig. 5.9. If the magnitude of these tensile stresses is high enough, it may switch off the sintering process otherwise it may lead to the inter-columnar mud- cracking. It is likely that the mud-cracking of GdZ columns took place during the cool-down of furnace cyclic testing. Mud cracking can partially relieve the tensile stresses built up in the system and promote subsequent

sintering. There has been another study where a shorter lifetime of PS GdZ- NiCrAlY TBC has been obtained due to a higher sintering in GDZ [168]. The failure of GdZ TBCs due to built up of stresses is also because of the lower toughness of GdZ, compared to 7YSZ [168].

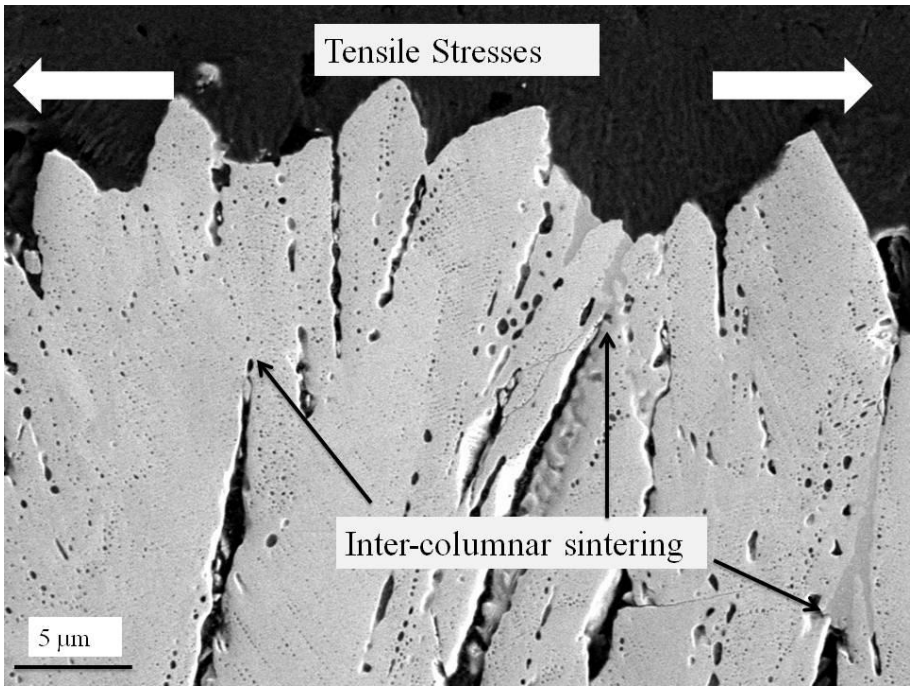

Fig. 5.9: Tensile stresses due to the inter-columnar sintering in GdZ columns

The failure location can also give an idea about the weakest location in the TBC system. In case of single layer GdZ on NiCoCrAlY system, the failure location has never been observed at the TBC-TGO interface. This is the location where the chemical reaction between GdZ and TGO resulting in the formation of Gd-aluminate has been observed. The failure location has been mostly the TGO- bond coat interface. This shows that the chemical reaction between GdZ and TGO doesn't reduce the adhesion at the TBC-TGO interface. Instead, it can be said that the new phase formed at the TBC-TGO interface for GdZ on NiCoCrAlY bond coats actually improves the adhesion since these TBC systems have shown a very long lifetime. In case of GdZ on NiCoCrAlY-2 bond coat also, a very similar mud-cracking type failure has been observed. Out of the three samples for GdZ- NiCoCrAlY-2 system, one of the samples had a failure location within the GdZ as well. A similar finding has been observed for GdZ on NiCoCrAlY bond coat. Out of the three samples tested for GdZ- NiCoCrAlY system, the sample with 5000 cycles lifetime was mechanically cut and the ceramic top coat spalled off as a result of mechanical cutting. The failure location is very similar to the one already shown in Fig. 4.26. It was observed that the weakest location in the system was within the GdZ layer which is also the location of failure. Both these cases confirm a good adhesion between GdZ and TGO which can also be due to the chemical reaction at the TBC-TGO interface.

A totally opposite result is obtained for GdZ on NiCoCrAlY-Hf bond coats where no chemical reaction between GdZ and TGO has been observed. The failure location for GdZ- NiCoCrAlY-Hf system has been found to be at TBC-TGO interface which has never been the case for GdZ-NiCoCrAlY systems. This shows that the adhesion between GdZ and NiCoCrAlY-Hf bond coat is not the best in the system and after failure, TGO has been found to be intact with the bond coat. However, it has been already reported that Hf- improves the adhesion between the bond coat and the TGO. Hf also forms stringers which play an anchoring role in the bond coat thereby improving the lifetime of TBC systems. However, despite the anchoring role of Hf- stringers; the failure location for 7YSZ- NiCoCrAlY-Hf systems has been found to be within the TGO. This failure location can be a result of the refractory elements diffusion towards the TGO as well. As it has been already mentioned that a Hf-depleted region, rich in refractory elements, starts to build up at the TGO- bond coat interface. This refractory- rich region is more likely to decrease the adhesion between the TGO and the bond coat. In case of NiCoCrAlY bond coat on CMSX-4 substrate, lower lifetimes have been obtained and the reason is more likely the diffusion of refractory elements from the substrate towards the TGO. The failure pattern in case of CMSX-4-NiCoCrAlY based systems show a large scale spallation with failure location at the TGO- bond coat interface, showing a low adhesion at that point. For NiCoCrAlY-Hf bond coats, the lifetime has been improved considerably due to the improved adhesion of Hf- stringers. However, after reaching a certain number of cycles, the negative impact of refractory elements at the TGO- bond coat interface becomes strong enough to cause spallation while the Hf- stringers still remain intact in the bond coat.

5.6 TGO Growth

TGO growth is one of the most important factors which lead to failure of TBC systems. Stresses accumulate in the TBC systems due to the TGO growth and ultimately result in the spallation of TBCs. Although there is no specific value for the critical TGO thickness, still a lower TGO growth is appreciated in TBC systems. In this study, TGO growth has been found to be different for different TBC systems. In case of NiCoCrAlY1 and NiCoCrAlY2 based systems, it has been observed that single layer GdZ TBCs show the slowest TGO growth and show the longest lifetimes. For the samples with longer lifetime, the difference between the TGO thicknesses becomes even more significant. TGO thicknesses up to 10 microns could be adopted in the system and do not lead to failure in some samples. In a similar study, GdZ showed a lower lifetime compared to DySZ as well [174]. In case of another rare earth zirconate, single layer samarium zirconate TBCs showed a higher TGO growth rate and a lower lifetime than the standard 7YSZ TBC system. In this study, it has been observed that addition of Hf to NiCoCrAlY bond coat increases the TGO growth rate. Hf- addition in NiCoCrAlY bond coats not only result in forming Hf- stringers which run deep into the bond coat but also the bulk TGO thickness has been found to be increased. The increase in the bulk TGO growth can be due to the fact that TGO for NiCoCrAlY-Hf bond coats doesn’t only consist of alumina but also contains a

lot of Hf oxide and spinels. An interesting finding of this study is that the bulk TGO growth for NiCoCrAlY-Hf bond coats has been increased when GdZ is deposited as the ceramic top coat. This is totally opposite to the findings on NiCoCrAlY bond coats where GdZ reduced the TGO growth compared to 7YSZ ceramic top coats. The main difference of GdZ based systems on NiCoCrAlY and NiCoCrAlY-Hf is that of the reaction phase which forms at the TBC-TGO interface, shown in Fig. 5.9.

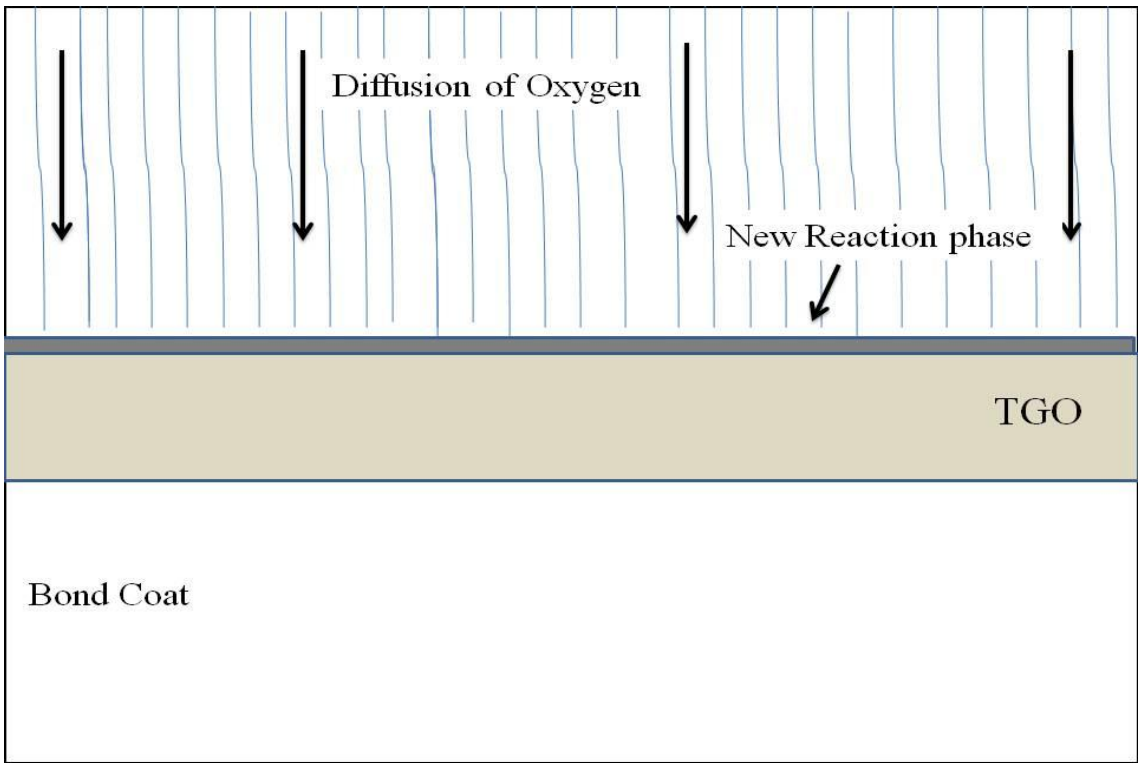

Fig.5.10: TGO growth through the reaction phase for GdZ-NiCoCrAlY systems.

It is possible that the new phase formed due to the chemical reaction between GdZ and the TGO causes more resistance in the flow of oxygen. The different morphology of GdZ columns play no role in this difference in TGO growth as the morphology of GdZ columns has been the same on both NiCoCrAlY and NiCoCrAlY-Hf bond coats. It has also been observed that the TGO growth on both NiCoCrAlY and NiCoCrAlY2 bond coats has been very similar although the reaction phase has been found to be slightly different on both the bond coats. In case of NiCoCrAlY-2 bond coats, the reaction phase consists of alternating Gd and Y- rich aluminates but still the TGO growth has been similar to NiCoCrAlY bond coats where the reaction phase consists only of Gd-aluminate. Only after the oxygen diffusivity through Gd and Y- aluminates is investigated, their role could be confirmed in affecting the TGO growth for GdZ- NiCoCrAlY TBC systems. However, in this study GdZ has improved the lifetime where TGO growth rate has been reduced and no effect on the lifetime is observed where TGO growth rate is not reduced.

6- CONCLUSIONS

TBCs are used to improve the high temperature capability and lifetime of gas turbine components. Since the efficiency of gas turbines is directly proportional to the turbine inlet temperature, new materials are constantly being introduced which have better high temperature properties and/ or longer lifetimes. This study has demonstrated some compositions which show better lifetime than the standard TBC systems. It has been observed that GdZ, when deposited on NiCoCrAlY bond coat, improves the lifetime of TBC systems to around 4 times than the standard TBC system. This improvement has been observed on both IN100 and CMSX-4 superalloys and is correlated with a chemical reaction between the TGO and GdZ which results in a better adhesion in the TBC systems. In case of standard 7YSZ- NiCoCrAlY TBC system, there is a zirconia- alumina mixed zone at the TGO- TBC interface with a columnar alumina zone underneath. For both double layer and 7YSZ TBCs, the mixed zone is continuously present at the TBC- TGO interface with a thickness of around 1µm. However, in case of single layer GdZ TBCs on NiCoCrAlY bond coats, the mixed zone at the TBC- TGO interface is not continuous due to the GdZ- alumina chemical reaction. The resulting new phase becomes more and more continuous with thermal cycling and after 5000 this new phase is continuously present at the TGO- TBC interface. This chemical reaction at the TBC-TGO interface also results in a lower TGO growth which means that the stresses accumulated in the system are lowered. When GdZ and NiCoCrAlY are deposited on IN100 substrate, the dominating failure pattern is mud-cracking which is totally different to the buckling- type failure observed in the standard 7YSZ systems. The main reason for this mud-cracking in GdZ columns is a heavy inter-columnar sintering which is observed for GdZ only at the tips of the columns. Due to the inter-columnar sintering, the EB-PVD columns cannot accommodate the tensile stresses in the system and as a result cracks propagate between the clusters of columns sintered together. In case of GdZ, the cracks are supposed to be initiated at the column tips which are the heavily sintered portion. The middle of the columns doesn't sinter as much as the tips of the columns. In case of GdZ- 7YSZ double layers, the extent of sintering can be easily compared at the double layer interface. It has been observed that the sintering at the middle of GdZ columns is lesser than in the 7YSZ columns.

The difference in sintering characteristics observed for GdZ at the tips and the middle of the columns can be due to the difference in the morphology of the columns. The EB-PVD columns for GdZ showed a different morphology than the standard 7YSZ, despite the same deposition parameters used. The columns for GdZ have a significant difference in the diameter at the top and the bottom of the columns. In addition, the GdZ columns are slightly bent in one direction. The direction of bending of GdZ columns has been found to tbe same as the direction of rotation of TBC samples during the EB-PVD deposition. This bent morphology and the different diameter of columns at the top and the bottom has not been observed for 7YSZ columns. This study also demonstrated the fluorite- pyrochlore ordering of GdZ during thermal cycling. In case

of 7YSZ, there is a slow diffusion of yttrium at elevated temperature which results in yttria-rich and yttria depleted regions. Yttria depleted regions upon cooling transform into monoclinic phase and this transformation is detrimental for the TBC lifetime. However, the fluorite to pyrochlore transformation in GdZ has not been found to be detrimental for the lifetime of TBC systems. Infact the pyrochlore phase of GdZ has a higher thermal stability than the fluorite phase.

In case of GdZ and NiCoCrAlY on CMSX-4 substrate, the failure pattern is more of chemical nature. The macroscopic view shows large scale spallation of TBC layer and for some samples, the whole TBC layer spalls off even after a lower number of thermal cycles. Careful investigations by EDX revealed diffusion of refractory elements from the substrate towards the TGO and this diffusion has been confirmed by XRF in this study. It has been observed that W, Ta and Re diffuse continuously towards the TGO during thermal cycling and the wt % of these elements near the TGO increases with thermal cycling. Out of the three refractory elements present in CMSX-4, W has been found to be diffusing more than both Ta and Re. It seems quite likely that W and Ta reduce the adhesion at the TGO- bond coat interface. The diffusion of refractory elements has been found in both 7YSZ and GdZ based TBC systems, however, GdZ based systems show a longer lifetime mainly because of their better adhesion at the TBC-TGO interface as a result of the chemical interaction at that location.

For the NiCoCrAlY-2 bond coat systems, the findings have been very similar to the NiCoCrAlY system. This study revealed that increasing the amount of yttrium from 0.19 wt % to 0.42 wt % does not cause a significant change in the lifetime of TBC systems with 7YSZ ceramic top coat. Infact, the lifetime has been slightly lower when NiCoCrAlY is replaced with NiCoCrAlY-2 on IN100 substrate with 7YSZ ceramic top coat. The TGO formation and growth remains similar with yttrium being the first element to oxidize in the system, forming yttria at the TBC-TGO interface. However, this higher yttria at the TBC-TGO interface doesn't improve the lifetime of TBC systems which has been demonstrated in this study also. When GdZ is deposited on NiCoCrAlY-2 bond coat, the reaction phase consists of alternating Gd and Y- rich phases. It can be due to the fact that yttria starts to form at the TBC-TGO interface even during the ceramic top coat deposition. This yttria acts as a barrier at the TBC- TGO interface for the GdZ- TGO chemical reaction. Consequently, the Gd- Al perovskite is formed where yttria is not present and at other locations yttrium reactions with the TGO to form different compositions of Y-aluminates. The lifetime of GdZ- NiCoCrAlY-2 TBC systems has been found to be the highest in this study which shows that the interaction at the TBC- TGO interface improves the adhesion at that interface. Also the TGO growth has been found to be very similar to the GdZ- NiCoCrAlY system which is slower than the standard 7YSZ system.

This study has demonstrated that addition of small amount of Hf in NiCoCrAlY bond coat improves the lifetime of standard 7YSZ- TBC system considerably when deposited on CMSX-4 substrate. A 10- time improvement in the TBC lifetime has been observed when the lifetime of NiCoCrAlY- based systems is compared to the NiCoCrAlY- Hf- based ones with 7YSZ as the

ceramic top coat. This improvement in the lifetime is mainly due to the improved adhesion which Hf imparts in the TBC systems and the formation of Hf- stringers at the TGO- bond coat interface. It has been observed that the TGO growth is increased by the addition of Hf in the NiCoCrAlY bond coat, however, the faster TGO growth has not been found detrimental to the lifetime. Due to the formation of Hf- stringers, the TGO growth is mainly governed and directed by Hf present in the bond coat. The TGO growth in NiCoCrAlY systems has been found to be more uniform than the Hf- doped systems. Due to the irregular TGO growth in NiCoCrAlY- Hf systems, the bond coat is entrapped in the TGO at several locations which oxidizes to form spinels in the later stages of thermal cycling. When 7YSZ is replaced with GdZ on NiCoCrAlY-Hf bond coat, the improvement in the lifetime is not observed which is observed when GdZ is deposited on NiCoCrAlY bond coat. One of the reasons can be that the lifetime of 7YSZ-NiCoCrAlY- Hf system is already very long and this lifetime is already comparable to the one achieved for GdZ- NiCoCrAlY systems. It is also possible that the longest lifetime for GdZ obtained after equilibrium between stress accumulation, sintering and stored interfacial energy is achieved is in the range of 3000 cycles. Another reason can be that the chemical reaction between the TBC and the TGO which is observed in the GdZ- NiCoCrAlY systems has not been observed in the GdZ- NiCoCrAlY- Hf system. This effect is also evident from the TGO growth in GdZ- NiCoCrAlY- Hf systems, which is faster as compared to the 7YSZ based system. In the GdZ- NiCoCrAlY system, where a new phase formed at the TBC-TGO interface, the TGO growth is slower than the standard system. It looks quite likely that the oxygen diffusion through the reaction phase is slower which results in the slower TGO growth.

In case of NiCoCrAlY-Hf systems, a relatively faster diffusion of Hf towards the TGO has been observed. However despite the Hf- diffusion, the refractory elements still diffuse towards the TGO and the rate of diffusion through NiCoCrAlY and NiCoCrAlY- Hf bond coats has been found to be very similar. The dominating failure mechanism for 7YSZ- NiCoCrAlY-Hf systems has been found to be buckling. In case of GdZ- NiCoCrAlY-Hf system, a combination of buckling and mud-cracking type of failure pattern has been observed.

The average lifetime and failure mechanisms for different TBC systems are shown in Table 6.1 in the order of decreasing lifetime. A rough upper temperature limit has also been added in the table to assess the high temperature capability of the TBC system. It is evident from the Table that GdZ, along with its better thermal properties, shows longer lifetimes than most of its 7YSZ counterpart systems.

Table 6.1: Average lifetime, upper temperature limit and the dominating failure pattern for various TBC systems investigated in this study.

TBC System	Cycles to Failure (Average)	Upper temperature limit	Dominating Failure pattern
IN100-NiCoCrAlY-2- GdZ	3685	>1200°C	Mud-cracking
CMSX-4-NiCoCrAlY-Hf-7YSZ	2984	Upto 1200°C	Buckling
IN100- NiCoCrAlY- GdZ	2896	>1200°C	Mud-cracking
CMSX-4- NiCoCrAlY-Hf- GdZ	2866	>1200°C	Mud-cracking + Buckling
IN100- NiCoCrAlY-7YSZ-GdZ	1297	>1200°C	Mud-cracking + Buckling
CMSX-4- NiCoCrAlY-GdZ	1065	>1200°C	Large scale spallation (chemical failure)
IN100- NiCoCrAlY-7YSZ	832	Upto 1200°C	Buckling
IN100- NiCoCrAlY-2-7YSZ	762	Upto 1200°C	Buckling

7- Future Work

This study presents several areas which could be a starting point for further research. These are explained as following:

Investigations on the diffusion of different elements from the substrate towards the TGO especially for the CMSX-4- based systems could be further improved by using GDOES technique. In this study, an attempt has been made to investigate the depth profile of different elements present close to the TGO. However, due to the cylindrical shape of the samples, GDOES could not be performed. For a disc shaped sample, GDOES can be done at the locations where TBC has been spalled off and the amount of refractory elements through the bond coat thickness could be investigated.

The addition of Hf in the NiCoCrAlY bond coats with CMSX-4 substrate and 7YSZ ceramic top coat improves the lifetime of TBC systems. In this study, an improvement of around 10times has been observed by the addition of 0.6 wt % of Hf. In a previous study, even longer lifetimes have been obtained with 1.0 wt % Hf additions. This remains to further study as to what maximum improvement can be obtained by the addition of Hf to NiCoCrAlY bond coats.

In this study, a chemical reaction has been observed between GdZ and the TGO for the NiCoCrAlY- based systems. EDX results revealed the different elements present in the new phase formed after the chemical reaction and from the literature survey, it is possible to expect a certain composition after such a chemical reaction. However, to find the exact composition of the new phase formed, transmission electron microscopy (TEM) is needed which could be a topic of future work. The significance of TEM is even more for the GdZ- NiCoCrAlY-2 system where the reaction zone consists of alternating Gd- and Y- rich phases.

8- REFERENCES

1. C. Soares, *Gas Turbines: A Handbook of Air, Land and Sea Applications.* Book, 2008. 2nd Edition.

2. R. C. Reed, *The Superalloys: Fundamentals and Applications.* Cambridge University Press, Cambridge, UK, 2006.

3. M. P. Boyce, *Gas Turbine Engineering Handbook.* 2012. Fourth Edition.

4. E. Logan Jr., *Handbook of Turbomachinery.* Book, 2003. 2nd Edition.

5. N. P. Padture, M. Gell, and E.H. Jordan, *Thermal barrier coatings for gas-turbine engine applications.* Science, 2002. 296(5566): p. 280-4.

6. R. Miller, *Current status of thermal barrier coatings- an overview.* Surface and Coatings Technology, 1987. 30: p. 1-11.

7. G.W. Goward, *Progress in coatings for gas turbine airfoils.* Surface and Coatings Technology, 1998. 108-109(1-3): p. 73-79.

8. R. Sivakumar and B. L. Mordike, H*igh temperature coatings for gas turbine blades: A review* Surface and Coatings Technology, 1989. 37(2): p. 139-160.

9. R. Miller, *History of thermal barrier coatings for gas turbine engines* Thermal Barrier Coatings 2 Conference, Germany, 2007.

10. D. S. Rickerby and H. C. Low, *Towards designers surfaces in the aero gas turbine.* Proceedings of 4th European Propulsion Forum, London: Royal Aeronautical Society, 1993.

11. T. M. Pollock and S. Tin, *Nickel-based superalloys for advanced turbine engines: chemistry, microstructure, and properties.* Journal of Propulsion and Power, 2006. 22(2): p. 361-374.

12. K. Haris, G.L. Erickson and R. E. Schwer, *Directionally solidified and single crystal superalloys.* ASM Handbook, 2002. ASM- International, Materials Park, Ohio. .

13. M. J. Pomoroy, *Coatings for gas turbine materials and long term stability issues.* Materials & Design, 2005. 26: p. 223-231.

14. P. Caron and O. Lavigne, *Recent studies at Onera on superalloys for single crystal turbine blades.* Journal of Aerospace Lab, 2011(3): p. 1-12.

15. P. Caron, *High γ' solvus New Generation Nickel-Based Superalloys for Single Crystal Turbine Blade Applications.* Superalloys 2000, TMS, Warrendale, PA, USA (T.M. Pollock et al., eds), 2000: p. 737-746.

16. X. Han, *Diffusion Coatings for High Temperature Applications on Ni- base superalloys.* PhD Thesis, Politechnico di Milano, 2011.

17. N. Birks, G.H.M., *Introduction to High Temperature Oxidation of Metals.* Edward Arnold Publishers Ltd. , 1983.

18. A. S. Radcliff, *Factors influencing Gas Turbine use and performance.* Material Science & Technology, 1987. 3: p. 554-561.

19. S. R. Levine and R. M. Caves, *Thermodynamics and Kinetics of Pack Aluminide Coating Formation on IN100.* Journal of Electrochemical Society, 1974. 121(8): p. 1051-1064.

20. G. W. Goward, Z. A. Foroulis and F. S. Petit (eds.), *properties of high temperature alloys.* Electrochemical Society, Princeton NJ, 1976: p. 806.

21. S. J. Grisaffe, C. T. Sims and W. C. Hagel, *The Superalloys.* Wiley, Newyork, 1972.

22. R. Sivakumar and L. L. Seigle, *On the Kinetics of the Pack-Aluminization Process.* Metallurgical Transactions A, Physical Metallurgy & Materials Science, 1976. 7: p. 1073.

23. R. Darolia, *Thermal barrier coatings technology: critical review, progress update, remaining challenges and prospects.* International Materials Reviews, 2013. 58(6): p. 315-348.

24. J. R. Nicolls, N. J. Simms, W. Y. Chan and H. E. Evans, *Smart Overlay Coatings - Concept and Practice.* Surface and Coatings Technology, 2002. 149(2-3): p. 236-244.

25. E. A. Jarvis and E. A. Carter, *The Role of Reactive Elements in Thermal Barrier Coatings.* Composites Science & Technology, 2002. 4(2): p. 33-41.

26. D.P. Whittle and J. Stringe, *Improvement in properties: Additives in oxidation resistance.* Philosophical Transactions of the Royal Society B, 1980. 295: p. 309-329.

27. A. Strawbridge and P. Y. Hou, *THE ROLE OF REACTIVE ELEMENTS IN OXIDE SCALE ADHESION.* Materials at High Temperature, 1994. 12: p. 177-181.

28. E. Lang, *The Role of Active Elements in the Oxidation Behavior of High Temperature Metals and Alloys.* Elsevier Applied Science, London, U.K., 1989.

29. D. P. Moon, *Role of Reactive Elements in Alloy Protection.* Material Science & Technology, 1989. 5: p. 754-764.

30. B. A. Pint, *Experimental observations in support of the dynamic-segregation theory to explain the reactive-element effect.* Oxidation of Metals, 1996. 45(1-2): p. 1-37.

31. W.E. King, (Ed.), *The Reactive Element Effect on High Temperature Oxidation- After Fifty Years.* Material Science Forum, 1989. 43.

32. B. A. Pint et al., *Substrate and Bond Coat compositions- factors affecting alumina scale adhesion.* Material Science & Engineering, 1998. 245: p. 201-211.

33. U. Schulz, K. Fritscher and A. Ebach-Stahl, *Cyclic behavior of EB-PVD thermal barrier coating systems with modified bond coats.* Surface and Coatings Technology, 2008. 203: p. 449-455.

34. J. Jedlinski, S.M., *The influence of implanted yttrium on the oxidation behavior of NiAl.* Material Science & Engineering, 1987. 87: p. 281-287.

35. G. J. Yurek and H. S. Schmalzried, *Deviations from Local Thermodynamic Equilibrium During Interdiffusion of CoO-MgO and CoO-NiO.* Berichte der Bunsengesellschaft für physikalische Chemie, 1975. 79(3): p. 255-262.

36. B. A. Pint, K. L. More and I. G. Wright, *The Effect of Quaternary Additions on the Oxidation Behavior of Hf-doped NiAl.* Oxidation of Metals, 2003. 59: p. 257-283.

37. B. A. Pint, *The role of chemical composition on the oxidation performance of aluminide coatings.* Surface and Coatings Technology, 2004. 188-189: p. 71-78.

38. P. Y. Hou and K. Priimak, *Interfacial segregation, Pore Formation and Scale Adhesion on NiAl Alloys.* Oxidation of Metals, 2005. 63: p. 113-130.

39. J. Liu, *Mechanisms of lifetime improvement in thermal barrier coatings with Hf and/ or Y modifications of CMSX-4 superalloy substrates.* PhD Thesis, University of Central Florida, 2007.

40. A. Hesnawi, H. Li., Z. Zhou, S. Gong, and H. Xu, *Isothermal oxidation behaviour of EB-PVD MCrAlY bond coat.* . Vacuum, 2007. 81: p. 947-952.

41. D. Naumenko, V. Shemet, L. Singheiser, and W. J. Quadakkers, *Failure mechanisms of thermal barrier coatings on MCrAlY-type bondcoats associated with the formation of the thermally grown oxide.* Journal of Materials Science, 2009. 44: p. 1687-1703.

42. C. Lee, H. Kim, H. Choi, and H. Ahn, *Phase transformation and bond coat oxidation behavior of plasma-sprayed zirconia thermal barrier coating.* Surface and Coatings Technology, 2000. 124: p. 1-12.

43. J. Toscano et al., *Parameters affecting TGO growth and adherence on MCrAlY-bond coats for TBC's.* Surface and Coatings Technology, 2006. 201: p. 3906-3910.

44. C. G. Levi, E. Sommer, S. G. Terry, A. Catanoiu and M. Rühle, *Alumina Grown during Deposition of Thermal Barrier Coatings on NiCrAlY.* Journal of American Ceramic Society, 2003. 86(4): p. 676-685.

45. B. M. Warnes, *Reactive element modified chemical vapor deposition low activity platinum aluminide coatings.* Surface and Coatings Technology, 2001. 146-147: p. 7-12.

46. J. Liu, J. W. Byeon and Y. H. Sohn, *Effects of phase constituents/ microstructure of thermally grown oxide on the failure of EB-PVD thermal barrier coating with NiCoCrAlY bond coat.* Surface and Coatings Technology, 2006. 200: p. 5869-5876.

47. W. Bruae, K. Fritscher, U. Schulz, C. Leyens and R. Wirth, *Nucleation and Growth of Oxide Constituents on NiCoCrAlY Bond Coats During the Different Stages of EB-PVD TBC Deposition and Upon Thermal Loading.* Material Science Forum, 2004. 461-464: p. 899-906.

48. H. Lau, *Influence of yttria on the cyclic lifetime of YSZ TBC deposited on EB-PVD NiCoCrAlY bond coats and its contribution to a modified TBC adhesion mechanism.* Surface and Coatings Technology, 2013. 235: p. 121-126.

49. J. D. Douglas, *The Oxidation Mechanism of Ni_3Al Containing Yttrium.* Oxidation of Metals, 1974. 8(3): p. 139.

50. K. Fritscher, W. Braue and U. Schulz, *Assessment of cyclic lifetime of NiCoCrAlY/ ZrO_2-based EB-PVD TBC systems via reactive element enrichment in the mixed zone of the TGO scale.* Metallurgical and Materials Transactions A, 2013. 44(5): p. 2070-2082.

51. A. J. Slifka, B. J. Filla, J. M. Phelps, G. Bancke and C. C. Berndt, *Thermal conductivity of a zirconia thermal barrier coating.* . journal of thermal technology, 1998. 7(1): p. 43-46.

52. X. Q. Cao, R. Vassen, and D. Stoever, *Ceramic materials for thermal barrier coatings.* Journal of the European Ceramic Society, 2004. 24(1): p. 1-10.

53. C. R. Lima and R. Trevisan, *Temperature measurements and adhesion properties of plasma sprayed thermal barrier coatings.* Journal of Thermal Spray Technology, 1999. 8(2): p. 323-327.

54. U. Schulz, B. Saruhan, K. Fritscher and C. Leyens, *Review on Advanced EB-PVD Ceramic Topcoats for TBC applications.* Journal of applied ceramic technology, 2004. 1(4): p. 302-315.

55. U. Schulz, *Phase Transformation in EB-PVD Yttria Partially Stabilized Zirconia Thermal Barrier Coatings during annealing.* Journal of American Ceramic Society, 2000. 83(4): p. 904-910.

56. J. R. Brandon and R. Taylor, *Phase stability of zirconia-based thermal barrier coatings Part-1. Zirconia-Yttria alloys.* Surface and Coatings Technology, 1991. 46: p. 75-90.

57. E. C. Subbarao, A. H. Heuer, L. W. Hobbs Eds., *Science and Technology of Zirconia.* American Ceramic Society, Columbus, OH, 1984. 3: p. 1.

58. L. Wang, *Thermal cycling and Thermal Radiation Performances of Novel Thermal Barrier Coatings.* PhD Thesis, Louisiana State University, 2013.

59. A. F. Renteria, *A small-angle scattering analysis of the influence of manufacture and thermal induced morphological changes on the thermal conductivity of EB-PVD PYSZ Thermal Barrier Coatings.* PhD Thesis- RWTH Aachen, 2006.

60. T. E. Strangmann, *Columnar ceramic thermal barrier coatings.* US Patent 4321311, European Patent 0042872B1, 1982.

61. E. Lugscheider, K.B., S. Barwulf and A. Etzkorn, *Mechanical properties of EB-PVD-thermal barrier coatings by nanoindentation.* . Surface and Coatings Technology, 2001. 138(1): p. 9-13.

62. U. Schulz, S. G. Terry and C. G. Levi, *Microstructure and texture of EB-PVD TBCs grown under different rotation modes* Material Science & Engineering, 2003. 360(1-2): p. 319-329.

63. T. Jeanine, D.-Marsin and Dinesh K. Gupta, *Protective coatings in the gas turbine engine.* Surface and Coatings Technology, 1994. 68/69: p. 1-9.

64. J. R. Nicolls, K. J. Lawson, A. Johnstone and D. S. Rickerby, *Methods to reduce the thermal conductivity of EB-PVD TBCs.* Surface and Coatings Technology, 2002. 151-152: p. 383-391.

65. P. D. Harmsworth and R. Stevens, *Phase composition and properties of plasma-sprayed zirconia thermal barrier coatings.* Journal of Material Science, 1992. 27: p. 611-615.

66. R. McPherson, *A review of microstructure and properties of plasma sprayed ceramic coatings.* Surface and Coatings Technology, 1989. 39/40: p. 173-181.

67. H. Lau, *Mikrostruktur und morphologie thermisch gewachsener oxidschichten von wärmedämmschichtsystemen für turbinenschaufeln.* PhD Thesis- RWTH Aachen, 2004.

68. D. R. Clarke et al., *Thermal barrier coatings for more efficient gas turbine engines.* MRS Bulletin, 2012. 37: p. 891-898.

69. S. Sampath, U. Schulz, M. Ophelia Jarligo and Seiji Kuroda, *Processing science of advanced thermal-barrier systems.* MRS Bulletin, 2012. 37: p. 903-910.

70. J. R. Nicolls, Y. Jaslier and D. S. Rickerby, *Erosion and foreign object damage of thermal barrier coatings.* 4th International symposium on High Temperature Corrosion, Les Embiez, France, 1996.

71. R. Wellman and J. R. Nicholls, *Some observation on erosion mechanisms of EB-PVD TBCs.* Wear, 20000. 242(1-2): p. 89-96.

72. E. Y. Lee, R. R. Biederman and D. S. Rickerby, *The microstructural characterization of plasma sprayed and physical vapor deposited partially stabilized zirconia thermal barrier coatings.* Plasma Surface Engineering, 1989.

73. O. Unal, T. E. Mitchell and A. H. Heuer, *Microstructure of Y_2O_3- stabilized ZrO_2 electron beam physical vapor deposition coatings on Ni- base Superalloys.* Journal of American Ceramic Society, 1994. 77(4): p. 984-992.

74. S. G. Terry, *Evolution of microstructure during the growth of thermal barrier coatings by Electron-Beam Physical Vapor Deposition.* Materials Department, University of California, Santa Barbara, 2001: p. 197.

75. M. Schmücker and U. Schulz, *Microstructure of ZrO_2 thermal barrier coatings applied by EB-PVD.* Material Science & Engineering, 2000. 276(A): p. 1-8.

76. B. Movchan and V. Demchisin, *Study of the structure and properties of thick vacuum condensates of nickels, titanium, aluminum oxide and zirconium dioxide.* Fiz. Metal. Metalloved, 1969. 28: p. 83-90.

77. A. V. Drift, *Evolutionary selection, a principle governing growth orientation in vapour-deposited layers.* Philips Res. Rep., 1967. 22.

78. J. R. VanValzah and H. E. Eaton, *Cooling rate effects on the tetragonal to monoclinic phase transformation in aged plasma-sprayed yttria partially stabilized zirconia.* Surface and Coatings Technology, 1991. 46: p. 289-300.

79. R. Taylor, J. R. Brandon and P. Morrell, *Microstructure, composition and property relationships of plasma-sprayed thermal barrier coatings.* Surface and Coatings Technology, 1992. 50: p. 141-149.

80. A. Cipitria, I. O. Golosnoy and T. W. Clyne, *A sintering model for plasma-sprayed zirconia TBCs. Part I: Free-standing coatings.* Acta Materialia, 2009. 57(4): p. 980-992.

81. A. Azzopardi, R. Mervel, B. Saint-Ramond, E. Olson and K. Stiller, *Influence of Aging on Structure and Thermal Conductivity of Y-PSZ and Y-FSZ EB-PVD Coatings.* Surface and Coatings Technology, 2004. 177-178: p. 131-139.

82. U. Schulz, K. Fritscher, C. Leyens and M. Peters, *High- Temperature Aging of EB-PVD TBCs.* Ceramic Engineering and Science Proceedings, 2001. 22(4): p. 347-356.

83. U. Schulz, K. Fritscher and M. Peters, *EB-PVD Y_2O_3 and CeO_2/Y_2O_3 Stabilized Zirconia TBCs- Crystal Habit and Phase Compositions.* Surface and Coatings Technology, 1996. 82: p. 259-269.

84. U. Schulz, K. Fritscher and M. Peters, *Thermocyclic Behavior of Variously Stabilized EB-PVD TBCs.* Journal of Engineering for Gas Turbine and Power, 1997. 119: p. 917-921.

85. C. Leyens, U. Schulz and K. Fritscher, *Oxidation and Lifetime of PYSZ and CeSZ coated Ni- base substrates with MCrAlY Bond Layers.* Materials at High Temperatures, 2003. 20(4): p. 475-480.

86. U. Schulz, K. Fritscher and C. Leyens, *Two-Source Jumping Beam Evaporation for Advanced EB-PVD TBC Systems.* Surface and Coatings Technology, 2000. 133-134: p. 40-48.

87. U. Schulz, K. Fritscher and W. A. Kaysser, *Cyclic lifetime of PYSZ and CeSZ EB-PVD TBC Systems on various Ni- Superalloy substrates.* COST 2002, Liege: J. Lecomte-Bechers, M. Carton, 2002: p. 483-492.

88. B. A. Nagaraj and D. J. Wortmann, *Burner Rig Evaluation of Ceramic Coatings with Vanadium- Contaminated Fuels.* ASME Journal of Engineering for Gas Turbine and Power, 1990. 112: p. 536-542.

89. C. G. Levi, *Emerging materials and processes for thermal barrier systems.* Current Opinion in Solid State and Materials Science, 2004. 8(1): p. 77-91.

90. S. Alperine, V. Arnault, O. Lavigne and R. Mevrel, *Heat Barrier Composition, A Mechanical superalloy article provided with a ceramic coating having such composition and a method of making the ceramic coating.* . U.S patent No. 6333118, EP patent No. 1085109, 2001.

91. U. Schulz et al., *Low thermal conductivity ceramics for turbine blade TBC application.* Ceramic Engineering and Science Proceedings, 2004. 25(4): p. 375-380.

92. R. L. Jones, *Experiences in seeking stabilizers for zirconia having hot corrosion resistance and high temperature tetragonal (t') stability.* Naval Research Laboratory, NRL/MR/6170, 1996. 96: p. 7841.

93. R. L. Jones, *Scandia, Yttria-stabilized zirconia (SYSZ): A candidate material for high temperature TBCs.* Proceedings of TBC Workshop NASA ed. N.I.R. Center, Cleveland, OH., 1997. 41.

94. J. Wu et al., *Low thermal conductivity rare-earth zirconates for potential thermal barrier coating applications.* Journal of American Ceramic Society, 2002. 85(12): p. 3031-3035.

95. G. Suresh et al., *Investigation of the thermal conductivity of selected compounds of gadolinium and lanthanum.* Journal of Nuclear Materials, 1997. 249: p. 259-261.

96. M. Maloney, *TBC systems and Materials.* U.S patent No. 6177200, U.S patent No. 617560, 2001.

97. Q.Xu et al., *Rare-Earth Zirconate Ceramics with Fluorite Structure for Thermal Barrier Coatings.* Journal of American Ceramic Society, 2006. 89(1): p. 340-342.

98. R. Subramanian, *TBC having high phase stability.* U.S patent No. 6258467, U.S patent No. 387539, 2002.

99. N. P. Bansal, D. Zhu, *Effects of doping on thermal conductivity of pyrochlore oxides for advanced thermal barrier coatings.* Material Science & Engineering: A, 2007. 459(1-2): p. 192-195.

100. D. R. Clarke and S. R. Phillpot, *Thermal Barrier Coating Materials.* Materials today, 2005. 8(6): p. 22-29.

101. R. Vaßen, F. Traeger and D. Stöver, *New thermal barrier coatings based on Pyrochlores/YSZ double-layer systems.* International Journal of Applied Ceramic Technology, 2004. 1(4): p. 351-361.

102. R. Vaßen, M. O. Jarligo, T. Steinke, D. E. Mack and D. Stöver, *Overview on advanced thermal barrier coatings.* Surface and Coatings Technology, 2010. 205: p. 938-942.

103. Z.-G. Liu et al., *(Ln0.9Gd0.05Yb0.05)2Zr2O7 Ceramics with Pyrochlore Structure as Thermal Barrier Oxides.* Advanced Engineering Materials, 2008. 10(8): p. 754-758.

104. C. G. Levi et al., *Environmental degradation of thermal barrier coatings by molten deposits.* MRS Bulletin, 2012. 37(10): p. 932-941.

105. W. Braue and P. Mechnich, *Volcanic ash induced decomposition of EB-PVD Gd2Zr2O7 thermal barrier coatings to Gd-Oxyapatite Zircon, and Gd, Fe-Zirconolite.* Journal of the American Ceramic Society, 2013. 96(6): p. 1958-1965.

106. S. Krämer, J. Yang, and C.G. Levi, *Infiltration-inhibiting reaction of gadolinium zirconate thermal barrier coatings with CMAS melts.* Journal of the American Ceramic Society, 2008. 91(2): p. 576-583.

107. R. M. Leckie et al., *Thermochemical compatibility between alumina and ZrO2–GdO3/2 thermal barrier coatings.* Acta Materialia, 2005. 53(11): p. 3281-3292.

108. S. Lakiza et al., *Phase diagram of the ZrO2–Gd2O3–Al2O3 system.* Journal of the European Ceramic Society, 2006. 26(3): p. 233-246.

109. B. Saruhan, P. Francois, K. Fritscher and U. Schulz, *EB-PVD processing of pyrochlore-structured $La_2Zr_2O_7$ based TBCs.* Surface and Coatings Technology, 2004. 182(2-3): p. 175-183.

110. K. Fritscher and B. Saruhan, *EB-PVD $La_2Zr_2O_7$- based TBCs.* International Symposium on Advanced TBCs and TiAls for gas turbines TURBOMAT, DLR 2002: p. 180-182.

111. X. Q. Cao, R. Vaßen, W. Jungen, S. Schwartz, F. Tietz and D. Stöver, *Thermal stability of Lanthanum Zirconate plasma-sprayed coating.* Journal of American Ceramic Society, 2001. 84(9): p. 2086-2090.

112. R. Vaßen et al., *Zirconates as new materials for thermal barrier coatings.* Journal of the American Ceramic Society, 2000. 83: p. 2023-2028.

113. W. Ma et al., *Yb_2O_3 and Gd_2O_3 doped strontium zirconate for thermal barrier coatings.* Journal of the European Ceramic Society, 2008. 28(16): p. 3071-3081.

114. W. Ma et al., *New generation perovskite thermal barrier coating materials.* Journal of Thermal Spray Technology, 2008. 17(5-6): p. 831-837.

115. P. S. Murti and M. V. Krishnaiah, *Investigation of the thermal conductivity of calcium cerate and calcium zirconate* Materials Chemistry and Physics, 1992. 31(4): p. 347-350.

116. R. Tarvin and K. Davies, *A-Site and B-Site Order in (Na1/2La1/2)(Mg1/3Nb2/3)O3 Perovskite.* Journal of the American Ceramic Society, 2004. 87(5): p. 859-863.

117. R. Guo et al., *Ba(Mg1/3Ta2/3)O3 single crystal fiber grown by the laser heated pedestal growth technique.* Journal of Applied Physics, 1994. 75: p. 4704.

118. R. C. Ropp and G. G. Libowitz, *The Nature of the Alumina-Rich Phase in the System La2O3-Al2O3.* journal of the American Ceramic Society, 1978. 61(11-12): p. 473-475.

119. Y. F. Zhang, Q.Li, X. F. Ma and X. Q. Cao, *Synthesis and high-pressure sintering of lanthanum magnesium hexaaluminate.* Materials Letters, 2008. 62: p. 923-925.

120. Y. Zhang, D. E. Mack, M. O. Jarligo, X. Cao, R. Vaßen and D. Stöver, *Partial evaporation of strontium zirconate during atmospheric plasma spraying.* Journal of Thermal Spray Technology, 2009. 18(4): p. 694-701.

121. R. N. German, *Sintering Theory and Practice.* John Wiley & Sons, 1996. 1st edition.

122. J. L. Shi, *Thermodynamics and densification kinetics in solid state sintering of ceramics.* Journal of Materials Research, 1999 14(4): p. 1398-1408.

123. K. W. Lay, *Grain growth during sintering. in 3rd International Conference on Sintering and Related Phenomena.* edited by Kuczynski, G.C., Indiana, USA: Plenum Press, 1972: p. 65-80.

124. S. A. Tsipas, *Thermophysical properties of plasma sprayed thermal barrier coatings.* PhD thesis- University of Cambridge, 2005.

125. W. S. Coblenz et al., Coble, *Initial Stage Solid State Sintering Models. A Critical Analysis and Assessment. in Sintering and Related Phenomena.* edited by Kuczynski, G.C.: Plenum Press, 1980: p. 36-43.

126. W. D. Kingery and M. Berg, *Study of the Initial Stages of Sintering Solids by Viscous Flow, Evaporation-Condensation and Self-Diffusion.* Journal of Applied Physics, 1955. 26(10): p. 1205-1212.

127. R. L. Coble, *Sintering crystalline solids: I. Intermediate and Final Stage Diffusion models.* Journal of Applied Physics, 1961. 32(5): p. 787-792.

128. M. I. Mendelev and D. J. Srolovitz, *Impurity effects on grain boundary migration.* Modelling and Simulation in Materials Science and Engineering, 2002. 10: p. 79-109.

129. J. W. Cahn, *The impurity-drag effect in grain boundary motion.* Acta Metallurgica, 1962. 10: p. 769-798.

130. W. H. Rhodes, *Agglomerate and particle size effects on sintering of yttria stabilzed zirconia.* Journal of the American Ceramic Society, 1981. 64(1): p. 19-22.

131. L. del Olmo, P. Duran and C. Moure, *Sintering behaviour of an yttria stabilized zirconia. in Sintering-theory and Practice.* edited by Kolar, D., Pejovnik, S., and Ristic, M.M., Portooz, Yugoslavia: Elsevier Scientific, Amsterdam, 1981: p. 401-408.

132. P. J. Jorgensen, *Diffusion controlled sintering in oxides. in Sintering and Related Phenomena.* edited by Kuczynski, G.C., Hooton, N.A., and Gibbon, C.F.: Gordon and Breach, New York, 1967: p. 401-422.

133. R. S. Nasar et al., *Sintering mechanisms of ZrO2 center dot MgO with addition of TiO2 and CuO.* Ceramics International, 2004. 30(4): p. 571-577.

134. M. Kilo et al., *Cation self-diffusion of Ca, Y, and Zr in single crystalline calcia- and yttria-doped zirconia.* Journal of Applied Physics, 2003. 94(12): p. 7547-7552.

135. M. Kilo et al., *Lanthanide transport in stabilized zirconias: Interaction between ionic radius and diffusion coefficient.* Journal of Chemical Physics, 2004. 12(11): p. 5482-5487.

136. H. Solmon, J. Chaumont, C. Dolin, and C. Monty, *Zr, Y and O self diffusion in Zr(1-x)YxO2-x/2. in Ceramic Transactions- Point Defects and Related Properties of Ceramics.* edited by Mason, T.O. and Routbort, J.L., 1991: p. 175-184.

137. F. R. Chien and A. H. Heuer, *Lattice diffusion kinetics in Y2O3-stabilized cubic ZrO2 single crystals: a dislocation loop annealing study.* Philosophical Magazine A,, 1996. 73: p. 681-697.

138. H. Tsubakino, T. Fujiwara, K. Satani and S. Ioku, *Composition of grain boundary phase formed in zirconia-3 mol% yttria containing alumina.* Journal of Materials Science Letters, 1997. 16(17): p. 1472-1475.

139. J. Shi, T. S. Yen and H. Schubert, *Effect of Small Amounts of Additives on the Sintering of High-Purity Y-TZP.* Journal of Materials Science, 1997. 32: p. 1341-1346.

140. M. Verkerk, A. Winnubst and A.Burggraaf, *Effect of Impurities on Sintering and Conductivity of Yttria-Stabilised Zirconia.* Journal of Materials Science, 1982. 17: p. 3113-3122.

141. S. Tekeli, M. Erdogan and B. Aktas, *Microstructural evolution in 8 mol% Y2O3-stabilized cubic zirconia (8YSCZ) with SiO2 addition.* Materials Science and Engineering a-Structural Materials Properties Microstructure and Processing, 2004. 386(1-2): p. 1-9.

142. S. X. Wu and R. J. Brook, *Sintering Aids for Zirconia Ceramics.* Transactions and journal of the British Ceramic Society, 1983. 82(6): p. 200-205.

143. J. S. Kirkaaldy and D. J. Young, *Diffusion in the condensed state.* The institute of Metals, London, 1987.

144. N. K. Adam, *The physics and chemistry of surfaces.* Oxford University Press, London, 1949.

145. P. K. Wright and A. G. Evans, *Mechanisms governing the performance of thermal barrier coatings.* Current Opinion in Solid State and Materials Science, 1999. 4: p. 255-265.

146. R. J. Christensen, V. K. Tolpygo and D. R. Clarke, *The influence of the reactive element yttrium on the stress in alumina scales formed by oxidation.* Acta Materialia, 1997 45(4): p. 1761-1766.

147. D. R. Clarke and V. K. Tolpygo, *Wrinkling of alpha-Alumina Films Grown By Thermal Oxidation: II. Oxide Separation and Failure.* Acta Materialia, 1998. 46(14): p. 5167-5174.

148. V. K. Tolpygo, J. Dryden and D. R. Clarke, *Determination of the Growth Stresses Generated During the Oxidation of Fe-22Cr-4.8Al-0.3Y Alloy.* Acta Materialia, 1998. 46(3): p. 927-937.

149. A. G. Evans, M. Y. He and J. W. Hutchinson, *Effect of interface undulations on the thermal fatigue of thin films and scales on metal substrates.* Acta Materialia, 1997. 45(9): p. 3543-3554.

150. G. C. Chang and W. Phucharoen, *Finite element thermal stress solutions for thermal barrier coatings.* Surface and Coatings Technology, 1987. 32(1-4): p. 307-325.

151. A. Strawbridge and H. E. Evans, *Mechanical Failure of Thin Brittle Coatings.* Engineering Failure Analysis, 1995. 2(2): p. 85-103.

152. J. S. Wang and A. G. Evans, *Measurement and analysis of buckling and buckle propagation in compressed oxide layers on superalloy substrates.* Acta Materialia, 1998. 46(14): p. 4993-5005.

153. R. D. Jackson, *The Effect of Bond Coat Oxidation on the Microstructure and Endurance of Two Thermal Barrier Coating Systems* PhD Thesis- University of Birmingham, 2009.

154. H. E. Evans and R. C. Lobb, *Conditions for the initiation of oxide-scale cracking and spallation.* Corrosion Science, 1984. 24(3): p. 209-222.

155. A. Rabiei and A. G. Evans, *Failure mechanisms associated with the thermally grown oxide in plasma sprayed thermal barrier coatings.* Acta Materialia, 2000. 48: p. 3963-3976.

156. R. Panat, S. Zhang and K. J. Hsia, *Bond coat surface rumpling in thermal barrier coatings.* Acta Materialia, 2002. 51: p. 239-249.

157. D. R. Clarke and V. K. Tolpygo, *Surface rumpling of a (Ni, Pt)Al bond coat induced by cyclic oxidation.* Acta Materialia, 2000. 48(13): p. 3283-3293.

158. D. R. Clarke and V. K. Tolpygo, *On the rumpling mechanism in nickel-aluminide coatings: Part II: characterization of surface undulations and bond coat swelling.* Acta Materialia, 2004. 52(17): p. 5129-5141.

159. H. E. Evans, *Oxidation failure of TBC systems: An assessment of mechanisms*. Surface and Coatings Technology, 2011. 206: p. 1512-1521.

160. D. R. Clarke and V. K. Tolpygo, *Rumpling of CVD (Ni,Pt)Al diffusion coatings under intermediate temperature cycling.* Surface and Coatings Technology, 2009. 203(20-21): p. 3278-3285.

161. V. K. Tolpygo and D. R. Clarke, *On the rumpling mechanism in nickel-aluminide coatings Part 1: an experimental assessment.* Acta Materialia, 2004. 52: p. 5115-5127.

162. R. T. Wu, X. Wang and A. Atkinson, *On the interfacial degradation mechanisms of thermal barrier coating systems: Effects of bond coat composition.* Acta Materialia, 2010. 58(17): p. 5578-5585.

163. R. Hutchinson, N.A. Fleck, and A.C.F. Cocks, *A sintering model for thermal barrier coatings.* Acta Materialia, 2006. 54(5): p. 1297-1306.

164. J. A. Haynes et al., *Effects of Interface Roughness on Residual Stresses in Thermal Barrier Coatings.* Journal of the American Ceramic Society, 1999. 82(4): p. 1073-1075.

165. M. P. Taylor, W. M. Pragnell and H. E. Evans, *The influence of bond coat surface roughness on chemical failure and delamination in TBC systems.* Materials and Corrosion, 2008. 59(6): p. 508-513.

166. H. E. Evans, A. T. Donaldson and T. C. Gilmour, *Mechanisms of Breakaway Oxidation and Application to a Chromia-Forming Steel.* Oxidation of Metals, 1999. 52(5-6): p. 379-402.

167. E. P. Busso, H. E. Evans, Z. Q. Qian and M. P. Taylor, *Effects of breakaway oxidation on local stresses in thermal barrier coatings.* Acta Materialia, 2010. 58(4): p. 1242-1251.

168. L. Wang et al., *Thermal Cycling Behavior of $Gd_2Zr_2O_7$ Based Thermal Barrier Coatings.* Material Science and Technology 2011. 2011 Conference & Exhibition, MS&T Partner Societies p. 1046-1053.

169. W. Ma, S. Gong, H. Li and H. Xu, *Novel thermal barrier coatings based on $La_2Ce_2O_7$/8YSZ double-ceramic-layer systems deposited by electron beam physical vapor deposition.* Surface and Coatings Technology, 2008. 202: p. 2704-2708.

170. H. Zhao et al., *Reaction, transformation and delamination of samarium zirconate thermal barrier coatings.* Surface and Coatings Technology, 2011. 205(19): p. 4355-4365.

171. U. Kaden, C. Leyens, M. Peters and W. A. Kaysser, *Thermal stability of an EB-PVD thermal barrier coating system on a single crystal nickel- base superalloy.* . Elevated Temperature Coatings 3 TMS, 1999: p. 27-38.

172. U. Schulz and B. Baufeld, *Life time dependency on the pre-coating treatment of a thermal barrier coating under thermal cycling.* Surface and Coatings Technology, 2006. 201: p. 2667-2675.

173. H. Lau, C. Leyens, U. Schulz and C. Friedrich, *Influence of bondcoat pre-treatment and surface topology on the lifetime of EB-PVD TBCs.* Surface and Coatings Technology, 2003. 165: p. 217-223.

174. A. U. Munawar, U. Schulz, G. Cerri and H. Lau, *Microstructure and cyclic lifetime of Gd and Dy-containing EB-PVD TBCs deposited as single and double-layer on various bond coats.* Surface and Coatings Technology, 2014. 245: p. 92-101.

175. H. Limin et al., *Substrate effects on the high-temperature xxidation behavior of thermal barrier coatings.* Journal of material Science and Technology, 2009. 25(6): p. 799-802.

176. U. Schulz, M. Menzebach, C. Leyens and Y. Q. Yang, *Influence of substrate material on oxidation behavior and cyclic lifetime of EB-PVD TBC systems.* Surface and Coatings Technology, 2001. 146-147: p. 117-123.

177. U. Kaden, *Einfluss der substratlegierung CMSX-4 auf die lebensdauer eines EB-PVD-Wärmedämmschichtsystems.* PhD Thesis- RWTH Aachen, 2001.

178. M. S. A. Karunaratne, D. C. Cox, P. Carter and R. C. Reed, *Modelling of the microsegregation in CMSX-4 superalloy and its homogenisation during heat treatment.* Superalloys, TMS (The Mineral, Metals and Materials Society) 2000, 2000.

179. M. S. A. Karunaratne, P. Carter and R. C. Reed, *Interdiffusion in the face-centred cubic phase of the Ni- Re, Ni- Ta and Ni- W systems between 900°C and 1300°C.* Material Science & Engineering, 2000. A281: p. 229-233.

180. B. A. Pint et al., *Some effects of metallic substrate composition on degradation of thermal barrier coatings.* In J. Nicholls and D. Rickerby, eds., High Temperature Surface Engineering., 2000. Institute of Materials, London. : p. 95-113.

181. D. S. Rickerby, S. R. Bell and D. K. White, *Thermal Barrier Coating for a superalloy article and method of application.* European Patent EP 0718419A2, 1995.

182. J. G. Goedjen and G. P. Wagner, *Evaluation of commercial coatings on MRM-002, IN-939 and CM-247 Substrates.* ASME international Gas Turbine and Aeroengine congress & Exhibition, 1996. Birmingham, UK.

183. A. U. Munawar, U. Schulz and G. Cerri, *Microstructural evolution of GdZ and DySZ based EB-PVD TBC systems after thermal cycling at high temperature.* Journal of Engineering for Gas Turbines and Power, 2013. 135(10).

184. O. Fabrichnaya et al., *The thermodynamic database of ZrO2-$YO_{3/2}$- $GdO_{3/2}$-$AlO_{3/2}$ system and application to TBCs.* Journal of Phase Equilibria and Diffusion, 2006. 27(4): p. 343-352.

185. X. Zhao, X. Wang and P. Xiao, *Sintering and failure behaviour of EB-PVD thermal barrier coating after isothermal treatment.* Surface and Coatings Technology, 2006. 200: p. 5946-5955

186. E. A. A. Jarvis and E. A. Carter, *An atomic perspective of a doped metal- oxide interface.* The Journal of Physical Chemistry B 106(33) p. 7995-8004

187 A. U. Munawar, U. Schulz, G. Cerri and H. Lau, "Substrate effect on the lifetime of "Substrate effect on the lifetime of EB-PVD TBC systems with 7YSZ and GdZ as ceramic top coat materials" Accepted for ASME Turbo Expo 2014 Conference, Düsseldorf, Germany.